A Multi-Method Approach for the Quantification of Surface Amine Groups on Silica Nanoparticles

By

Ying Sun

Supervisor

Dr. Linda J. Johnston

Thesis submitted to the Faculty of Graduate and Postdoctoral Studies

University of Ottawa

In partial fulfillment of the requirements for the

M.Sc. Degree in the

Ottawa Carleton Chemistry Institute

University of Ottawa

Abstract

As nanomaterials continue to garner interest in a wide range of industries and scientific fields, commercial suppliers have met growing consumer demand by readily offering custom particles with size, shape and surface functionality made-to-order. By circumventing the challenging and complex synthesis of functionalized nanoparticles, these businesses seek to provide greater access for the experimentation and application of these nanoscale platforms.

In many cases, amine functional groups are covalently attached as a surface coating on a nanoparticle to provide a starting point for chemical derivatization and commonly, conjugation of biomolecules in medical science applications. Successful conjugation can improve the compatibility, interfacing and activity of therapeutic and diagnostic nanomedicines. Amines are amongst the most popular reactive groups used in bioconjugation pathways owing to the many high-yield alkylation and acylation reaction are involved in.

For the design of functionalized nanomaterials with precisely tuned surface chemical properties, it is important to develop techniques and methods which can accurately and reproducibly characterize these materials. Quantification of surface functional groups is crucial, as these groups not only allow for conjugation of chemical species, but they also influence the surface charge and therefore aggregation behavior of nanomaterials. The loss of colloidal stability of functionalized nanomaterials can often correspond to a significant if not complete loss of functionality.

Thus, we sought to develop multiple characterization approaches for the quantification of surface amine groups. Silica nanoparticles were selected as a model nanomaterial as they are widely used, commercially available, and their surface chemistry has been investigated and studied for decades. Various commercial batches of silica nanoparticles were procured with sizes ranging from 20 – 120 nm. Two colorimetric assays were developed and adapted for their ease-of-use, sensitivity, and convenience. In addition, a fluorine labelling technique was developed which enabled analysis by quantitative solid-state ^{19}F NMR and X-ray photoelectron spectroscopy (XPS). XPS provided data on surface chemical composition at a depth of ≈ 10 nm, which allowed us to determine coupling efficiencies of the fluorine labelling technique and evaluate the reactivity of the two assays.

The ensemble of surface-specific quantification techniques was used to evaluate multiple commercial batches of aminated silica and investigate batch-to-batch variability and the influence of particle size with degree of functionalization. In addition, resulting measurements of surface amine content were compared and validated by an independent method based on quantitative solution ^{1}H NMR, which was developed for total functional group content determination. This allowed for us to assess the role of accessibility and reactivity of the amine groups present in our silica particles.

Overall, the objective of this study was to develop a multi-method approach for the quantification of amine functional groups on silica nanoparticles. At the same time, we hoped to set a precedent for the development and application of multiple characterization techniques with an emphasis of comparing them on the basis of reproducibility, sensitivity, and mutual validation.

Acknowledgements

I would like to first thank Dr. Linda Johnston, who has supported and guided me not only during my graduate research, but also my undergraduate honours project. I want to express my gratitude for her steady patience and mentorship at every step along the way. It has been quite some time since she opened the door to 100 Sussex, and I will always appreciate and reflect on her many lessons and teachings.

I'd like to sincerely thank a long list of group members at Sussex who have guided and pushed me along the way. Thank you Maohui, Greg, and Zygmunt, who each helped and taught me a great deal. Thank you, Shan, for your support and making me feel so welcome within the group. Thank you, Brian, Valerie and Mike, who were always willing to lend me a hand with anything. A special thank you goes to Andreas, who has been a great teacher, colleague and friend during my experiments at M-40. And of course, thank you to my dear friend Filip, who was an irreplaceable part of my Master's. The silica project and my caffeine dependence would not be where they are today without you.

To my parents, you have both set such a soaring example for me, Michael, and Wei Wei. You have always encouraged and spurred on my learning and scholarship. I can't recall an earlier memory than of Dad sharing stories from university, whether it was preaching and agitating Mom as the student chairman in Chongqing, or living in that small apartment flat in downtown Montreal.

Lastly, I want to thank my girlfriend, Morganne, who has been by my side from the start to the end of this memorable chapter. I vividly remember the day I shared with you my hopes of going back to school and completing my Master's degree. That moment will always be a special part of our story together.

Table of Contents

List of Abbreviations

4-NBA	4-nitrobenzaldehyde
AFM	Atomic Force Microscopy
APTES	(3-aminopropyl)triethoxysilane
AuNP	Gold Nanoparticles
BODIPY	Boron-dipyrromethene
BTFBA	3,5-bistrifluoromethylbenzaldehyde
BTFMBA	3,5-bis-(trifluoromethyl)-benzoic acid
CBB	Coomassie Brillant Bleu
CD-XPS	Chemical Derivatization X-ray Photoelectron Spectroscopy
CP	Cross-polarization
DLS	Dynamic Light Scattering
DNA	Deoxyribonucleic acid
DNP	Dynamic Nuclear Polarization
EASY	Elimination of Artifacts in NMR Spectroscopy
ECSA	Electron Spectroscopy for Chemical Analysis
ERETIC	Electronic REference To access In vivo Concentrations
FID	Free-induction Decay
FT	Fourier-transform

FTIR	Fourier-transform Infrared Spectroscopy
ISO	International Organisation for Standardization
LOD	Limit of Detection
LOQ	Limit of Quantification
MAS	Magic-angle Spinning
MCM-41	Mobil Composition of Matter No. 41
MS/IR	Mass Spectrometry/Infrared Spectroscopy
MSN	Mesoporous Silica Nanoparticle
NMR	Nuclear Magnetic Resonance
NP	Nanoparticle
PAA	Poly(acrylic acid)
PEG	Poly(ethylene glycol)
PEI	Poly(ethyleneimine)
PMMA	Poly(methylmethacrylate)
PTFE	Poly(tetrafluoroethylene)
QD	Quantum Dot
qNMR	Quantitative NMR
RBC	Red Blood Cell
RF	Radiofrequency
S/N	Signal-to-Noise

SAM	Self-assembled Monolayer
SESSA	Simulation of Electron Spectra for Surface Analysis
ss NMR	Solid-state NMR
TEM	Transmission Electron Microscope
TFAA	Trifluoroacetic acid
TFEA	2,2,2-trifluoroethylamine
TGA	Thermogravimetric Analysis
W/O	Water in Oil
XPS	X-ray Photoelectron Spectroscopy

List of Figures

intramolecular interactions and degrees of polymerization, which gives rise to structural complexity.

Figure 2-1: The ninhydrin reaction mechanism between alpha amino acids and primary amines. A shows the equilibrium state of ninhydrin and it -trione form, while B shows the widely accepted mechanism that follows.

Figure 2-2: Comparison of calibration curves prepared with primary amine standard APTES (3-aminopropyl)triethoxysilane in ethanol and 60% ethanol/H_2O.

Figure 2-3: Comparison of calibration curves prepared with primary amine octylamine in ethanol and 60% ethanol/H_2O.

Figure 2-4: Varying percentage of ethanol in aqueous reaction solution and effect on determining concentration of primary amine calibrant octylamine by the ninhydrin assay. n = 2, 2, 1, 6, 2 and 6 for 20, 40, 60, 80 and 100% respectively. A polynomial (2) fit was used as a guide.

Figure 2-5: Ninhydrin assay tests with amino acid Leucine in Ethanol 60%.

Figure 2-6: Ninhydrin reaction time kinetics experiment, with amine standards APTES and Leucine in ethanol 60%. A Sigma Aldrich assay kit was used for these experiments. Each point represents a single replicate.

Figure 2-7: Ninhydrin reaction time kinetics experiment, with amine standard octylamine and Leucine in ethanol 60%. 5 mM aliquots were used to monitor output. Each point represents a single replicate.

Figure 2-8: Ninhydrin calibration curve of leucine in Ethanol 60%, using the ninhydrin protocol from the Dawson publication. Each point represents a single replicate.

Figure 2-9: Ninhydrin reaction time kinetics with octylamine in ethanol 60%. A 2.47 mM aliquot was used. Each point represents a single replicate.

Figure 2-10: Stability of ninhydrin assay dye product over time. Data points represent the average of a triplicate, from the reaction with 50 nm aminated silica nanoparticles.

Figure 5-4: Correlation plots of fractional monolayer coverage with ^{1}H qNMR and ^{19}F ssNMR and XPS N/Si and F/Si ratios.

List of Tables

Chapter 1: Introduction

1.1 Introduction to Nanomaterials

In 1974 at a conference in Tokyo, Norio Taniguchi's proceedings stressed the increasing capability of large-scale manufacturing processes to prepare precise and fine features at the nanoscale. He envisioned a confluence of scientific disciplines enabled by technological processing, which translated into the first use of the word "nanotechnology".[1]

Nanomaterials can possess drastically different and remarkable physical, chemical, optical and electric properties in comparison to their bulk equivalents. Furthermore, unique phenomena such as quantum effects begin to appear in the nanoscale regime (~100 nm). These effects are of intense interest to semiconductor and electronics industries, where nanotechnology proffers smaller and more precise fabrication techniques. Doping and adding small amounts of nanomaterials to bulk plastics and fibers can improve conductive and mechanical properties, pushing the limits of synthetic materials.

No longer a distant vision, nanotechnology has arrived with commercial applications in electronics, energy and biomedical industries expected to exceed 100 billion USD globally in 2020. Meanwhile, international organizations have yet to establish universally accepted definitions and nomenclature to define and classify the rapidly expanding field.[2] The International Organisation for Standardization (ISO), defines a "nano-object" as a discrete material with one, two or three external dimensions in the nanoscale, which ranges from 1-100 nm. The ISO definition of a nanoparticle is a nano-object with all three dimensions in the nanoscale.

Nanomaterials are already packaged and sold on shelves, as a part of lotions and beauty products from the cosmetics industry. Everyday consumers are in closer proximity as ever to nanomaterials, as seen in **Fig 1-1**., making it essential to understand the nature of prolonged exposure and the potential effects to our health and the environment.

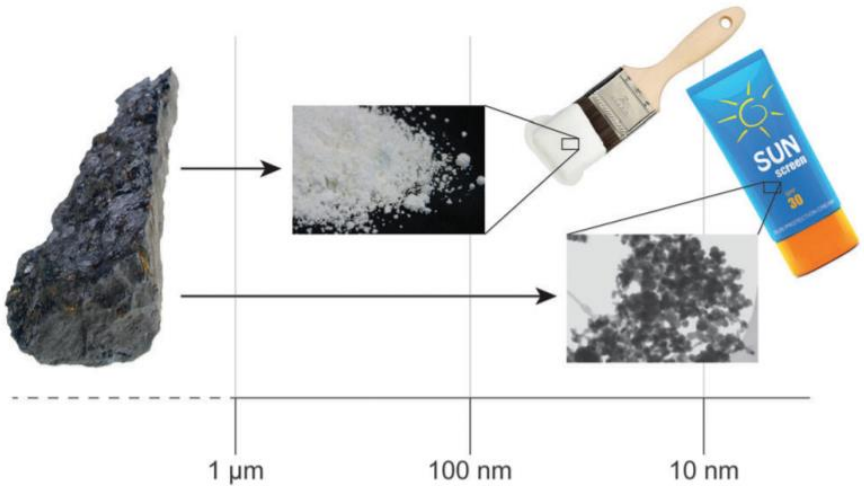

Figure 1-1: The industrial use of TiO_2 at the micro and nanoscale as a pigment in paints and opacifier in sunscreen. Nanoscale TiO_2 was shown to reduce undesired skin-whitening while maintaining UV-absorptive qualities. Illustration from reference (3).

Regulatory bodies seek to understand the safety, toxicology and the environmental outcomes of nanotechnology in our lives.[4,5] This has proven to be a great challenge, as materials in the nanoscale possess additional physical and chemical characteristics compared to their bulk counterparts. For example, a bulk material such as steel, an iron alloy, has discrete dimensions, surface area, mass and density. Manufacturing and processing of steel is relatively consistent at a large scale. In contrast, a batch of nanoparticles made from iron oxide has a *distribution* of sizes, surface areas, morphologies, and densities. Furthermore, at the nanoscale, additional

properties such as surface charge, and solubility play a greater role in governing behaviors in different chemical environments. The issue is further compounded due to the fact that nanomaterials can transform and change during their preparation, use and disposal.[6] In a dynamic state, they are capable of dissolving, aggregating or agglomerating, corroding, and oxidizing over time. This transformative behavior, termed the “chameleon effect”, makes not only regulatory efforts more difficult, but also reproducing and replicating results in scientific literature.[7,8]

One of the main causes of the “chameleon effect” of nanomaterials, is the number of different methods for their preparation and fabrication, and their impact on the properties of the resulting material. Materials produced in large-scale, “top-down” industrial processes may possess entirely different structure, composition, and morphology than lab-scale “bottom-up” syntheses. Despite carrying the same name, iron oxide nanoparticles prepared by different means can possess significantly different internal structure and composition.

Moreover, there are issues beyond drawing distinctions between nanomaterials produced by different fabrication or synthetic methods. Reproducing a particular method to arrive with a batch with consistent physiochemical properties is often non-trivial. For example, a group of researchers attempted without success to replicate synthesis of ceria nanoparticles after moving to a different laboratory.[7] Despite producing the NPs for years, the new particles were considerably less stable, suggesting that subtle and unnoticed differences in the conditions can fundamentally alter the final product.

Notably, the surfaces of nanomaterials can be very challenging to prepare consistently and uniformly. Sacher et. al, in a comparative study of preparing surface

functionalized nanomaterials for drug delivery,[9] stressed the "… lack of reproducibility in nanomaterial fabrication [creates a] worrisome situation for the research community... One crux of the problem is surely a lack of standards and techniques for surface characterization, and their use in quantifying reproducibility." This is concerning, as the surface is one of the principal determinants of a nanomaterial's behavior and function.

This problem does not only plaque the reproducibility of research data and syntheses, but stands in the way of clinical translation of nanomaterials in the diagnosis, treatment and prevention of diseases, one of the areas for which nanotechnology stands to make the most impact.[10] The development of reference standards and methods of characterization of physicochemical properties and surface chemistry is an enormous task given the sheer number of the different parameters and variety of types of nanomaterials.[11–13] Initiative must be taken to improve the quality of materials characterization, which will foster more quantitative and useful data for meta-analyses and review.[14] Only then can we critically assess the consequence of the growing role of nanotechnology in our lives.

1.2 Surface Chemistry of Nanomaterials

At the nanoscale, materials have a greater ratio of atoms facing the surface which results in a higher surface area to volume ratio. This relationship (which is exemplified in **Fig. 1-2**) can result in "surface effects" which are often responsible for the drastic differences in physicochemical properties between bulk materials and their nanoscale equivalents.[15] For example, surface atoms have a comparatively lower coordination number from fewer neighboring atoms, which can lead to higher affinities

for bonding and adsorption.[15] Thus, surface chemistry is frequently exploited to enhance and improve nanomaterial characteristics in their applications. They are most commonly covalently modified with chemical groups or biomolecules to impart active targeting in bioapplications. Additionally, the chemical groups may alter the surface charge of the particle, which is a critical parameter in maintaining colloidal stability. And further, when used as part of fillers and plastics, the surfaces of nanomaterials can be modified with a polymer coating, to ensure homogenous distribution throughout the bulk.

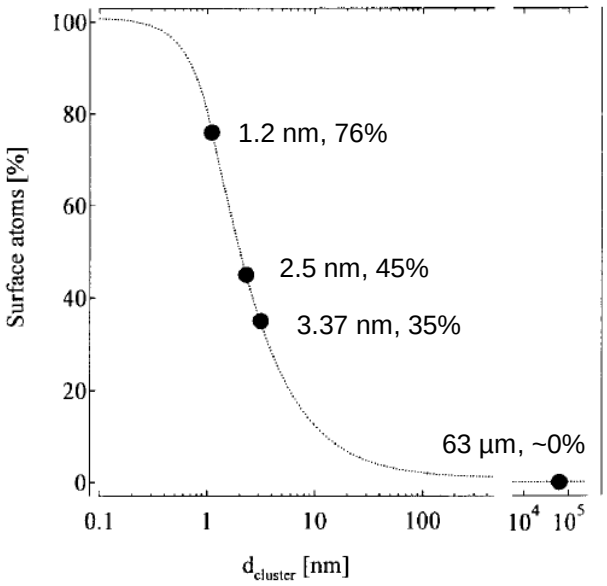

Figure 1-2: The percentage of surface atoms relative to the diameter of various prepared Pd clusters. Adapted from reference (16).

One of the most promising applications of nanotechnology is in medicine.[17] Nanomaterials have been exhaustively researched as platforms for diagnostic imaging and drug delivery in the last 20 years. One of the most important domains within this broad field is in the customization and tailoring of the nanomaterial's surface for improved recognition and targeting.[18] An expansive range of biomolecules have been

demonstrated as ‘smart’ targeting ligands, various surface chemistry properties have been tuned and manipulated, and materials of different elemental composition, structure and morphology have been investigated, as shown in **Figure 1-3**.

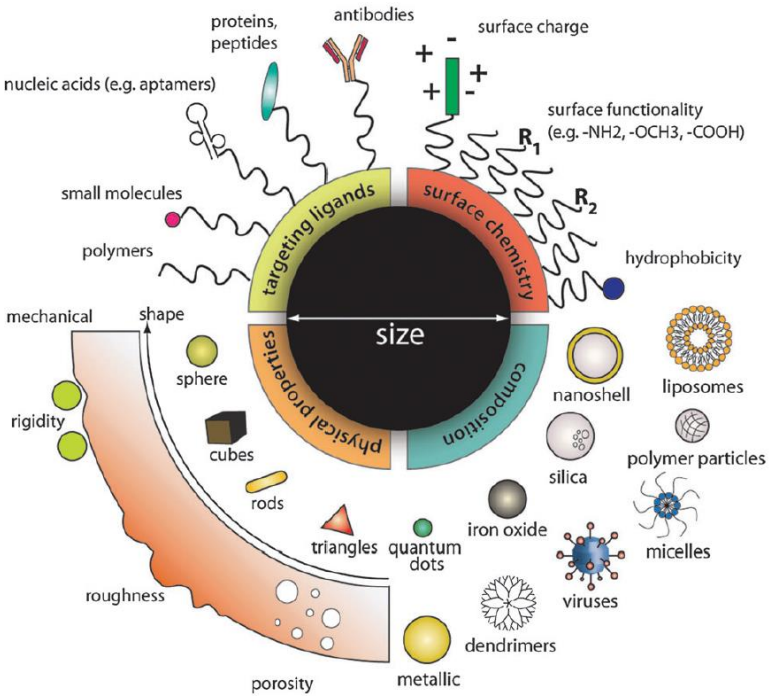

Figure 1-3: An illustration of the various ways a nanoparticle can be customized for intracellular delivery. Many of the properties outside of the quadrant termed “surface chemistry” still influence and are influenced by the nature of the nanoparticle’s surface. Image from reference (19).

To ensure nanomedicines can successfully reach their target site and perform their function, it is essential to understand their stability and behavior in the relevant environment. One major area of concern for colloidal nanoparticles is controlling their agglomeration and aggregation. This refers to the common tendency of nanoscale objects to adhere to one another when in solution, provoking the formation of large clusters or agglomerates, which precipitate or ‘crash out’ of solution. This comes with

severe reduction of available surface area due to the points of adhesion, and generally loss of desired functionality. The short range and long range thermodynamic forces which drive the aggregation of particles have been subject to a great deal of study and theorization.[20,21] Monitoring and tuning the surface charge of nanoparticles is one strategy to manage aggregation, as increasing surface charge results in more electrostatic repulsion, which can stabilize dispersions. Even for nanoparticles which can form stable dispersions in ideal solvents and conditions, their colloidal stability suffers in biological applications, where salt and ion concentration, temperature and pH can fluctuate and change. Carefully prepared surface coatings, which may involve a combination of surfactants, polymers or electrolytes can improve stability of nanoparticles suspensions and prevent aggregation.[20] This is crucial in biomedical applications, as there are many cases where toxicology of nanotherapeutics has been shown to be size-dependent and related to aggregation state.

When introduced into living systems the surface of a nanomaterial can give rise to a host of non-covalent interactions with biomacromolecules. A complex of proteins often accumulates around a nanoparticle, which is termed the ‘protein corona.[22] It is understood that many biological responses should be attributed to the protein-NP complex, rather than the bare nanoparticle.[23] Addressing and controlling the formation of the protein corona is one of the most important reasons for functionalizing and tailoring the nanomaterial surface in bioapplications.

In **Fig 1-4**., we can see a detailed breakdown of the protein corona into the hard and soft coronas. Proteins which inhabit the hard corona possess higher binding affinity to the surface, whereas the soft corona proteins are more weakly bound, and can be

removed by washing and purification. The exposure time indicates the dynamic nature of the protein-NP complex, where proteins may exchange between soft and hard coronas. In the chart (C), various factors are listed which determine the formation of the protein corona. The composition, surface, size, charge and shape are in fact, all attributes which can be controlled and tuned through surface functionalization techniques.

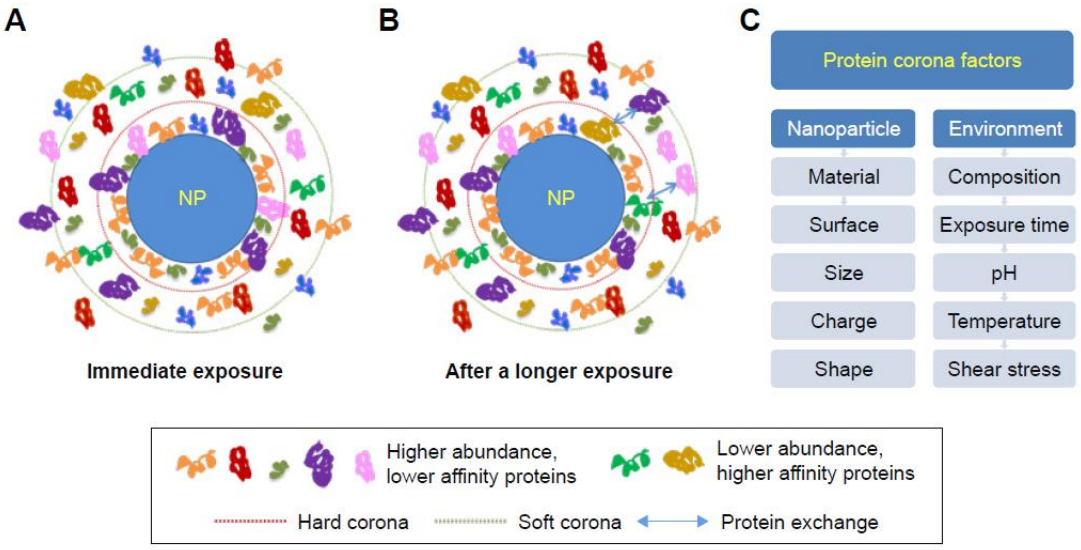

Figure 1-4: Accumulation of non-specific binding of proteins onto the surface of nanoparticles in biological conditions, resulting in the “protein corona”. (C) shows the various factors which contribute to its formation. Image from reference (22).

Although the core of a nanomaterial will interact to some degree with the outside environment by physical interactions (i.e. van der Waals)[24], the surface is still the principal determinant to yield specific and desired biological responses and signals. For therapeutics and diagnostics, specially designed surfaces can improve internalization into cells, non-toxicity, and circulation characteristics.[25] Polyethylene glycol (PEG) coatings are widely used to minimize the formation of the protein corona, and there is

work that suggests that grafting density can influence the attachment of opsonins, which is linked to the phagocytic response.[26] Improving the circulation time of PEGylated NPs gives them a greater chance to reach the target site, often by the enhanced permeation and retention effect.[27]

A unique strategy to alter the surface character of nanotherapeutics was demonstrated with gold nanoparticles wrapped with red blood cell (RBC) membranes, seen in **Fig. 1-5**.[28] These membranes incorporate natural markers such as membrane proteins, glycans and other moieties that camouflage the nanomaterial. Purified mouse RBC vesicles were treated to remove intracellular contents, and then extruded at a size of 100 nm. AuNPs were mixed and extruded alongside the treated RBC membranes which resulted in fused RBC-membrane-coated gold nanoparticles. Repeating this process resulted in a homogenous shell with excellent immunosuppressive qualities, demonstrating a unique approach to produce advanced hybrids of biological and inorganic materials. This work has been extended to magnetic iron oxide NPs, polymeric and silica nanomaterials and is one of the most frequently used approaches to introduce a cell-membrane exterior as a surface coating. Incorporating different types of cell membranes, such as cancer cell, fibroblast or platelet can provide a more targeting-based approach, and further improve the outcomes of these nano-based therapeutics.

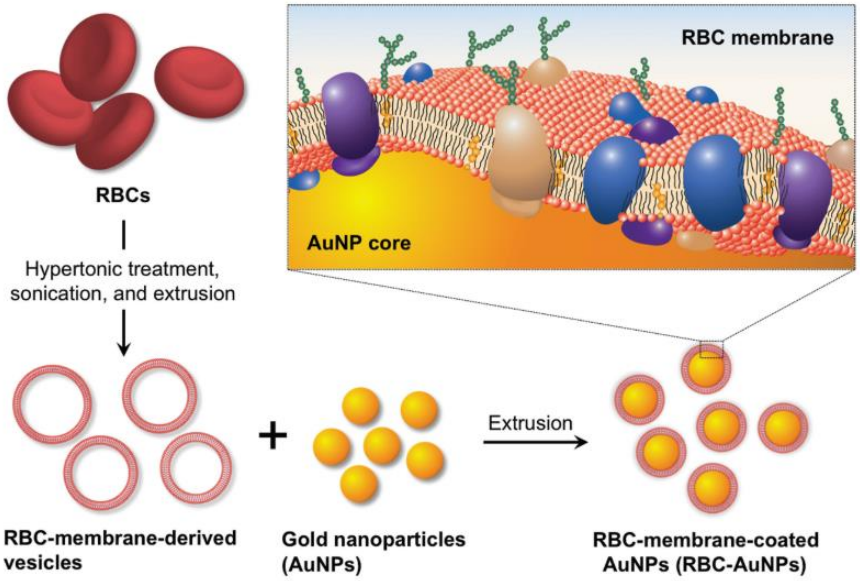

Figure 1-5: Surface coatings of red blood cell membranes onto gold nanoparticles for enhanced biocompatibility. Image from reference (28).

Beyond drug delivery systems and therapeutics, surface chemistry has wide ranging effects on the electronic and optical properties of certain nanomaterials. Semiconductor quantum dots, which are comprised of group II-VI or III-V elements exhibit unique optical properties, resulting from confinement of charges at the nanoscale. Their quantized discrete energy levels are primarily dependent on the size of the quantum dots. The surfaces of QDs can harbor defect sites which can quench the fluorescence activity of neighboring dots. Their activity can also deteriorate from oxidation and photodegradation during photoactivation. As a result, there is a large focus on surface capping strategies that can protect and insulate the optical and electronic properties.[29] Furthermore, quantum dots have been assessed as potential systems for solar energy conservation as part of photovoltaic and photoelectrochemical devices. Design and characterization of surface ligands and coatings is crucial to control

interparticle distances and organization in the devices.[30] Beyond the example of quantum dots, the use of nanomaterials in the development of electronics with exceptional physical and chemical properties is wide-ranging in scope. Nanostructures have been beneficial in the development of lithium-ion batteries, supercapacitors, and hydrogen storage systems.[31]

Another major area of research is in the development of composite hybrid materials which possess a component in the nanoscale. These ‘nanocomposites’ utilize nanomaterials as fillers which can confer significant improvements and changes to physical and chemical characteristics to the bulk properties. In examples with ceramic and polymer composites, improved dielectric electronics can be prepared by combining ceramic nanoparticles with high permittivity and polymers with desirable mechanical properties.[32] The success of most nanocomposite applications heavily depends on the controlled spatial distribution of the nanofillers. Where homogenous distribution is often desired, uneven distribution and accumulation can result in defect centers with unexpected electronic properties. Aggregates of nanofillers can also lead to stress points with poor mechanical properties, and thereby deterioration and destruction of the nanocomposite. Surface coatings are one of the key means of controlling the distribution of nanomaterials in composite materials. Inorganic oxide fillers such as silica and alumna are often used within polymer composites. The former is known improve thermal[33], mechanical[34], optical[35] properties in the bulk. Utilizing both silica-based nanomaterials and silica coatings has been shown to reduce aggregation and retain the beneficial characteristics in the bulk.[36]

1.3 Nanoscale Silica

Nanoscale silica is one of the most widely used and produced engineered nanomaterials. There are various methods for its large-scale preparation and processing,[3,37] as well as small-scale laboratory syntheses.[38] As nanoparticles, their tunable size, density and porosity has led to intense interest and their application as drug delivery platforms.[39–41] Furthermore, silicon dioxide (SiO_2) is frequently used as a coating for organic and inorganic nanoparticles, providing colloidal stability in aqueous media, chemical inertness, optical transparency and a platform for facile surface chemistry.[42] Although silica nanoparticles are often regarded as biocompatible and "well-tolerated",[38,43] their cytotoxicity is a subject to ongoing study and investigation due to contradictory reports.[39,44] Cytotoxicity has also been shown to be governed by particle size, surface charge and degree of porosity.[45,46] While their toxicity is not entirely clear, nanosilica possess desirable characteristics required in bioapplications. Alongside their previously stated strengths, they are biodegradable and their circulation characteristics can be easily tuned and controlled.[43]

The most popular method for small-scale synthesis is the Stöber process, which prepares monodisperse silica nanoparticles from silica precursors, aqueous alcohol solution and base catalyst (ammonia). Particle size from several micrometers to tens of nanometers is controlled by ratio of precursor to catalyst.

There are two principal reactions which occur during the Stöber process (see **Fig. 1-6**). The first is the hydrolysis of the precursor which results in silanol monomers. The second is the condensation of the silanols, which generates water or ethanol as a

by-product, depending on the substituents and extent of hydrolysis of the precursors. As these reactions proceed, the particles can grow in size and decrease in number, with smaller particles dissolving giving way to larger precipitates, a process named Ostwald ripening. The systematic study on the role of each reagent was a major contribution by Stöber in 1968.[47] The kinetic balance between precursor hydrolysis and condensation of the resultant monomers has been identified as a major determinant in controlling size, polydispersity, and interior structure of the Stöber silica nanoparticles.[48]

$$(1)\ \mathrm{Si(OEt)_4} + x\mathrm{H_2O} \rightleftharpoons \mathrm{Si(OEt)_{4-x}(OH)_x} + x\mathrm{EtOH}$$

$$(2)\ 2\,\mathrm{Si(OEt)_{4-x}(OH)_x} \rightleftharpoons \mathrm{(EtO)_{8-2x}(Si-O-Si)(OH)_{2x-2}} + \mathrm{H_2O}$$

$$(3)\ \mathrm{Si(OEt)_4} + \mathrm{Si(OEt)_{4-x}(OH)_x} \rightleftharpoons \mathrm{(EtO)_{7-x}(Si-O-Si)_1(OH)_{x-1}} + \mathrm{EtOH}$$

Figure 1-6: Principal reactions of the Stöber process: (1) hydrolysis of the precursor and condensation via silanols (2) and by unhydrolyzed precursors (3). From reference (48).

The reverse micro-emulsion method is the second most frequently used synthetic route and involves a reverse micelle or water in oil (W/O) microemulsion.[49] Water droplets at the nanometer scale in the oil phase create a confined space for particle growth, and also determine the particle size distribution. Silicate precursors penetrate these droplets with the aid of surfactants, with the type of surfactant and concentration providing additional control over particle size.[50] The strength of the surfactant restricts droplet exchange and combination, which leads to larger sizes of particles.

Silica materials with controlled porosity have been avidly investigated since the discovery of MCM-41 (Mobil Composition of Matter No. 41) in the early 90s. The material's porosity provides an additional platform for loading of dyes, imaging agents and therapeutics. Methods of preparing colloidal mesoporous silica nanoparticles (MSNs) came later, as MCM-41 is an amorphous silicate. MSNs have garnered great interest in applications as zeolites and solid supports for catalysis.

The Stöber process can be easily modified to produce mesoporous silica nanoparticles.[51] The inclusion of a cationic surfactant induces formation of micelles within silicate micelles, which was a major contribution by Grun et al.[52] Once the silica matrix has condensed, the surfactants can be removed afterwards by calcination, leaving behind the pores. Although the degree of porosity and diameter is influenced by a multitude of factors (solvent, temperature, water content, pH), the surfactant concentration and length is one of the most direct means of control.[51]

Silica nanoparticles can form stable dispersions in aqueous solutions and various polar organic solvents (alcohols, toluene etc.), although this behavior is dependent on their size and their surface chemistry. The surface silanol groups (Si-OH) are hydrophilic and form hydrogen bonds with water and polar solvents. Their suitability for aqueous conditions has enabled their use in biological applications.[53] The presence of salts and electrolytes is known to increase the rate of aggregation, although this behavior is not fully understood, along with the effects of temperature and pH.[54] Agglomeration of silica nanoparticles, as is consistent with other nanomaterials, is provoked by drying processes (i.e. freeze-drying, thermal drying). It has been reported that the presence of water in the dispersion of particles can increase the agglomeration

of particles after the drying process.[37] It remains one of the major production challenges, as silica nanoparticles are known to be sensitive to certain processing and handling conditions. The presence of moisture is believed to initiate interparticle condensation during drying.[37]

Silica and silica-based nanostructures are also biodegradable, which is important as the persistence of inorganic nanoparticles is an important issue regarding clinical translation.[11] It appears that structure, density and porosity are all materials properties which influence the rate of biodegradation, while temperature and pH increase the rate of dissolution.[39] Controlling or tuning the rate of degradation in biological environments may benefit kinetics of drug delivery systems which utilize silica nanomaterials or coatings.[55–57]

1.4 Surface Functionalization of Silica Nanoparticles

One of the major advantages of using silica nanoparticles and silica-based coatings is the relative ease of chemically modifying their surface. The surface chemistry of silica has been exploited for over thirty years to prepare functionalized materials. This is due to the extensive body of research on silicon substrates and films, as a great deal of their surface chemistry is shared. Since the 1980s,[58] alkylsiloxanes have been studied and exploited for their ability to form self-assembled monolayers (SAMs) on thin films and substrates. Provided the surface has available hydroxyl groups, and even in cases where there are trace amounts, monolayers (and multilayers) of siloxanes can be grown, a process termed *silanization*. The diverse variety of

organofunctional alkoxysilanes allows for the custom tailoring of the surface chemistry in silica-based coatings and nanomaterials.

The general structure of an alkoxysilane is divided into three parts: the head group, the alkyl chain and the terminal group.[59] The head group is the point of attachment onto the substrate and is typically trimethoxy- or triethoxy-. Other halide substituents such as trichloro- are sometimes used for their increased reactivity, but also have issues with undesired side reactions. The alkyl chain is the next region, and an important feature to consider as its length directly influences the thickness. Depending on heteroatom substitutions along the alkyl chain, van der Waal interactions may influence the packing and ordering of the surface coating. The last region of the silane, facing outwards, is the terminal group. It primarily determines the chemical functionality of the monolayer. Organic functional groups such as amine, carboxyl, thiol, acetates etc. are frequently used to allow for further chemical derivatization through diverse reaction pathways. See **Table 1-1** for reference to some popular silane coupling reagents. From biomolecules such as antibodies, polypeptides and DNA to supramolecular ligands, fullerenes and pyridine complexes, the potential for surface customization has been explored extensively on SAMs.

Table 1-1. The most popular functional silane coupling reagents, their chemical functional groups and their surface applications. Table from reference (43).

Silane	Functional Group	Application and Effects
(3-Aminopropyl)trimethoxysilane (**APTMS**) (3-Aminopropyl)triethoxysilane (**APTES**)	$–NH_2$	Reduced aggregation, fluorescent labeling, surface charge modification, DNA binding and protection from enzymatic cleavage
(3-Mercaptopropyl)-trimethoxysilane (**MPTMS**)	–SH	Conjugate with maleimides, thiol/disulfide exchange reactions to attach oligonucleotides, surface charge modification
Polyethylene glycol-silane (**PEG-silane**)	–PEG	Increased circulation time, reduced aggregation and increases particle dispersity in aqueous solution
Alkylsilane	Alkyl chain	Hydrophobic coating, increase ultrasound contrast
Carboxyethylsilanetriol	–COOH	Functionalize silica NPs and provide reactive sites for amine
3-Trihydroxysilylpropyl methylphosphonate	$–PO_3^-$	Functionalize silica NPs and provide reactive sites for amine
(3-Isocyanatopropyl)-triethoxysilane	–NCO	Functionalize silica NPs and provide reactive sites for amine

As shown in **Fig. 1-7**, the spontaneous reaction between alkoxysilane and surface hydroxyl begins with hydrolysis of the head group's substituents, which allows for the condensation reaction. The rate of hydrolysis will depend on the concentration of the silane solution, as well as the relative reactivity of the substituents. Condensation and attachment of the silane to the surface can occur at any of the three available sites and the different degrees of binding can influence the order of the surface coating.

At a macromolecular scale, the reaction generates a cross-linked network of siloxane bridges (Si-O-Si) between both silanes and substrate and silane to silane. The growth of these networks is categorized between homogenous growth vs. island type growth. In the former, individual groups attach throughout the surface evenly, while island type growth involves attachment of larger pre-formed oligomers to the surface. It is believed that the latter is a consequence of the tendency of alkoxysilanes to form oligomers in solution, where hydrolysis can occur in the presence of moisture in the reagent, but also without.[60] The means to control the different growth mechanisms have been the focus of a great deal of research that continued throughout studies on thin films and nanoscale silica. The type of solvent, age of silanes, concentration (water content) of reactive silane solution and temperature have been identified as contributing factors.[53,61–63]

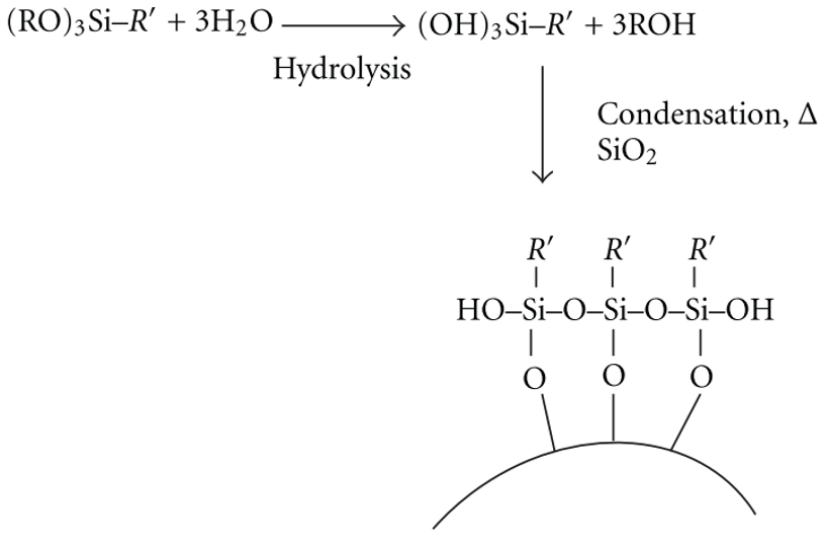

Figure 1-7: Surface functionalization with alkoxysilane by self-assembled monolayers on oxide surfaces. Adapted from reference (37).

Alkoxysilanes can also bind and adhere to the surface through non-covalent interactions (physisorption) as shown in the example below (**Fig. 1-8**). The various modes of binding possible for alkoxysilanes can result in different orientations and structural features. Here, we can see single bond attachment through the head group, as well as electrostatic adsorption, cyclization and formation of a multilayer of alkoxysilanes. Non-covalent functionalization with large molecules (i.e. lipids, polymers, proteins etc.) typically depends on opposite charged species and electrostatic interactions and is often simpler to perform.[64] Adsorption has been widely studied and reported as an alternative route of functionalization for applications where reversible binding is desired.[65,66]

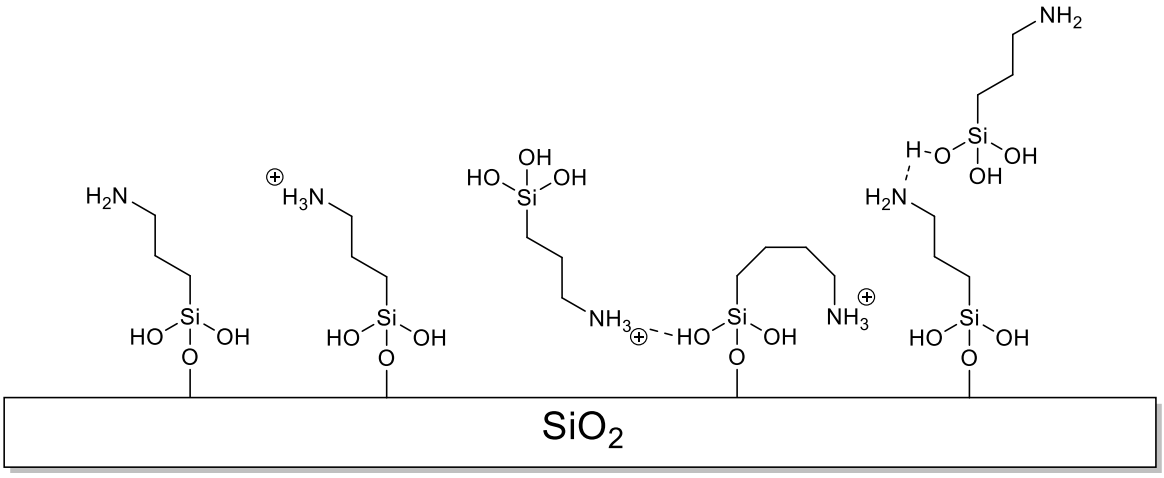

Figure 1-8: Various modes of binding of an alkoxysilane (3-APTES) which possesses a functional group capable of hydrogen bonding and charged ion form. Adapted from reference (67).

The mechanism of formation of self-assembled monolayers is also described as a *post-modification* surface functionalization. In contrast, *co-condensation* techniques require inclusion of functional chemical species during particle growth and synthesis.

There are various examples of incorporating fluorescent organic dyes, MRI-active contrast agents, and metal ion chelators, although these are not strictly surface species.[43] Co-condensation functionalization techniques are most frequently used in the preparation of highly porous nanoparticles, such as in mesoporous silica, where functional group content is intended to be both surface bound and distributed throughout the interior matrix and pores.[39]

APTES, (3-Aminopropyl)triethoxysilane, is one of the most frequently used organofunctional alkoxysilanes, as it introduces primary amine chemical groups to silica surfaces. Although it is typically used for post-synthetic surface modification, it can also be incorporated throughout particles by co-condensation. Primary amine groups are useful because of their various reactive pathways, particularly for the conjugation of biomolecules. Many biologically relevant, high-yield acylation and alkylation coupling reactions utilize primary amines.[68] Accordingly, some of the earliest examples of surface functionalized silica nanoparticles utilized APTES for the surface immobilization of polypeptides[69], folic acid[70] and DNA[71]. Alternatively, APTES can be used to pre-conjugate biomolecules, such as fluorescent dyes, allowing for their encapsulation within the particle matrix.[72] There are numerous instances of improved photostability of fluorescent dyes when encapsulated within silica nanoparticles.[73,74] APTES monolayers impart a net positive charge to silica nanoparticles which not only can provide colloidal stability,[75] but also enable electrostatic immobilization of negatively charged species.[72] APTES-modified silica nanoparticles have been extensively studied as non-viral gene delivery systems through surface adsorption of plasmid DNA.[76] In respect to polymeric nanocomposites, APTES-coated silica nanoparticles have been shown to impart

improved tensile strength, abrasion resistance and rheological properties.[77] Lastly, APTES functionalized catalysts and zeolites have been frequently shown to improve adsorption and complexation of a variety of molecular guests.[78–82]

Silica nanoparticles have been highlighted as potential platforms for the design of *theranostics*: agents capable of both performing imaging/diagnostics and targeted therapy.[40,43,83–86] This is largely owing to the flexibility and different modes of functionalization of nanoscale silica, which enables the design of multifunctional particles. In many examples with mesoporous silica nanoparticles, their pores are typically loaded with small molecule pharmaceuticals. Capping of the pores with photosensitive nanomaterials and molecules such as quantum dots[87], gold nanoparticles[88] and coumarin[89] have demonstrated this mechanism of activatable gatekeeping and delivery. More advanced, 'mechanized' theranostics were outlined by Stoddart and others, whose work on stimuli responsive (pH, redox and light) supramolecular capping molecules allowed for the design of what they termed 'nanovalves', shown in **Fig. 1-9.**[84]

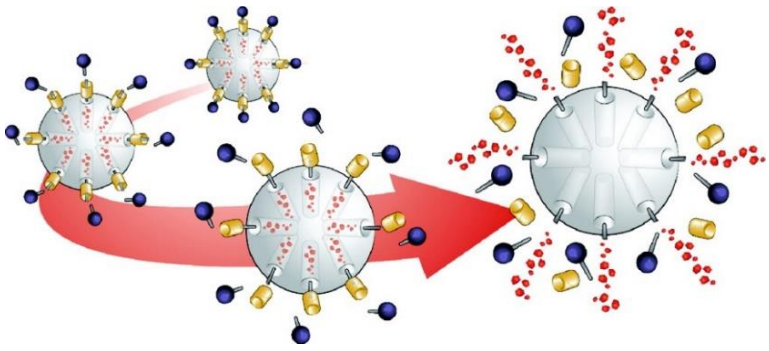

Figure 1-9: An illustration of activatable gatekeeping on mesoporous silica nanoparticles showcasing a multifunctional drug delivery system. Image from reference (84).

1.5 Quantification of Surface Functional Groups

As functionalized nanomaterials stand to make enormous impacts in a diverse variety of fields and industries, their methods of characterization are a critical factor for their development, quality control and regulation. Since the nanomaterial's surface chemistry has a significant influence on the material's properties and behavior, it is imperative to establish reproducible and validated methods to determine chemical composition and structure.

In respect to silica nanoparticles and their functionalization, there are various methods and conditions which allow for control over the grafting density or concentration of surface functional groups.[77,90–92] In addition, surface functional group density has been shown repeatedly to influence the performance and outcome of these materials in various applications.

In one such case, mesoporous silica nanoparticles were surface functionalized with poly(ethyleneimine) (PEI) which improves their CO_2 adsorption capacity for carbon-capturing applications.[93] The authors noted that although most studies typically use highly-loaded PEI surfaces, there was a middle ground between CO_2 adsorption and diffusion resistance. Accordingly, they recommended a level of functionalization below the maximum they could achieve with PEI functionalization, demonstrating the improved performance two loadings in **Fig. 1-10**.

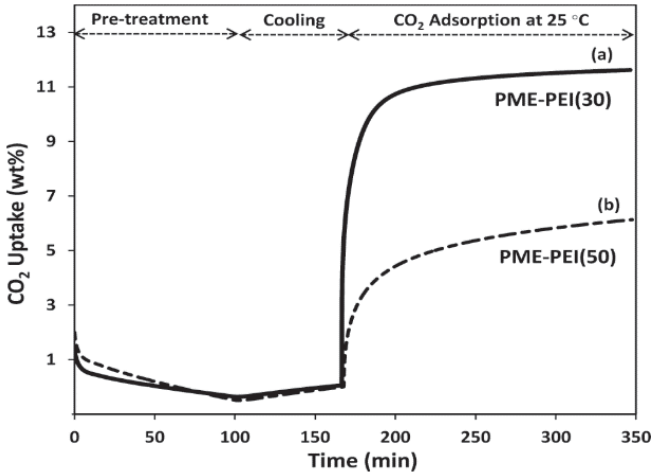

Figure 1-10: Comparison of CO_2 uptake of two mesoporous silica nanoparticles which were surface functionalized with poly(ethyleneimine) at different loadings. Image from reference (93).

In another example, mesoporous silica nanoparticles were functionalized with aminopropyl and aminobutyl surface groups for the adsorption of drug molecules.[94] A similar case was found, where a lower than maximum amount of functionalization gave optimal performance. Although other studies with ibuprofen and captopril indicated high loading density was preferable for drug release kinetics, results with a model pharmaceutical, methylprednisolone sodium succinate suggested a reduced degree of surface functionalization was more advantageous.

In the context of bioconjugation for the design of nanomedicines and therapeutics, a study by Kenneth Dawson's group stressed the impact of controlling the degree of surface functionalization and its impact on the rate of cellular uptake and potentially the specific pathway.[95] Silica nanoparticles were prepared with various surface concentrations of APTES and subsequently PEGylated to improve their colloidal stability in aqueous media. The aminated silica NPs were then conjugated with a

protein, Transferrin (Tf), to yield a range of particles with different loadings of both PEG and Tf. The authors found that through controlling surface functionalization, they were able to achieve greater cellular uptake in studies with A549 human alveolar epithelial cells. While the protein loading appeared to stay relatively constant, the amount of PEGylation had a strong influence of the uptake characteristics.

In general, the surface grafting density of biomolecules to nanomaterials has been the subject of extensive discussion as multiple non-ideal behaviors can arise: molecular crowding, neighbor-to-neighbor interactions, altered charge density, electrostatic repulsion, and loss of colloidal stability.[72] While there are reasonably effective methods for characterizing and quantifying certain biomolecules such as proteins and their grafting density, it is a significantly greater challenge to measure them when complexed and bound to nanomaterials.[96] This is an issue, as most bioconjugation applications require a specific degree of conjugation to retain colloidal stability, activity and proper conformation and/or orientation of grafted biomolecules[72].

Therefore, it is critical to effectively characterize and quantify the surface functional group density prior to bioconjugation and to precisely determine the number of available binding sites. Furthermore, it is imperative to utilize multiple characterization techniques, as with all analytical tools, there are no all-encompassing and definitive methods. Each approach possesses its own advantages and disadvantages, usability, limitations and sources of error.

For silica-based nanomaterials, although many graphical representations suggest a highly ordered and well-behaved surface and interior matrix, the amount of disorder, complexity and variability in structure and morphology has been well-

documented for decades. With respect to the characterization of surface functional groups, particularly those which depend on chemical derivatization and assume a quantitative coupling yield, this can result in tremendous differences and large sources of systematic error.[97,98] This is very concerning, as two of the most frequently used characterization methods for surface functional group content are photometric and fluorescent-based assays, which depend on the reactivity of the reporter or dye molecule. On silica, functional groups may be arranged in a variety of modes[99], with an example shown in **Figure 1-11**; a more accurate representation of the surface content may require further dividing it into chemical groups which are more accessible or reactive and those which are sterically hindered, crowded or even encapsulated.[97] Determining the surface accessible/reactive groups vs. total groups can provide a more complete and detailed picture of the nanomaterial's degree of functionalization.

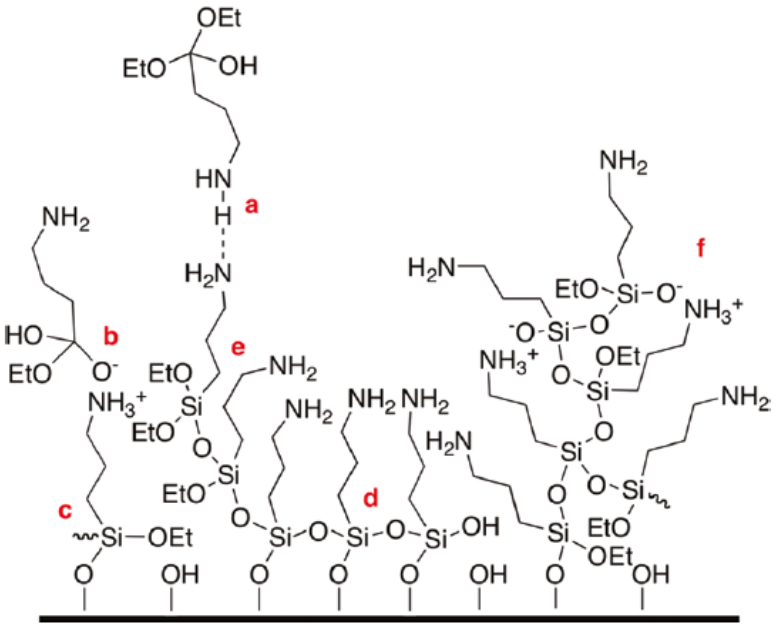

Figure 1-11: The various irregular and disordered arrangements of silanes that are possible on surface-functionalized silica. (a-f) illustrate different intermolecular and

intramolecular interactions and degrees of polymerization, which gives rise to structural complexity. a) hydrogen bonding, b) and c) ionic interactions, d) and e) lateral and vertical growth, and f) irregular growth. Image from reference.[61]

There are several characterization techniques for quantification of organic functional groups on inorganic scaffolds and nanoparticles. Those which require destruction or dissolution of the nanomaterial include elemental analysis,[100–102] thermogravimetric analysis (TGA),[103] and some solution NMR approaches.[103,104] Total functional group content determination is a useful measurement for nanomaterials which may contain chemical moieties below the surface, within pores, or distributed homogenously through the matrix. Elemental analysis is limited to providing total elemental organic content and offers no identification of origin. TGA can not only provide total functional group content, but also additional information such as moisture content, residual or trapped solvent, and detect any contaminants depending on coupling to MS/IR. However, TGA can be limited by materials which are not thermally stable throughout the temperature program. In our groups work, we have found that loss of silanols due to condensation occurs at a similar temperature range as organic functional groups, and therefore requires additional efforts to deconvolute this effect.[105]

Non-destructive approaches such as Fourier-transform infrared spectroscopy (FTIR), conductometric titration, mass spectrometry and solid-state NMR are also useful for materials that are not compatible with the aforementioned methods. FTIR is mostly used in a qualitative manner to identify functional groups and compare relative amounts.[90] Conductometric titrations can be performed quantitatively for acidic and basic groups, but require samples to be fully protonated/deprotonated and can require

large amounts of sample.[106–108] Additionally, variations in the surface structure determines functional group orientation and position, altering reactivity and thus pKa's, which can complicate conductometric titration analysis.[97] Mass spectrometry techniques are challenging to use with silicates, due to the high ionization potential and competing isotopes. Solid-state NMR instrumentation is less accessible, expensive, and sample preparation often requires additional agents in the case of sensitivity enhancement techniques.[109]

For quantification of surface functional groups on nanomaterials, colorimetric and fluorescence-based assays are the most popular, largely owing to their convenience and simplicity.[110–115] Labelling with colorimetric and fluorescent probes can provide an estimate of 'reactive' or 'accessible' functional groups, although it is not straightforward to relate coupling efficiency of molecular probes to bioconjugation of bulky macromolcules.[115] Direct measurement of these probes when bound to the surface can also be challenging. Fluorescence-based approaches despite being relatively sensitive, are affected by self-quenching, particularly when surface functional groups are densely packed.[13] Self-quenching can be studied and partially addressed by using nanomaterials with controlled surface functionality and the use of fluorescence lifetime measurements.[115] However, for quantitative measurements, fluorescent-based approaches have been shown to detrimentally affected by changes to molar absorption coefficients and fluorescent quantum yield when bound.[97] Recently, a class of rationally designed probes demonstrated one strategy of circumventing this issue, by using cleavable structures which have distinct emissions when bound and unbound.[116,117] Unfortunately, colorimetric and fluorescent labeling approaches are limited in their ability

to quickly and conveniently determine what types of chemical groups are bound to the surface, which is a strength of characterization techniques such as NMR and FTIR. Furthermore, performing quantitative measurements requires careful consideration of the emission mechanism, as well as the coupling yield to the functional group of interest.[13,97]

X-ray-based techniques such as X-ray photoelectron spectroscopy and Auger electron spectroscopy can be used to determine chemical composition of surfaces, although they are less commonly applied in a quantitative manner on nanomaterials.[98,118,119] Both require sophisticated modelling and analysis to account for the structural complexity of certain nanoparticles, as both techniques were designed for analysis of flat, planar samples. Chemical derivatization or labelling for XPS can be performed but is also restricted by coupling yield.[120]

As is it clear that each characterization technique has both its strengths and weaknesses, it is most appropriate to utilize a combination of methods. When quantitatively measuring surface functionalization on a nanomaterial, it is logically more suitable to implement surface-specific techniques over methods which provide total functional group content. However, it can still be beneficial to include total functional group determination to validate surface methods which may be sensitive to surface group reactivity and accessibility. In some cases where the method for surface functionalization of a nanomaterial is not known, using both surface and total determinations may point to whether functionality was derived post-synthetically, or during particle growth/co-condensation.

1.6 Objective of Thesis

The objective of this thesis was to develop methods for the quantitative determination of amine functional groups on silica nanomaterials. Through the implementation of multiple instrumental techniques and surface chemistry reactions, we sought to establish a multi-method approach. Each method was critically assessed based on reproducibility, sensitivity, and sources of error. For the reasons highlighted in the introduction, and as they are widely used and commercially available, silica nanoparticles served as a model nanomaterial. APTES functionalized silica nanoparticles possessing a primary amine functionality, and bare, non-functionalized particles were procured from a commercial supplier. Multiple production batches were compared to investigate the batch-to-batch reproducibility of commercial surface-functionalized nanomaterials. Their physicochemical properties, such as size, surface charge and dispersive state were routinely analyzed to ensure measurements collected were representative of stable colloidal nanoparticles. Through the study of multiple quantitative methods, some which are suitable for routine measurements (two colorimetric assays) and those which require more sophisticated instrumentation (solid-state NMR and XPS analysis), we aimed to provide an ensemble of characterization techniques with clear comparisons of advantages and limitations.

1.7 References

(1) Toumey, C. Let There Be Nano. *Nat. Nanotechnol.* **2018**, *13* (10), 872–873. https://doi.org/10.1038/s41565-018-0276-y.

(2) Jeevanandam, J.; Barhoum, A.; Chan, Y. S.; Dufresne, A.; Danquah, M. K. Review on Nanoparticles and Nanostructured Materials: History, Sources, Toxicity and Regulations. *Beilstein J. Nanotechnol.* **2018**, *9* (1), 1050–1074. https://doi.org/10.3762/bjnano.9.98.

(3) Stark, W. J.; Stoessel, P. R.; Wohlleben, W.; Hafner, A. Industrial Applications of Nanoparticles. *Chem. Soc. Rev.* **2015**, *44* (16), 5793–5805. https://doi.org/10.1039/c4cs00362d.

(4) Miernicki, M.; Hofmann, T.; Eisenberger, I.; von der Kammer, F.; Praetorius, A. Legal and Practical Challenges in Classifying Nanomaterials According to Regulatory Definitions. *Nat. Nanotechnol.* **2019**, *14* (3), 208–216. https://doi.org/10.1038/s41565-019-0396-z.

(5) Clausen, L. P. W.; Hansen, S. F. The Ten Decrees of Nanomaterials Regulations. *Nat. Nanotechnol.* **2018**, *13* (9), 766–768. https://doi.org/10.1038/s41565-018-0256-2.

(6) Lowry, G. V. Inching Closer to Realistic Exposure Models. *Nat. Nanotechnol.* **2018**, *13* (11), 983–985. https://doi.org/10.1038/s41565-018-0299-4.

(7) Baer, D. R. The Chameleon Effect: Characterization Challenges Due to the Variability of Nanoparticles and Their Surfaces. *Front. Chem.* **2018**, *6* (May), 1–7. https://doi.org/10.3389/fchem.2018.00145.

(8) Baer, D. R.; Gilmore, I. S. Responding to the Growing Issue of Research Reproducibility. *J. Vac. Sci. Technol. A* **2018**, *36* (6), 068502. https://doi.org/10.1116/1.5049141.

(9) Mireles, L. K.; Sacher, E.; Yahia, L.; Laurent, S.; Stanicki, D. A Comparative Physicochemical, Morphological and Magnetic Study of Silane-Functionalized

Superparamagnetic Iron Oxide Nanoparticles Prepared by Alkaline Coprecipitation. *Int. J. Biochem. Cell Biol.* **2016**, *75*, 203–211. https://doi.org/10.1016/j.biocel.2015.12.002.

(10) D'Mello, S. R.; Chen, M.-L.; Lee, S. L.; Cruz, C. N.; Tyner, K. M.; Kapoor, M. The Evolving Landscape of Drug Products Containing Nanomaterials in the United States. *Nat. Nanotechnol.* **2017**, *12* (6), 523–529. https://doi.org/10.1038/nnano.2017.67.

(11) Hua, S.; de Matos, M. B. C.; Metselaar, J. M.; Storm, G. Current Trends and Challenges in the Clinical Translation of Nanoparticulate Nanomedicines: Pathways for Translational Development and Commercialization. *Front. Pharmacol.* **2018**, *9* (JUL), 1–14. https://doi.org/10.3389/fphar.2018.00790.

(12) Mulvaney, P.; Parak, W. J.; Caruso, F.; Weiss, P. S. Standardizing Nanomaterials. *ACS Nano* **2016**, *10* (11), 9763–9764. https://doi.org/10.1021/acsnano.6b07629.

(13) Hennig, A.; Dietrich, P. M.; Hemmann, F.; Thiele, T.; Borcherding, H.; Hoffmann, A.; Schedler, U.; Jäger, C.; Resch-Genger, U.; Unger, W. E. S. En Route to Traceable Reference Standards for Surface Group Quantifications by XPS, NMR and Fluorescence Spectroscopy. *Analyst* **2015**, *140* (6), 1804–1808. https://doi.org/10.1039/c4an02248c.

(14) Caruso, F.; Corrie, S. R.; Thordarson, P.; Kavallaris, M.; Boyd, B. J.; Crampin, E. J.; Gooding, J. J.; Parton, R. G.; Faria, M.; Johnston, A. P. R.; et al. Minimum Information Reporting in Bio–Nano Experimental Literature. *Nat. Nanotechnol.* **2018**, *13* (9), 777–785. https://doi.org/10.1038/s41565-018-0246-4.

(15) Roduner, E. Size Matters: Why Nanomaterials Are Different. *Chem. Soc. Rev.* **2006**, *35* (7), 583–592. https://doi.org/10.1039/b502142c.

(16) Nützenadel, C.; Züttel, A.; Chartouni, D.; Schmid, G.; Schlapbach, L. Critical Size and Surface Effect of the Hydrogen Interaction of Palladium Clusters. *Eur. Phys. J. D* **2000**, *8* (2), 245–250. https://doi.org/10.1007/s100530050033.

(17) Chan, W. C. W.; Udugama, B.; Kadhiresan, P.; Kim, J.; Mubareka, S.; Weiss, P. S.; Parak, W. J. Patients, Here Comes More Nanotechnology. *ACS Nano* **2016**, *10* (9), 8139–8142. https://doi.org/10.1021/acsnano.6b05610.

(18) Nicolas, J.; Mura, S.; Brambilla, D.; MacKiewicz, N.; Couvreur, P. Design, Functionalization Strategies and Biomedical Applications of Targeted Biodegradable/Biocompatible Polymer-Based Nanocarriers for Drug Delivery. *Chem. Soc. Rev.* **2013**, *42* (3), 1147–1235. https://doi.org/10.1039/c2cs35265f.

(19) Chou, L. Y. T.; Ming, K.; Chan, W. C. W. Strategies for the Intracellular Delivery of Nanoparticles. *Chem. Soc. Rev.* **2011**, *40* (1), 233–245. https://doi.org/10.1039/c0cs00003e.

(20) Hotze, E. M.; Phenrat, T.; Lowry, G. V. Nanoparticle Aggregation: Challenges to Understanding Transport and Reactivity in the Environment. *J. Environ. Qual.* **2010**, *39* (6), 1909. https://doi.org/10.2134/jeq2009.0462.

(21) Mudunkotuwa, I. A.; Grassian, V. H. The Devil Is in the Details (or the Surface): Impact of Surface Structure and Surface Energetics on Understanding the Behavior of Nanomaterials in the Environment. *J. Environ. Monit.* **2011**, *13* (5), 1135–1144. https://doi.org/10.1039/c1em00002k.

(22) Nguyen, V. H.; Lee, B. J. Protein Corona: A New Approach for Nanomedicine Design. *Int. J. Nanomedicine* **2017**, *12*, 3137–3151. https://doi.org/10.2147/IJN.S129300.

(23) Thompson, M.; Nel, A. E.; Somasundaran, P.; Mädler, L.; Klaessig, F.; Velegol, D.; Hoek, E. M. V.; Castranova, V.; Xia, T. Understanding Biophysicochemical Interactions at the Nano–Bio Interface. *Nat. Mater.* **2009**, *8* (7), 543–557. https://doi.org/10.1038/nmat2442.

(24) Walczyk, D.; Bombelli, F. B.; Monopoli, M. P.; Lynch, I.; Dawson, K. A. What the Cell “Sees” in Bionanoscience. *J. Am. Chem. Soc.* **2010**, *132* (16), 5761–5768. https://doi.org/10.1021/ja910675v.

(25) Dawson, K. A.; Baldelli Bombelli, F.; Mahon, E.; Salvati, A.; Lynch, I. Designing

the Nanoparticle–Biomolecule Interface for “Targeting and Therapeutic Delivery.” *J. Control. Release* **2012**, *161* (2), 164–174. https://doi.org/10.1016/j.jconrel.2012.04.009.

(26) del Pino, P.; Hartmann, R.; de la Fuente, J. M.; Maffre, P.; Parak, W. J.; Pelaz, B.; Rivera-Fernández, S.; Nienhaus, G. U.; Gallego, M. Surface Functionalization of Nanoparticles with Polyethylene Glycol: Effects on Protein Adsorption and Cellular Uptake. *ACS Nano* **2015**, *9* (7), 6996–7008. https://doi.org/10.1021/acsnano.5b01326.

(27) Biswas, S.; Kumari, P.; Lakhani, P. M.; Ghosh, B. Recent Advances in Polymeric Micelles for Anti-Cancer Drug Delivery. *Eur. J. Pharm. Sci.* **2016**, *83*, 184–202. https://doi.org/10.1016/j.ejps.2015.12.031.

(28) Gao, W.; Hu, C. M. J.; Fang, R. H.; Luk, B. T.; Su, J.; Zhang, L. Surface Functionalization of Gold Nanoparticles with Red Blood Cell Membranes. *Adv. Mater.* **2013**, *25* (26), 3549–3553. https://doi.org/10.1002/adma.201300638.

(29) Karakoti, A. S.; Shukla, R.; Shanker, R.; Singh, S. Surface Functionalization of Quantum Dots for Biological Applications. *Adv. Colloid Interface Sci.* **2015**, *215*, 28–45. https://doi.org/10.1016/j.cis.2014.11.004.

(30) Selinsky, R. S.; Ding, Q.; Faber, M. S.; Wright, J. C.; Jin, S. Quantum Dot Nanoscale Heterostructures for Solar Energy Conversion. *Chem. Soc. Rev.* **2013**, *42* (7), 2963–2985. https://doi.org/10.1039/c2cs35374a.

(31) Zhang, Q.; Uchaker, E.; Candelaria, S. L.; Cao, G. Nanomaterials for Energy Conversion and Storage. *Chem. Soc. Rev.* **2013**, *42* (7), 3127–3171. https://doi.org/10.1039/c3cs00009e.

(32) Niu, Y.; Wang, H. Dielectric Nanomaterials for Power Energy Storage: Surface Modification and Characterization. *ACS Appl. Nano Mater.* **2019**, *2*, 627–642. https://doi.org/10.1021/acsanm.8b01846.

(33) Chang, K. C.; Hsu, C. H.; Peng, C. W.; Huang, Y. Y.; Yeh, J. M.; Wan, H. P.; Hung, W. C. Preparation and Comparative Properties of Membranes Based on

PANI and Three Inorganic Fillers. *Express Polym. Lett.* **2014**, *8* (3), 207–218. https://doi.org/10.3144/expresspolymlett.2014.24.

(34) Ribeiro, T.; Baleizão, C.; Farinha, J. P. S. Functional Films from Silica/Polymer Nanoparticles. *Materials (Basel).* **2014**, *7* (5), 3881–3900. https://doi.org/10.3390/ma7053881.

(35) Yoshinaga, K.; Yang, Y.; Ohno, T.; Motokucho, S.; Kojio, K. Inclusion of Fullerene in Polymer Chains Grafted on Silica Nanoparticles in an Organic Solvent. *Polym. J.* **2014**, *46* (9), 623–627. https://doi.org/10.1038/pj.2014.24.

(36) Guerrero-Martínez, A.; Pérez-Juste, J.; Liz-Marzán, L. M. Recent Progress on Silica Coating of Nanoparticles and Related Nanomaterials. *Adv. Mater.* **2010**. https://doi.org/10.1002/adma.200901263.

(37) Rahman, I. A.; Padavettan, V. Synthesis of Silica Nanoparticles by Sol-Gel: Size-Dependent Properties, Surface Modification, and Applications in Silica-Polymer Nanocomposites—A Review. *J. Nanomater.* **2012**, *2012*, 1–15. https://doi.org/10.1155/2012/132424.

(38) Liberman, A.; Mendez, N.; Trogler, W. C.; Kummel, A. C. Synthesis and Surface Functionalization of Silica Nanoparticles for Nanomedicine. *Surf. Sci. Rep.* **2014**, *69* (2–3), 132–158. https://doi.org/10.1016/j.surfrep.2014.07.001.

(39) Tang, F.; Li, L.; Chen, D. Mesoporous Silica Nanoparticles: Synthesis, Biocompatibility and Drug Delivery. *Adv. Mater.* **2012**, *24* (12), 1504–1534. https://doi.org/10.1002/adma.201104763.

(40) Kumar, P.; Tambe, P.; Paknikar, K. M.; Gajbhiye, V. Mesoporous Silica Nanoparticles as Cutting-Edge Theranostics: Advancement from Merely a Carrier to Tailor-Made Smart Delivery Platform. *J. Control. Release* **2018**, *287* (August), 35–57. https://doi.org/10.1016/j.jconrel.2018.08.024.

(41) Slowing, I. I.; Trewyn, B. G.; Giri, S.; Lin, V. S.-Y. Mesoporous Silica Nanoparticles for Drug Delivery and Biosensing Applications. *Adv. Funct. Mater.* **2007**, *17* (8), 1225–1236. https://doi.org/10.1002/adfm.200601191.

(42) Dong, X.; Wu, P.; Hellmann, G. P.; Wang, C.; Schäfer, C. G. Morphology-Controlled Coating of Colloidal Particles with Silica: Influence of Particle Surface Functionalization. *Langmuir* **2017**, *33* (9), 2235–2247. https://doi.org/10.1021/acs.langmuir.6b04069.

(43) Chen, F.; Hableel, G.; Zhao, E. R.; Jokerst, J. V. Multifunctional Nanomedicine with Silica: Role of Silica in Nanoparticles for Theranostic, Imaging, and Drug Monitoring. *J. Colloid Interface Sci.* **2018**, *521*, 261–279. https://doi.org/10.1016/j.jcis.2018.02.053.

(44) Hsiao, I.; Fritsch-Decker, S.; Leidner, A.; Al-rawi, M.; Hug, V.; Diabaté, S.; Grage, S. L.; Meffert, M.; Stoeger, T.; Gerthsen, D.; et al. Biocompatibility of Amine-Functionalized Silica Nanoparticles : The Role of Surface Coverage. **2019**, *1805400*, 1–11. https://doi.org/10.1002/smll.201805400.

(45) Yu, T.; Malugin, A.; Ghandehari, H. Impact of Silica Nanoparticle Design on Cellular Toxicity and Hemolytic Activity. *ACS Nano* **2011**, *5* (7), 5717–5728. https://doi.org/10.1021/nn2013904.

(46) Lin, Y.-S.; Haynes, C. L. Supporting Information: Impacts of Mesoporous Silica Nanoparticle Size, Pore Ordering,and Pore Integrity on Hemolytic Activity. *J Am Chem Soc* **2010**, *132* (16), 4834–4842.

(47) W. Stober; A. Fink; E. Bohn. Controlled Growth of Monodisperse Silica Spheres in the Micron Size Range. *J. Colloid Interface Sci.* **1968**, *26* (1), 62–69. https://doi.org/10.1016/0021-9797(68)90272-5.

(48) Han, M.-Y.; Wang, D.; Guo, Z.; Han, Y.; Liang, J.; Teng, Z.; Yang, W.; Lu, Z. Unraveling the Growth Mechanism of Silica Particles in the Stöber Method: In Situ Seeded Growth Model. *Langmuir* **2017**, *33* (23), 5879–5890. https://doi.org/10.1021/acs.langmuir.7b01140.

(49) Yamauchi, H.; Ishikawa, T.; Kondo, S. Surface Characterization of Ultramicro Spherical Particles of Silica Prepared by w/o Microemulsion Method. *Colloids and Surfaces* **1989**, *37* (C), 71–80. https://doi.org/10.1016/0166-6622(89)80107-6.

(50) Chang, C.-L.; Fogler, H. S. Controlled Formation of Silica Particles from Tetraethyl Orthosilicate in Nonionic Water-in-Oil Microemulsions. *Langmuir* **2002**, *13* (13), 3295–3307. https://doi.org/10.1021/la961062z.

(51) Wu, S. H.; Lin, H. P. Synthesis of Mesoporous Silica Nanoparticles. *Chem. Soc. Rev.* **2013**, *42* (9), 3862–3875. https://doi.org/10.1039/c3cs35405a.

(52) Grün, M.; Lauer, I.; Unger, K. K. The Synthesis of Micrometer- and Submicrometer-Size Spheres of Ordered Mesoporous Oxide MCM-41. *Adv. Mater.* **1997**, *9* (3), 254–257. https://doi.org/10.1002/adma.19970090317.

(53) Smith, E. A. How to Prevent the Loss of Surface Functionality. *Langmuir* **2008**, *24* (21), 12405–12409. https://doi.org/10.1021/la802234x

(54) Metin, C. O.; Lake, L. W.; Miranda, C. R.; Nguyen, Q. P. Stability of Aqueous Silica Nanoparticle Dispersions. *J. Nanoparticle Res.* **2011**, *13* (2), 839–850. https://doi.org/10.1007/s11051-010-0085-1.

(55) Kuroda, K.; Yamauchi, Y.; Aoyama, Y.; Urata, C.; Yamada, H.; Osada, S. Preparation of Colloidal Mesoporous Silica Nanoparticles with Different Diameters and Their Unique Degradation Behavior in Static Aqueous Systems. *Chem. Mater.* **2012**, *24* (8), 1462–1471. https://doi.org/10.1021/cm3001688.

(56) Van Gool, S.; Locquet, J.-P.; Seo, J. W.; Vervaele, M.; De Roo, B.; Seré, S.; Jacobs, S. Altering the Biodegradation of Mesoporous Silica Nanoparticles by Means of Experimental Parameters and Surface Functionalization. *J. Nanomater.* **2018**, *2018*, 1–9. https://doi.org/10.1155/2018/7390618.

(57) Nishiyama, N.; Koyama, H.; Takemoto, H.; Lee, Y.; Miyata, K.; Kataoka, K.; Itaka, K.; Oba, M.; Gouda, N.; Yamasaki, Y. Enhanced Transfection with Silica-Coated Polyplexes Loading Plasmid DNA. *Biomaterials* **2010**, *31* (17), 4764–4770. https://doi.org/10.1016/j.biomaterials.2010.02.033.

(58) Sagiv, J. Organized Monolayers by Adsorption. 1. Formation and Structure of Oleophobic Mixed Monolayers on Solid Surfaces. *J. Am. Chem. Soc.* **1980**, *102* (1), 92–98. https://doi.org/10.1021/ja00521a016.

(59) Haensch, C.; Hoeppener, S.; Schubert, U. S. Chemical Modification of Self-Assembled Silane Based Monolayers by Surface Reactions. *Chem. Soc. Rev.* **2010**, *39* (6), 2323–2334. https://doi.org/10.1039/b920491a.

(60) Jenkner, P.; Metternich, H. J.; Monkiewicz, J.; Lehnert, R.; Siesler, H. W.; Beari, F.; Brand, M. Organofunctional Alkoxysilanes in Dilute Aqueous Solution: New Accounts on the Dynamic Structural Mutability. *J. Organomet. Chem.* **2002**, *625* (2), 208–216. https://doi.org/10.1016/s0022-328x(01)00650-7.

(61) Zhu, M.; Lerum, M. Z.; Chen, W. How to Prepare Reproducible, Homogeneous, and Hydrolytically Stable Aminosilane-Derived Layers on Silica. *Langmuir* **2012**. https://doi.org/10.1021/la203638g.

(62) Pasternack, R. M.; Amy, S. R.; Chabal, Y. J. Attachment of 3-(Aminopropyl)Triethoxysilane on Silicon Oxide Surfaces: Dependence on Solution Temperature. *Langmuir* **2008**, *24* (22), 12963–12971. https://doi.org/10.1021/la8024827.

(63) Simon, A.; Cohen-Bouhacina, T.; Porté, M. C.; Aimé, J. P.; Baquey, C. Study of Two Grafting Methods for Obtaining a 3-Aminopropyltriethoxysilane Monolayer on Silica Surface. *J. Colloid Interface Sci.* **2002**, *251* (2), 278–283. https://doi.org/10.1006/jcis.2002.8385.

(64) Gomes, M. C.; Cunha, Â.; Trindade, T.; Tomé, J. P. C. The Role of Surface Functionalization of Silica Nanoparticles for Bioimaging. *J. Innov. Opt. Health Sci.* **2016**, *09* (04), 1630005. https://doi.org/10.1142/S1793545816300056.

(65) Belder, G. F.; ten Brinke, G.; Hadziioannou, G. Influence of Anchor Block Size on the Thickness of Adsorbed Block Copolymer Layers. *Langmuir* **2002**, *13* (15), 4102–4105. https://doi.org/10.1021/la960379w.

(66) Zhao, B.; Brittain, W. J. Polymer Brushes: Surface-Immobilized Macromolecules. *Prog. Polym. Sci.* **2000**, *25* (5), 677–710. https://doi.org/10.1016/S0079-6700(00)00012-5.

(67) Okhrimenko, D. V.; Budi, A.; Ceccato, M.; Cárdenas, M.; Johansson, D. B.;

Lybye, D.; Bechgaard, K.; Andersson, M. P.; Stipp, S. L. S. Hydrolytic Stability of 3-Aminopropylsilane Coupling Agent on Silica and Silicate Surfaces at Elevated Temperatures. *ACS Appl. Mater. Interfaces* **2017**, *9* (9), 8344–8353. https://doi.org/10.1021/acsami.6b14343.

(68) Hermanson, G. T. *Bioconjugate Techniques*; 2008. https://doi.org/10.1016/B978-0-12-370501-3.X0001-X.

(69) Fong, B.; Russo, P. S. Organophilic Colloidal Particles with a Synthetic Polypeptide Coating. *Langmuir* **1999**, *15* (13), 4421–4426. https://doi.org/10.1021/la9815648.

(70) Mericle, R. A.; Tan, W.; Batich, C. D.; Dutta, D.; Liesenfeld, B.; Santra, S.; Moudgil, B. M.; Chatel, D. Folate Conjugated Fluorescent Silica Nanoparticles for Labeling Neoplastic Cells. *J. Nanosci. Nanotechnol.* **2005**, *5* (6), 899–904. https://doi.org/10.1166/jnn.2005.146.

(71) Schirra, H.; Kneuer, C.; Lehr, C.-M.; Schmidt, H.; Haltner, E. G.; Schiestel, T.; Sameti, M. Silica Nanoparticles Modified with Aminosilanes as Carriers for Plasmid DNA. *Int. J. Pharm.* **2002**, *196* (2), 257–261. https://doi.org/10.1016/s0378-5173(99)00435-4.

(72) Sapsford, K. E.; Algar, W. R.; Berti, L.; Gemmill, K. B.; Casey, B. J.; Oh, E.; Stewart, M. H.; Medintz, I. L. Functionalizing Nanoparticles with Biological Molecules: Developing Chemistries That Facilitate Nanotechnology. *Chem. Rev.* **2013**, *113* (3), 1904–2074. https://doi.org/10.1021/cr300143v.

(73) Ow, H.; Larson, D. R.; Srivastava, M.; Baird, B. A.; Webb, W. W.; Wiesnert, U. Bright and Stable Core-Shell Fluorescent Silica Nanoparticles. *Nano Lett.* **2005**, *5* (1), 113–117. https://doi.org/10.1021/nl0482478.

(74) Burns, A.; Ow, H.; Wiesner, U. Fluorescent Core-Shell Silica Nanoparticles: Towards “Lab on a Particle” Architectures for Nanobiotechnology. *Chem. Soc. Rev.* **2006**, *35* (11), 1028–1042. https://doi.org/10.1039/b600562b.

(75) García, I.; Liz-Marzán, L. M.; González-Rubio, G.; Henriksen-Lacey, M.;

Mosquera, J. Reducing Protein Corona Formation and Enhancing Colloidal Stability of Gold Nanoparticles by Capping with Silica Monolayers. *Chem. Mater.* **2018**, *31* (1), 57–61. https://doi.org/10.1021/acs.chemmater.8b04647.

(76) Kim, Y.-K.; Ryoo, S.-R.; Ryoo, R.; Min, D.-H.; Kim, M.-H.; Cho, H. S.; Na, H.-K.; Jeon, H.; Lee, K. E. Facile Synthesis of Monodispersed Mesoporous Silica Nanoparticles with Ultralarge Pores and Their Application in Gene Delivery. *ACS Nano* **2011**, *5* (5), 3568–3576. https://doi.org/10.1021/nn103130q.

(77) Qiao, B.; Wang, T. J.; Gao, H.; Jin, Y. High Density Silanization of Nano-Silica Particles Using γ-Aminopropyltriethoxysilane (APTES). *Appl. Surf. Sci.* **2015**. https://doi.org/10.1016/j.apsusc.2015.05.174.

(78) Zhang, F.; Jiang, H.; Wu, X.; Mao, Z.; Li, H. Organoamine-Functionalized Graphene Oxide as a Bifunctional Carbocatalyst with Remarkable Acceleration in a One-Pot Multistep Reaction. *ACS Appl. Mater. Interfaces* **2015**, *7* (3), 1669–1677. https://doi.org/10.1021/am507221a.

(79) Huynh, J.; Palacio, R.; Safizadeh, F.; Lefèvre, G.; Descostes, M.; Eloy, L.; Guignard, N.; Rousseau, J.; Royer, S.; Tertre, E.; et al. Adsorption of Uranium over NH2-Functionalized Ordered Silica in Aqueous Solutions. *ACS Appl. Mater. Interfaces* **2017**, *9* (18), 15672–15684. https://doi.org/10.1021/acsami.6b16158.

(80) Kong, L.; Shen, Z.; Zhang, W.; Xia, M.; Gu, M.; Zhou, X.; Zhang, Y. Conversion of Sucrose into Lactic Acid over Functionalized Sn-Beta Zeolite Catalyst by 3-Aminopropyltrimethoxysilane. *ACS Omega* **2018**, *3* (12), 17430–17438. https://doi.org/10.1021/acsomega.8b02179.

(81) Zhang, F.; Jiang, H.; Li, X.; Wu, X.; Li, H. Amine-Functionalized Go as an Active and Reusable Acid-Base Bifunctional Catalyst for One-Pot Cascade Reactions. *ACS Catal.* **2014**, *4* (2), 394–401. https://doi.org/10.1021/cs400761r.

(82) Nayab, S.; Farrukh, A.; Oluz, Z.; Tuncel, E.; Tariq, S. R.; Rahman, H. U.; Kirchhoff, K.; Duran, H.; Yameen, B. Design and Fabrication of Branched Polyamine Functionalized Mesoporous Silica: An Efficient Absorbent for Water

Remediation. *ACS Appl. Mater. Interfaces* **2014**, *6* (6), 4408–4417. https://doi.org/10.1021/am500123k.

(83) Xie, J.; Lee, S.; Chen, X. Nanoparticle-Based Theranostic Agents. *Adv. Drug Deliv. Rev.* **2010**, *62* (11), 1064–1079. https://doi.org/10.1016/j.addr.2010.07.009.

(84) Ambrogio, M. W.; Thomas, C. R.; Zhao, Y. L.; Zink, J. I.; Stoddart, J. F. Mechanized Silica Nanoparticles: A New Frontier in Theranostic Nanomedicine. *Acc. Chem. Res.* **2011**, *44* (10), 903–913. https://doi.org/10.1021/ar200018x.

(85) Lee, J. E.; Lee, N.; Kim, T.; Kim, J.; Hyeon, T. Multifunctional Mesoporous Silica Nanocomposite Nanoparticles for Theranostic Applications. *Acc. Chem. Res.* **2011**, *44* (10), 893–902. https://doi.org/10.1021/ar2000259.

(86) Bagheri, E.; Ansari, L.; Abnous, K.; Taghdisi, S. M.; Charbgoo, F.; Ramezani, M.; Alibolandi, M. Silica Based Hybrid Materials for Drug Delivery and Bioimaging. *J. Control. Release* **2018**, *277* (January), 57–76. https://doi.org/10.1016/j.jconrel.2018.03.014.

(87) Song, D. P.; Shahin, S.; Xie, W.; Mehravar, S.; Liu, X.; Li, C.; Norwood, R. A.; Lee, J. H.; Watkins, J. J. Directed Assembly of Quantum Dots Using Brush Block Copolymers for Well-Ordered Nonlinear Optical Nanocomposites. *Macromolecules* **2016**, *49* (14), 5068–5075. https://doi.org/10.1021/acs.macromol.6b00926.

(88) Vivero-Escoto, J. L.; Slowing, I. I.; Wu, C. W.; Lin, V. S. Y. Photoinduced Intracellular Controlled Release Drug Delivery in Human Cells by Gold-Capped Mesoporous Silica Nanosphere. *J. Am. Chem. Soc.* **2009**, *131* (10), 3462–3463. https://doi.org/10.1021/ja900025f.

(89) Mal, N. K.; Fujiwara, M.; Tanaka, Y. Photocontrolled Reversible Release of Guest Molecules from Coumarin-Modified Mesoporous Silica. *Nature* **2003**, *421* (6921), 350–353. https://doi.org/10.1038/nature01362.

(90) Lu, H.-T. Synthesis and Characterization of Amino-Functionalized Silica Nanoparticles. *Colloid J.* **2013**, *75* (3), 311–318.

https://doi.org/10.1134/S1061933X13030125.

(91) Jung, H. S.; Moon, D. S.; Lee, J. K. Quantitative Analysis and Efficient Surface Modification of Silica Nanoparticles. *J. Nanomater.* **2012**, *2012*. https://doi.org/10.1155/2012/593471.

(92) Hristov, D. R.; Rocks, L.; Kelly, P. M.; Thomas, S. S.; Pitek, A. S.; Verderio, P.; Mahon, E.; Dawson, K. A. Tuning of Nanoparticle Biological Functionality through Controlled Surface Chemistry and Characterisation at the Bioconjugated Nanoparticle Surface. *Sci. Rep.* **2015**, *5* (August), 17040. https://doi.org/10.1038/srep17040.

(93) Heydari-Gorji, A.; Belmabkhout, Y.; Sayari, A. Polyethylenimine-Impregnated Mesoporous Silica: Effect of Amine Loading and Surface Alkyl Chains on CO2 Adsorption. *Langmuir* **2011**, *27* (20), 12411–12416. https://doi.org/10.1021/la202972t.

(94) Morales, V.; Idso, M. N.; Balabasquer, M.; Chmelka, B.; García-Muñoz, R. A. Correlating Surface-Functionalization of Mesoporous Silica with Adsorption and Release of Pharmaceutical Guest Species. *J. Phys. Chem. C* **2016**, *120* (30), 16887–16898. https://doi.org/10.1021/acs.jpcc.6b06238.

(95) Hristov, D. R.; Rocks, L.; Kelly, P. M.; Thomas, S. S.; Pitek, A. S.; Verderio, P.; Mahon, E.; Dawson, K. A. Tuning of Nanoparticle Biological Functionality through Controlled Surface Chemistry and Characterisation at the Bioconjugated Nanoparticle Surface. *Sci. Rep.* **2015**, *5* (August), 17040. https://doi.org/10.1038/srep17040.

(96) Lynch, I.; Cedervall, T.; Lundqvist, M.; Cabaleiro-Lago, C.; Linse, S.; Dawson, K. A. The Nanoparticle-Protein Complex as a Biological Entity; a Complex Fluids and Surface Science Challenge for the 21st Century. *Adv. Colloid Interface Sci.* **2007**, *134–135*, 167–174. https://doi.org/10.1016/j.cis.2007.04.021.

(97) Hennig, A.; Borcherding, H.; Jaeger, C.; Hatami, S.; Würth, C.; Hoffmann, A.; Hoffmann, K.; Thiele, T.; Schedler, U.; Resch-Genger, U. Scope and Limitations

of Surface Functional Group Quantification Methods: Exploratory Study with Poly(Acrylic Acid)-Grafted Micro- and Nanoparticles. *J. Am. Chem. Soc.* **2012**, *134* (19), 8268–8276. https://doi.org/10.1021/ja302649g.

(98) Hennig, A.; Dietrich, P. M.; Hemmann, F.; Thiele, T.; Borcherding, H.; Hoffmann, A.; Schedler, U.; Jäger, C.; Resch-Genger, U.; Unger, W. E. S. En Route to Traceable Reference Standards for Surface Group Quantifications by XPS, NMR and Fluorescence Spectroscopy. *Analyst* **2015**, *140* (6), 1804–1808. https://doi.org/10.1039/c4an02248c.

(99) Acres, R. G.; Ellis, A. V.; Alvino, J.; Lenahan, C. E.; Khodakov, D. A.; Metha, G. F.; Andersson, G. G. Molecular Structure of 3-Aminopropyltriethoxysilane Layers Formed on Silanol-Terminated Silicon Surfaces. *J. Phys. Chem. C* **2012**, *116* (10), 6289–6297. https://doi.org/10.1021/jp212056s.

(100) Zhang, Y.; Chen, Y. Fmoc-Cl Fluorescent Determination for Amino Groups of Nanomaterial Science. *IET Nanobiotechnol* **2012**, *6* (2), 76–80. https://doi.org/10.1049/iet-nbt.2011.0027.

(101) Jarre, G.; Heyer, S.; Memmel, E.; Meinhardt, T.; Krueger, A. Synthesis of Nanodiamond Derivatives Carrying Amino Functions and Quantification by a Modified Kaiser Test. *Beilstein J. Org. Chem.* **2014**, *10*, 2729–2737. https://doi.org/10.3762/bjoc.10.288.

(102) Maria Chong, A. S.; Zhao, X. S. Functionalization of SBA-15 with APTES and Characterization of Functionalized Materials. *J. Phys. Chem. B* **2003**, *107* (46), 12650–12657. https://doi.org/10.1021/jp035877+.

(103) Crucho, C. I. C.; Baleizão, C.; Farinha, J. P. S. Functional Group Coverage and Conversion Quantification in Nanostructured Silica by 1H NMR. *Anal. Chem.* **2017**, *89* (1), 681–687. https://doi.org/10.1021/acs.analchem.6b03117.

(104) Kunc, F.; Balhara, V.; Brinkmann, A.; Sun, Y.; Leek, D. M.; Johnston, L. J. Quantification and Stability Determination of Surface Amine Groups on Silica Nanoparticles Using Solution NMR. *Anal. Chem.* **2018**.

https://doi.org/10.1021/acs.analchem.8b02803.

(105) Burleigh, M. C.; Markowitz, M. A.; Spector, M. S.; Gaber, B. P. Direct Synthesis of Periodic Mesoporous Organosilicas: Functional Incorporation by Co-Condensation with Organosilanes. *J. Phys. Chem. B* **2001**, *105* (41), 9935–9942. https://doi.org/10.1021/jp011814k.

(106) Jung, H.-S.; Moon, D.-S.; Lee, J.-K. Quantitative Analysis and Efficient Surface Modification of Silica Nanoparticles. *J. Nanomater.* **2012**, *2012*, 1–8. https://doi.org/10.1155/2012/593471.

(107) Hennig, A.; Hoffmann, A.; Borcherding, H.; Thiele, T.; Schedler, U.; Resch-Genger, U. Simple Colorimetric Method for Quantification of Surface Carboxy Groups on Polymer Particles. *Anal. Chem.* **2011**, *83* (12), 4970–4974. https://doi.org/10.1021/ac2007619.

(108) Kralj, S.; Drofenik, M.; Makovec, D. Controlled Surface Functionalization of Silica-Coated Magnetic Nanoparticles with Terminal Amino and Carboxyl Groups. *J. Nanoparticle Res.* **2011**, *13* (7), 2829–2841. https://doi.org/10.1007/s11051-010-0171-4.

(109) Kobayashi, T.; Lafon, O.; Lilly Thankamony, A. S.; Slowing, I. I.; Kandel, K.; Carnevale, D.; Vitzthum, V.; Vezin, H.; Amoureux, J. P.; Bodenhausen, G.; et al. Analysis of Sensitivity Enhancement by Dynamic Nuclear Polarization in Solid-State NMR: A Case Study of Functionalized Mesoporous Materials. *Phys. Chem. Chem. Phys.* **2013**, *15* (15), 5553–5562. https://doi.org/10.1039/c3cp00039g.

(110) Moser, M.; Schneider, R.; Behnke, T.; Schneider, T.; Falkenhagen, J.; Resch-Genger, U. Ellman's and Aldrithiol Assay as Versatile and Complementary Tools for the Quantification of Thiol Groups and Ligands on Nanomaterials. *Anal. Chem.* **2016**, *88* (17), 8624–8631. https://doi.org/10.1021/acs.analchem.6b01798.

(111) Noel, S.; Liberelle, B.; Robitaille, L.; De Crescenzo, G. Quantification of Primary Amine Groups Available for Subsequent Biofunctionalization of Polymer Surfaces. *Bioconjug. Chem.* **2011**, *22* (8), 1690–1699. https://doi.org/10.1021/bc200259c.

(112) Qu, Z.; Xu, H.; Ning, P.; Gu, H. A Facile, One-Step Method for the Determination of Accessible Surface Primary Amino Groups on Solid Carriers. *Surf. Interface Anal.* **2012**, *44* (10), 1309–1313. https://doi.org/10.1002/sia.4912.

(113) Kong, N.; Zhou, J.; Park, J.; Xie, S.; Ramstr??m, O.; Yan, M. Quantitative Fluorine NMR to Determine Carbohydrate Density on Glyconanomaterials Synthesized from Perfluorophenyl Azide-Functionalized Silica Nanoparticles by Click Reaction. *Anal. Chem.* **2015**, *87* (18), 9451–9458. https://doi.org/10.1021/acs.analchem.5b02507.

(114) Fischer, T.; Dietrich, P. M.; Streeck, C.; Ray, S.; Nutsch, A.; Shard, A.; Beckhoff, B.; Unger, W. E. S.; Rurack, K. Quantification of Variable Functional-Group Densities of Mixed-Silane Monolayers on Surfaces via a Dual-Mode Fluorescence and XPS Label. *Anal. Chem.* **2015**, *87* (5), 2685–2692. https://doi.org/10.1021/ac503850f.

(115) Fischer, T.; Dietrich, P. M.; Unger, W. E. S.; Rurack, K. Multimode Surface Functional Group Determination: Combining Steady-State and Time-Resolved Fluorescence with X-Ray Photoelectron Spectroscopy and Absorption Measurements for Absolute Quantification. *Anal. Chem.* **2016**, *88* (2), 1210–1217. https://doi.org/10.1021/acs.analchem.5b03468.

(116) Moser, M.; Nirmalananthan, N.; Behnke, T.; Geißler, D.; Resch-Genger, U. Multimodal Cleavable Reporters versus Conventional Labels for Optical Quantification of Accessible Amino and Carboxy Groups on Nano-and Microparticles. *Anal. Chem.* **2018**, *90* (9), 5887–5895. https://doi.org/10.1021/acs.analchem.8b00666.

(117) Shiota, S.; Yamamoto, S.; Shimomura, A.; Ojida, A.; Nishino, T.; Maruyama, T. Quantification of Amino Groups on Solid Surfaces Using Cleavable Fluorescent Compounds. *Langmuir* **2015**, *31* (32), 8824–8829. https://doi.org/10.1021/acs.langmuir.5b02548.

(118) Tougaard, S. Accuracy of the Non-Destructive Surface Nanostructure Quantification Technique Based on Analysis of the XPS or AES Peak Shape.

Surf. Interface Anal. **1998**, *26* (4), 249–269. https://doi.org/10.1002/(SICI)1096-9918(199804)26:4<249::AID-SIA368>3.0.CO;2-A.

(119) Wang, Y. C.; Engelhard, M. H.; Baer, D. R.; Castner, D. G. Quantifying the Impact of Nanoparticle Coatings and Nonuniformities on XPS Analysis: Gold/Silver Core-Shell Nanoparticles. *Anal. Chem.* **2016**, *88* (7), 3917–3925. https://doi.org/10.1021/acs.analchem.6b00100.

(120) Graf, N.; Lippitz, A.; Gross, T.; Pippig, F.; Holländer, A.; Unger, W. E. S. Determination of Accessible Amino Groups on Surfaces by Chemical Derivatization with 3,5-Bis(Trifluoromethyl)Phenyl Isothiocyanate and XPS/NEXAFS Analysis. *Anal. Bioanal. Chem.* **2010**, *396* (2), 725–738. https://doi.org/10.1007/s00216-009-3233-7.

Chapter 2: Colorimetric Assays

This chapter primarily appears in the first publication. Preliminary experiments were performed by Vinod Balhara on the ninhydrin assay. Optimization of ninhydrin the adaptation of the second assay was performed by myself which include the results which appear in the publication.

1. Sun, Y.; Kunc, F.; Balhara, V.; Coleman, B.; Kodra, O.; Raza, M.; Chen, M.; Brinkmann, A.; Lopinski, G.; Johnston, L. Quantification of Amine Functional Groups on Silica Nanoparticles: A Multi-Method Approach. *Nanoscale Adv.* **2019**. https://doi.org/10.1039/C9NA00016J.

This second publication is focused on the quantitative ^{1}H NMR method. My contribution was in the ninhydrin assay data which appears in the publication.

2. Kunc, F.; Balhara, V.; Brinkmann, A.; Sun, Y.; Leek, D. M.; Johnston, L. J. Quantification and Stability Determination of Surface Amine Groups on Silica Nanoparticles Using Solution NMR. *Anal. Chem.* **2018**. https://doi.org/10.1021/acs.analchem.8b02803.

2.1 Background

Owing to their simplicity, sensitivity and convenience, UV-visible spectroscopic assays are widely used for routine surface group detection and quantification. UV-visible spectrophotometers can be found in nearly all laboratories, as benchtop instruments and plate readers are made both increasingly affordable and portable. Many popular colorimetric assays were originally designed to detect or quantify chemical species in solution. From there, many were adapted for the analysis of functionalized thin films and supports, such as those prepared by self-assembly of silanes. Colorimetric assays remain one of the most popular choices for the characterization and quantification of surface functionality on nanomaterials.

Careful selection of the appropriate assay for one's nanomaterial is important to ensure measurements are reproducible, reliable and quantitative. Most colorimetric assays operate by one of three general approaches. The first is by covalent attachment of a probe or dye. Upon binding, purification is required to remove excess reagent and loosely bound probes to the substrate or in our case, nanomaterial. Afterwards, dye is either measured directly on the nanoparticle, or is released and measured in solution. Nanoparticles can scatter, absorb and reflect light which can be a significant hindrance to assays of this type. Photo-cleavable reporters can address this issue, such as those proposed by the groups of Maruyama[1] and Ute-Resch Genger[2]. Their structures typically include disulfide bonds which can be photocleaved to release a dye into solution. They are still in early development as there are cases of inconsistency and limited coupling yield. Overall, assays of this type are limited by steric crowding between

covalently attached dyes or reporters, which can prevent complete coupling and detection of surface groups.

The second approach is through electrostatic adsorption of the dye. Purification is again required to remove excess dye, and as before, the dye can be measured along with the nanoparticle, or after release. Popular examples include Orange II and Coomassie Brillant Bleu (CBB).[3,4] These assays often require multiple stages of washing (to adsorb sufficient dye to the surface), purification (to remove excess, lightly bound dye) and removal (allowing for measurement in the UV-visible instrument). Furthermore, acidic/basic conditions may be necessary for optimal performance, which may not be compatible for certain nanomaterials.[3] One advantage of adsorption-based assays is that they avoid the issue of measuring bound dye with the nanoparticles, as the dye is released into solution in the final step. However, steric crowding remains an issue, especially in cases of bulky compounds such as CBB.

The third and final approach involves reaction of the functional group with a probe which results in the generation and release of a dye into solution. This method has the added benefit of limiting particle scattering effects, and further, can address the issue of steric crowding since the probes are not required to be concurrently bound.

In this project, two assays were used for quantification of surface amine groups. The first, ninhydrin, works through the third approach: surface reaction to generate dye species directly into solution. The second, 4-nitrobenzaldehyde, requires covalent attachment of the dye (first approach), but can be hydrolyzed and removed to allow for dye measurement in solution.

The ninhydrin assay has been a staple of biochemistry laboratories for decades. It is used for the detection and measurement of amino acids and primary amine groups in solution and on solid-supports for peptide synthesis[5,6]. The reagent, ninhydrin (Indane-1,2,3-trione) was first discovered in 1911 by Siegfried Ruhemann, who observed its colored reaction with amino acids and peptides.[7] Regarded as one of the most important findings in biochemistry, the reaction has found wide applicability in biomedical, clinical, agricultural, forensic, microbiological and plant studies.[8] Recently, it has also been adapted for primary amine group quantification on apatite ceramics[3], chitosans[9,10], nanodiamond[11], and on amine functionalized silica.[12–15]

The reagent ninhydrin is in equilibrium between its geminal-diol (ninhydrin hydrate) and its carbonyl form (Indan-1,2,3-trione), shown in **Fig. 2-1A**. Nucleophilic addition of the primary amine group at the carbonyl center is known to be the rate determining step and is influenced by polar and steric parameters.[16] What follows is a series of proton transfers which results in condensation of water, decarboxylation and cleavage of the amine group to yield an aldehyde (noted as deamination in the reaction scheme, Fig. 2-1B), forming the colored product. Aptly named Ruhemann's Purple, it is the dimer of two ninhydrin-hydrates linked via imine bond. The assay does not require discrete steps for binding, purification, and removal of dye. Through the course of the reaction, the product is continuously generated, as primary amine groups react, and are transformed to free aldehyde groups. This should reduce the impact of steric crowding of multiple dye molecules occupying neighboring sites, which could obstruct unreacted amines and result in lower than expected quantification.[3,14]

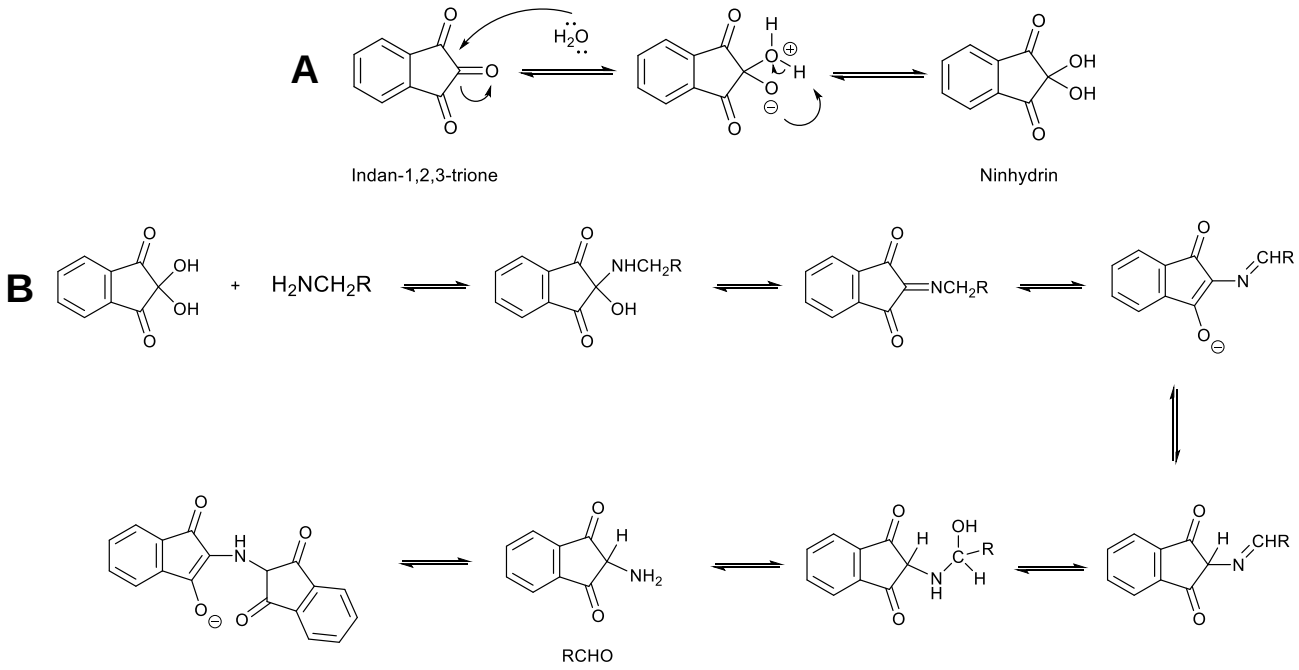

Figure 2-1: The ninhydrin reaction mechanism between alpha amino acids and primary amines.[16] A shows the equilibrium state of ninhydrin and it -trione form, while B shows the widely accepted mechanism that follows. Mechanism is adapted from reference.[16]

A wide range of conditions can be found in the literature for the ninhydrin assay. In fact, several modifications have been made to the original procedure for analysis of amino acids to improve reproducibility, stability of the reagents, and stability of the colored product.[17–20] This has continued to be the case for ninhydrin's use for the study of functional groups on various supports and materials. For quantification of amine groups on silica nanoparticles there are differences in reaction time, solvent, temperature, vessel, and amine standard used (see **Table 2-1**). Therefore, we concluded that careful evaluation and testing of conditions was necessary to ensure the assay performed under optimal conditions for our materials.

Table 2-1. Summary of reaction conditions used in the literature for the ninhydrin assay on aminated silica nanoparticles.

	Reaction Vessel	Solvent	Temperature (°C)	Reaction Time (min.)	Amine Standard
Dawson (2015)	Capped microcentrifuge tubes	Ethanol	60	40-45	Propylamine, Octylamine
Poli (2014)	Test tubes closed with bung and parafilm	Ethanol	100	90	Hexylamine
Sotu-Cantu (2012)	Capped vial	Ethanol	65	30	Hexylamine
Hsu-Tung Lu (2012)	-	Aq. Ethanol (Buffer)	100	15	APTMS

In comparison to ninhydrin, the 4-nitrobenzaldehyde (4-NBA) assay has been used relatively less frequently or the quantification of surface groups on nanomaterials. Its straightforward mechanism involves Schiff base condensation of the aldehyde with the primary amine group to form an imine. Upon covalent attachment of 4-NBA, excess and loosely bound dye is removed during purification, typically with anhydrous organic solvent. It is important to use dry solvent during purification, as introducing water hydrolyzes the imine, which is in fact the final step of the assay. Release of dye with an aqueous solvent mixture allows for its measurement without interference from particle scattering effects.

The assay was first established by Moon et. al in 1996, who demonstrated its quantitative performance on various functional amino-silanes on fused silica and oxidized silicon wafer.[21] 10 years later, the assay was adapted with a fluorinated benzaldehyde analog in a multi-method comparison utilizing FT-IR, UV-Visible and X-ray photoelectron spectroscopy. In that exemplary study, Kim et. al quantitatively

determined the surface density of primary amine groups on plasma-polymerized ethylenediamine films on platinum with 4-NBA assay. Afterwards, the researchers attempted to correlate the results with FT-IR peak intensity in a qualitative manner, and later the XPS results in a quantitative manner. Citing a good linear correlation ($R^2=0.97$) with the XPS and UV-Visible results, the researchers stressed the importance of multiple chemical derivatization approaches for effective surface group quantification. More recent examples of the 4-NBA's use on silica-magnetite nanoparticles[22,23] and mesoporous silica[24] reinforced the assay as promising for further study.

For the effective application of these two colorimetric assays for the quantification of amine groups on nanomaterials, it was necessary that the results are compared with other techniques to verify coupling yields and performance. Examples in the literature detail the difficulty and challenges of applying ninhydrin in a quantitative manner for different materials.[10–12] Similarly, 4-nitrobenzaldehyde was shown to give variable results in positive and negative controls which was attributed to non-specific binding that could not be addressed.[25] For ninhydrin, potential causes for non-quantitative output can be broad and substrate specific. It is well documented that side reactions, slow formation, and instability of the colored product lead to non-ideal behavior of the assay.[16] Herein, we applied the two colorimetric assays in conjunction for quantification of amine groups on silica nanoparticles, and compare them in a detail.

2.2 Experimental

2.2.1 Materials and Instruments

Silica nanoparticles were purchased from Nanocomposix USA as ethanol suspensions (≈ 10 mg mL^{-1}) or dry powdered form. Sizes ranged from 20 – 120 nm across multiple commercial batches, which were confirmed by TEM (and DLS for samples in suspensions) performed and provided by the supplier. Commercial batches which were used in published results were numbered B1, B2 and B3 while B0 represents batches used for internal testing and experimentation. Particles were prepared by the Stöber process and functionalized with 3-aminopropyl.

Gravimetric determinations of mass fraction of silica in suspensions was done by drying at 125 ^{o}C to constant mass. Suspensions of NPs were prepared by preparing 10 mg mL^{-1} ethanol or methanol suspensions, and sonicating for 20-25 min. Ninhydrin reagent (Kaiser kit) was purchased from Anaspec (USA). 4-Nitrobenzaldehyde (4-NBA) was purchased from Sigma Aldrich (Canada). Deionized water (18.2 MΩ cm, MilliQ) was used to prepare aqueous solutions. Centrifugation was performed at 14 000 rpm with a benchtop microcentrifuge.

UV-visible spectrophotometry was performed with a Cary 5000, and zeta-potential and Z-average (hydrodynamic diameter) measurements were collected with a Malvern Zetasizer Nano DLS instrument.

2.2.2 Ninhydrin Assay

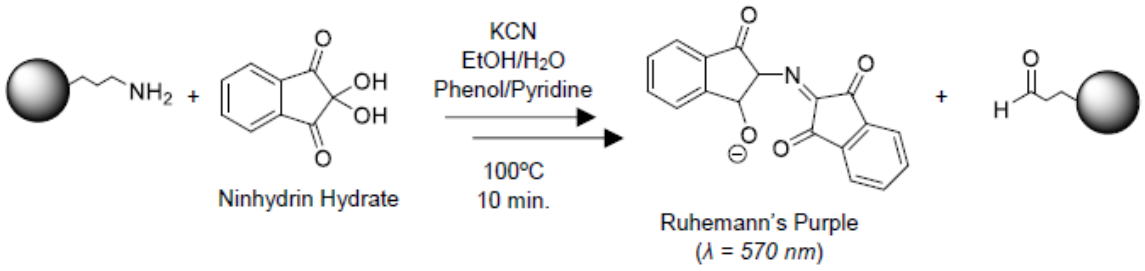

Beginning with a stable suspension of silica nanoparticles at a concentration of 10 (mg/mL), 500 µL of the suspension is pipetted into a 1 mL microcentrifuge tube, and pelleted by centrifugation (14K RPM, 20 minutes). 200 µL of the supernatant is removed by pipette and replaced with 200 µL of Milli-Q H_2O. The silica particles are re-suspended by bath sonication (>5 minutes) until there is a visibly clear dispersion and no remaining aggregates. DLS measurements were performed in some cases to monitor the aggregation state of particles and any effects of centrifugation.

The assay was performed in glass test tubes (approximately 7 mL volume), with the 500 µL of the prepared silica nanoparticle suspension added first; 100 µL KCN and 75 µL of phenol solution were added afterwards (Kaiser Kit, Anaspec). The test tubes were vortexed and then 75 µL of ninhydrin reagent was added last. The tube was stoppered with a glass marble and placed in a preheated water bath with a heat block, incubated for 10 minutes at 97 ^{o}C (boiling). The test tubes were removed and cooled in ice water, and then poured into 5 mL volumetric flasks. The tube was rinsed with 60% EtOH and added to the volumetric flask to reach a final volume of 5 mL. A 200 µL aliquot of the suspension was transferred to a microcentrifuge tube, diluted to a final volume of 1 mL in 60% EtOH and centrifuged for 20 minutes. The concentration of dye

was then quantified by removing an aliquot of the supernatant and measuring absorbance at 570 nm in a 1 cm path length cell. Additional dilutions were performed (typically between 2X to 20X) depending on the concentration of the dye and the resulting optical density. Care was taken to ensure samples were within safe levels for the linearity of the spectrometer (~0.2 to ~0.8).

For calibrations, a minimum of 5 concentrations of octylamine were prepared by serial dilution and was measured by the same protocol as described above.

2.2.3 4-NBA Assay

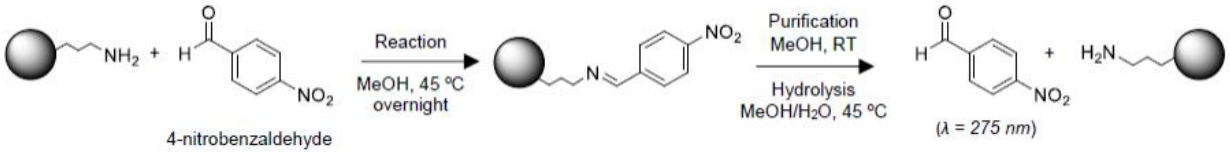

A 500 µL aliquot of silica NP dispersion in ethanol was pipetted into a microcentrifuge tube and centrifuged for 20 min. The supernatant was removed, and the NPs were re-dispersed by bath sonication (for at least 5 min) in 1 mL methanol containing an excess of 4-nitrobenzaldehyde (~ 100 fold, based on the estimated amine content corresponding to full monolayer coverage) and reacted by heating overnight at 45 ^{o}C at 1100 rpm in a Ther-Mix heated mixer (Vitl Life Science Solutions).

To remove the unreacted and excess reagent, the particles were purified the next day by first centrifugation for 20 min, after which the supernatant and reagent was discarded, and the particles were re-dispersed with fresh methanol. The centrifuge/re-dispersal steps were repeated a total of 4 times.

The NPs were isolated by centrifugation/removal of the supernatant, re-dispersed in hydrolysis solution, (1:1 Methanol/H_2O) and incubated at 45 ^oC overnight. Two additional rounds of hydrolysis were performed for 1 h each. The three hydrolytic washes were saved and diluted for measurement of optical density at 275 nm. In most cases, dilutions of 5-20X were required to stay within the working range of the spectrophotometer.

Monitoring of individual hydrolysis solutions indicated that 4-NBA was removed quantitatively with three hydrolysis steps. Calibration curves were prepared using 4-NBA in hydrolysis solution.

2.3 Results and Discussion

2.3.1 Optimization of Ninhydrin's Reaction Conditions with Primary Amine Standards

To evaluate the ninhydrin assay's performance, a procedure was adapted from the literature, intended for use with a widely available ninhydrin 'kit', called the Kaiser kit. The inclusion of reducing agents and solvents has been shown to improve the reproducibility, reaction time and stability of reagents.[5,26,27]

Initially, experiments were performed with the use of primary amine standards to monitor the yield of the colored product. For each standard, an appropriate amount was prepared in solvent, and reacted with the assay kit, with the colored product analyzed by the UV-Vis spectrophotometer. A plot of expected concentration (by gravimetry from prepared solutions) against "experimental concentration" ($\frac{Absorbance \times Dilution\ Factor}{Molar\ Extinciton\ Coefficient}$)

expresses the yield and performance of the assay through the slope of the linear regression, where 1.00 is quantitative output.[1] This approach differs from typical calibration plots, where the colored product is prepared in series, and a plot of concentration and absorbance provides the molar extinction coefficient. Several examples from the literature describe this method of monitoring the output of the assay. This was particularly relevant in the early stages of ninhydrin's development, as certain amino acids were known to give less than expected color yield. Tables of amino acids with their expected output can be found, which suggests the expected output of the assay should be taken into consideration when ninhydrin is used as a quantitative method.

The first primary amine we selected for testing was APTES (3-aminopropyl)triethoxysilane, since it is the coupling reagent that is used for surface amination on our commercial silica. A series of concentrations that reflected expected loadings of aminated silica nanoparticles as provided by the commercial supplier (Nanocomposix) were used for the tests. The resulting plots, example shown in **Fig. 2-2**, indicated less than quantitative output for the assay when APTES was used. Incidentally, it was also found that yield of the colored product was highly dependent on the reaction solvent. While the assay originally was performed in anhydrous ethanol, introducing variable amounts of water in the reaction solvent mixture had a significant effect on the final yield of the dye. This is exemplified in the calibration plot below, where APTES in anhydrous ethanol (♦) has an output of 48.7% according to the linear regression analysis, while APTES in 60% ethanol/H_2O (■) mixture has an output of

[1] *Molar extinction coefficient* ($\varepsilon = 22\,000\ \mathrm{L} \cdot \mathrm{mol} - 1 \cdot \mathrm{cm} - 1$). [8, 31]

83.9%. To the best of our knowledge, this “solvent effect” has not been highlighted in examples of ninhydrin’s use to analyze functionalized nanomaterials. There are a few older examples in the literature which touch on the performance of the assay in different solvents, but do not demonstrate effects to this degree.

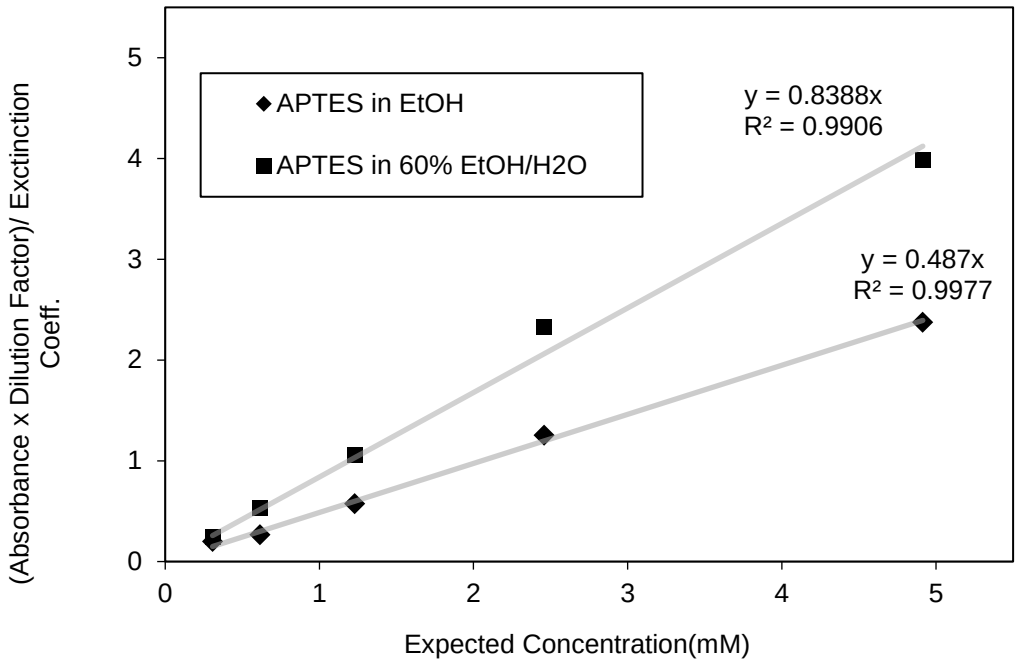

Figure 2-2: Comparison of calibration curves prepared with primary amine standard APTES (3-aminopropyl)triethoxysilane in ethanol and 60% ethanol/H_2O.

During attempts to monitor the repeatability of the assay with the primary amine standard, it was found that APTES was not a suitable choice. Inconsistent yields of the colored product were found day-to-day, shown in the following **Table 2-2**. APTES’ tendency to self-condense and co-polymerize is well documented in the literature.[28] The presence of large oligomers or networked APTES could potentially lead to reduced accessibility and a bulkier nucleophile, reducing reactivity of the assay. However, the deteriorating performance of the standard did not change with purchase and use of new

assay kits, or APTES reagent, which contradicts the reasoning of condensation and polymerization of the standard.

Table 2-2. The ninhydrin assay's colorimetric yield with primary amine standard, APTES. These tests were performed with a single assay kit and reagent bottle.

Date of Exp.	**Ninhydrin product yield with APTES in Ethanol**
June 12	53%
June 20	50%
Aug 15	37%
Aug 17	32%

It is notable that may of the literature examples of ninhydrin with APTES-functionalized nanomaterials (refer to **Table 2-1**) do not use APTES as the standard for calibration and optimization of the assay. This may be indicative of its unreliability as a standard.

Propylamine, while a logical choice for a standard due to its structural similarity to the amines on silica, has a low molecular weight and boiling point (59.112 g/mol, 47.8^{o}C), that would result in vaporization at the high temperatures required in the reaction conditions of our assay.[26] To reduce the likelihood of producing harmful amine vapors, we selected a higher MW amine standard, octylamine, which would be less volatile at elevated temperatures (129.24 g/mol, 176 ^{o}C).

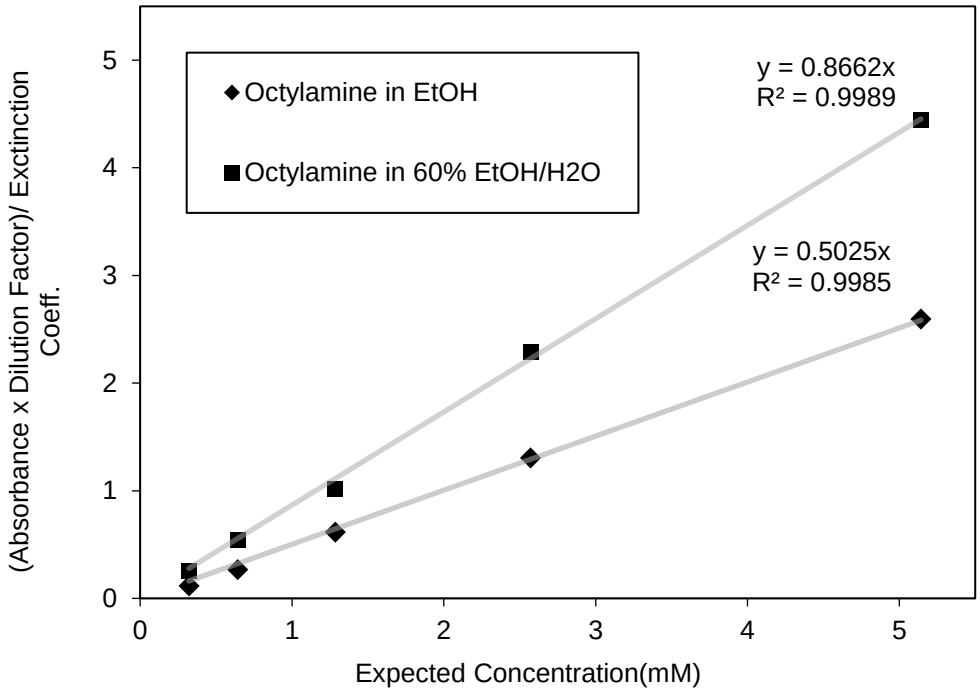

Figure 2-3: Comparison of calibration curves prepared with primary amine octylamine in ethanol and 60% ethanol/H_2O.

Results with octylamine, as shown in the comparison **Fig. 2-3**, show comparable output in anhydrous ethanol conditions as well as 60% ethanol/H_2O solution to early tests with APTES. However, as shown in the results in **Table 2-3**, the output of the assay remained stable throughout a similar time period as the previous study with APTES. Subsequently, octylamine was used as the primary amine standard for measurements on aminated silica nanoparticles. To explore the effects of the solvent on the output with octylamine, the fraction of ethanol to water was systematically varied in the experiment shown in **Fig. 2-4**. The results indicate that the 60% ethanol and water solvent mixture is within the range of optimal yield for the ninhydrin reaction.

Table 2-3. The ninhydrin assay's colorimetric yield with primary amine standard, octylamine.

Date of Exp.	Ninhydrin product yield with Octylamine in Ethanol/H_2O 60%
June 30	87%
July 5	89%
Aug 26	91%
Sept 1	90%
Sept 1	90%

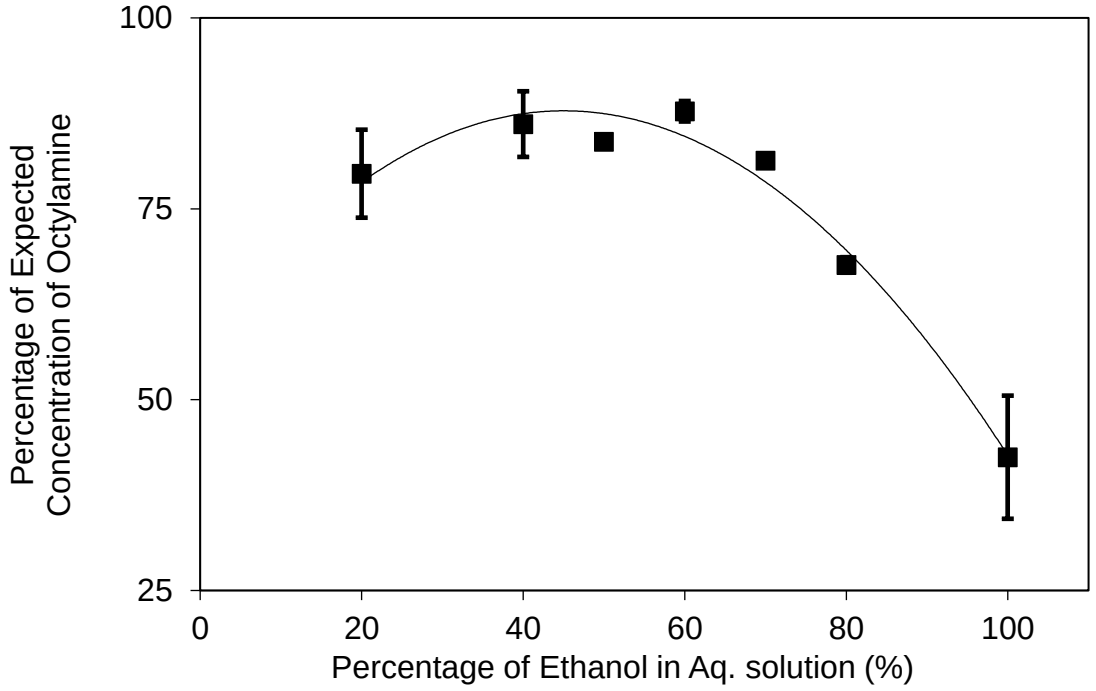

Figure 2-4: Varying percentage of ethanol in aqueous reaction solution and effect on determining concentration of primary amine calibrant octylamine by the ninhydrin assay. n = 2, 2, 1, 6, 2 and 6 for 20, 40, 60, 80 and 100% respectively. A polynomial (2) fit was used as a guide.

Additional tests were performed with the amino acid Leucine, which has been the widely used in literature for the ninhydrin reaction as a standard for quantitative output.[8] **Figure 2-5** shows the plot and quantitative output (0.998), which further validates the conditions used in our protocol, as well as confirms the molar extinction coefficient, as there are some inconsistencies found in the literature.

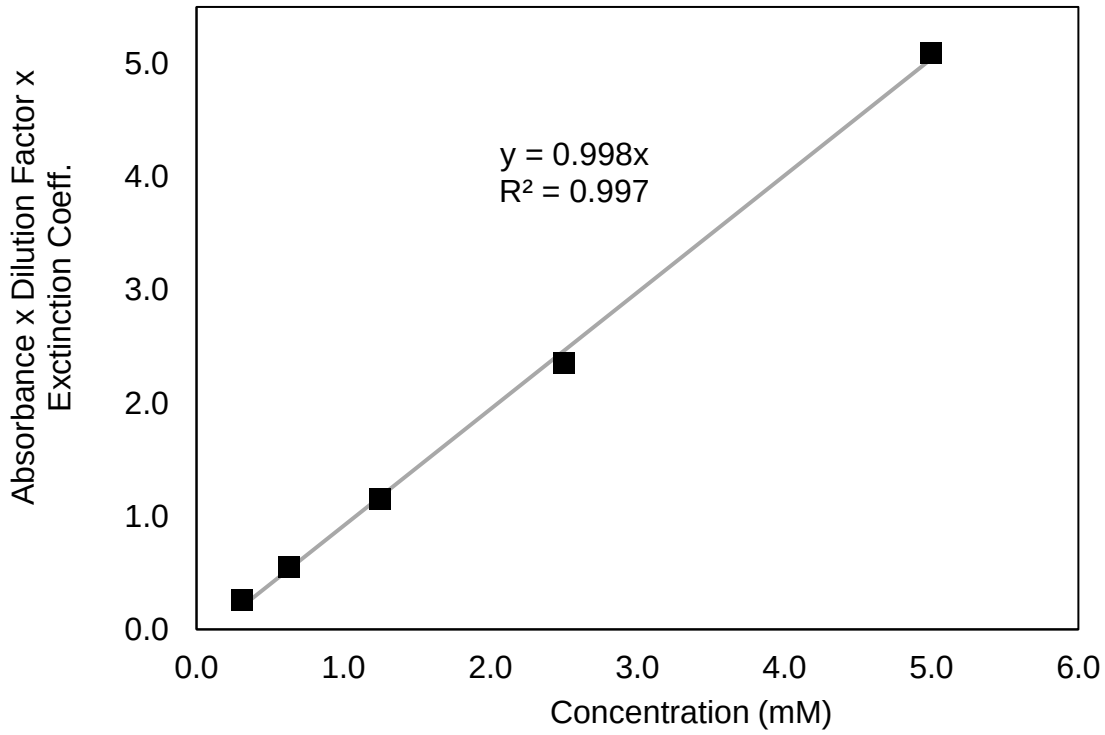

Figure 2-5: Ninhydrin assay tests with amino acid Leucine in Ethanol 60%.

Additional experimentation was performed to evaluate other reaction conditions prior to the study of aminated silica nanoparticles. These tests also served to evaluate conditions such as reaction time and temperature (**Fig. 2-6**).

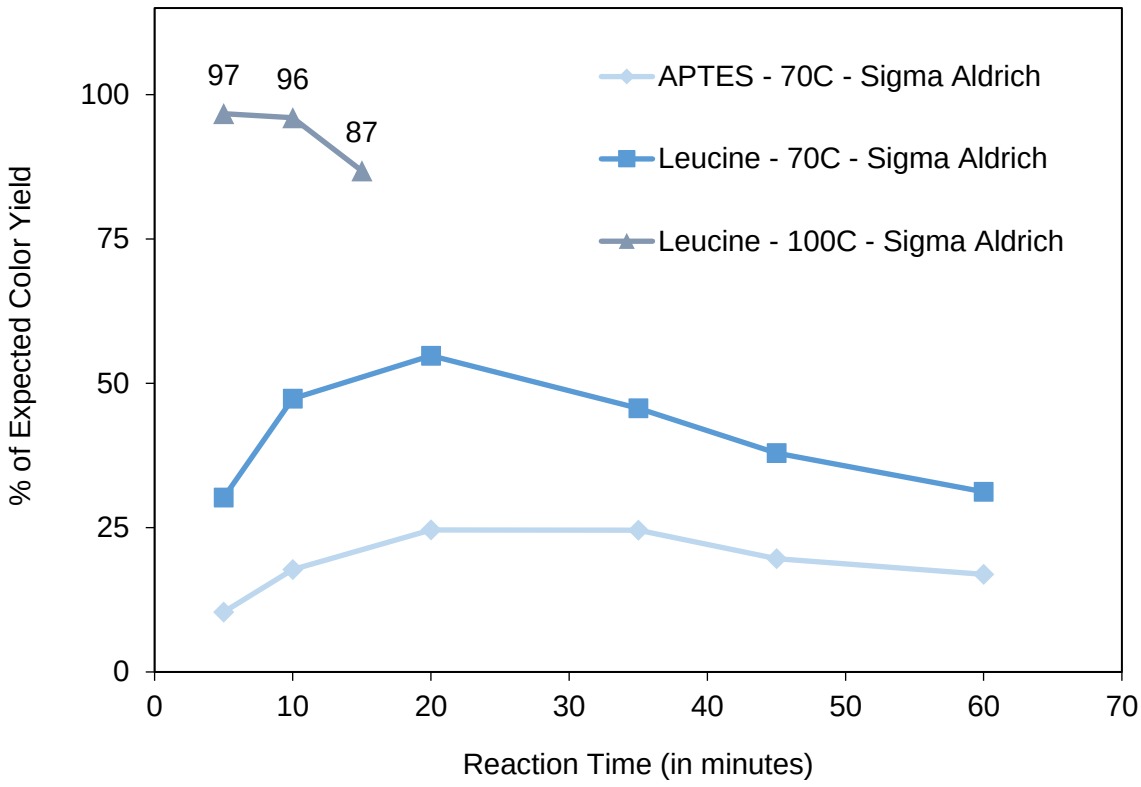

Figure 2-6: Ninhydrin reaction time kinetics experiment, with amine standards APTES and Leucine in ethanol 60%. A Sigma Aldrich assay kit was used for these experiments. Each point represents a single replicate.

The example in **Fig. 2-6** shows attempts to replicate and adapt conditions used by Soto-Cantu (65ºC, 30 minutes, capped vial).[14] A series of aliquots of leucine in ethanol 60% (2.25 µmol) were prepared and assayed by ninhydrin in microcentrifuge tubes in a shaker/stirrer. Lower than expected color yield was found. For comparison, reaction conditions with leucine in a water bath at 100ºC is shown with near quantitative color yield at 10 minutes, although the output begins to fall with 5 additional minutes of reaction.

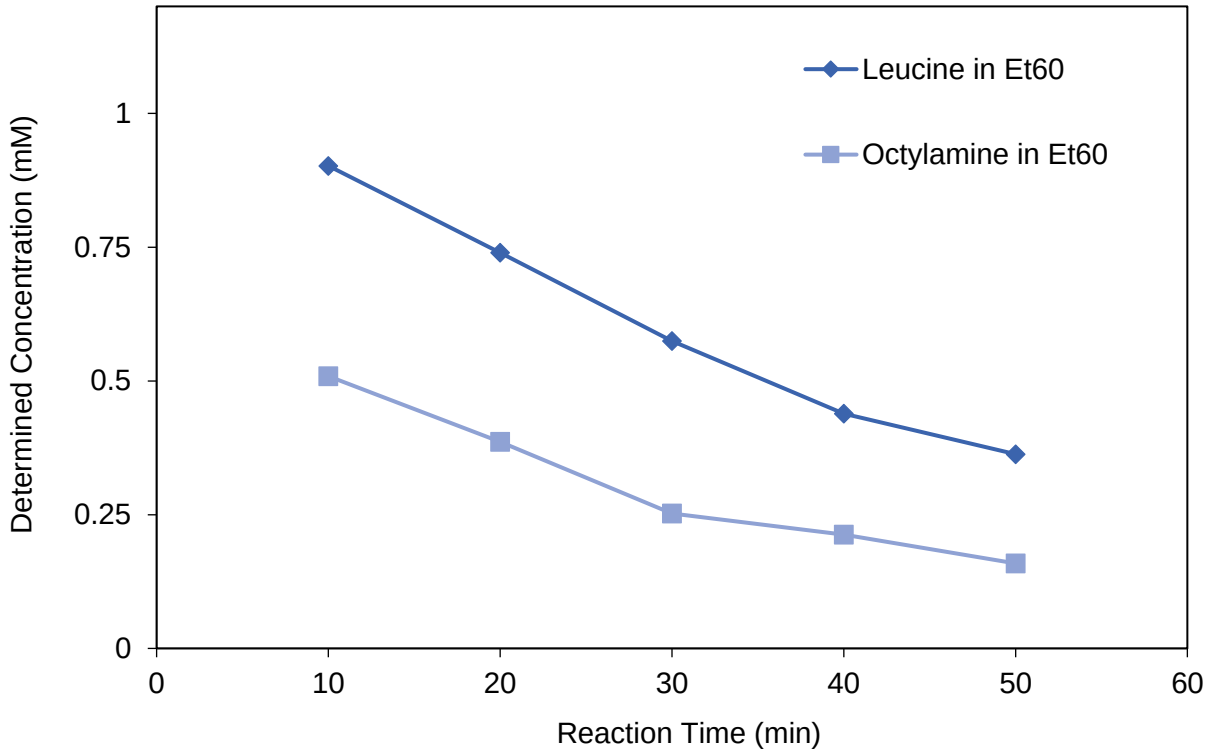

Figure 2-7: Ninhydrin reaction time kinetics experiment, with amine standard octylamine and Leucine in ethanol 60%. 5 mM aliquots were used to monitor output. Each point represents a single replicate.

Repeating the experiment with octylamine in ethanol 60% at 70 ^{o}C did not show improvement, shown in **Fig. 2-7**. Color yields with a 5 mM aliquot of leucine and octylamine showed very poor output and suggest that a higher reaction temperature is required to drive the reaction to completion and expected color yield.

An attempt to replicate Dawson's conditions (60^{o}C, 40-45 min, centrifuge tubes)[29] with a calibration curve of leucine in ethanol 60% also showed significantly lower than expected color yield, shown in **Fig. 2-8**.

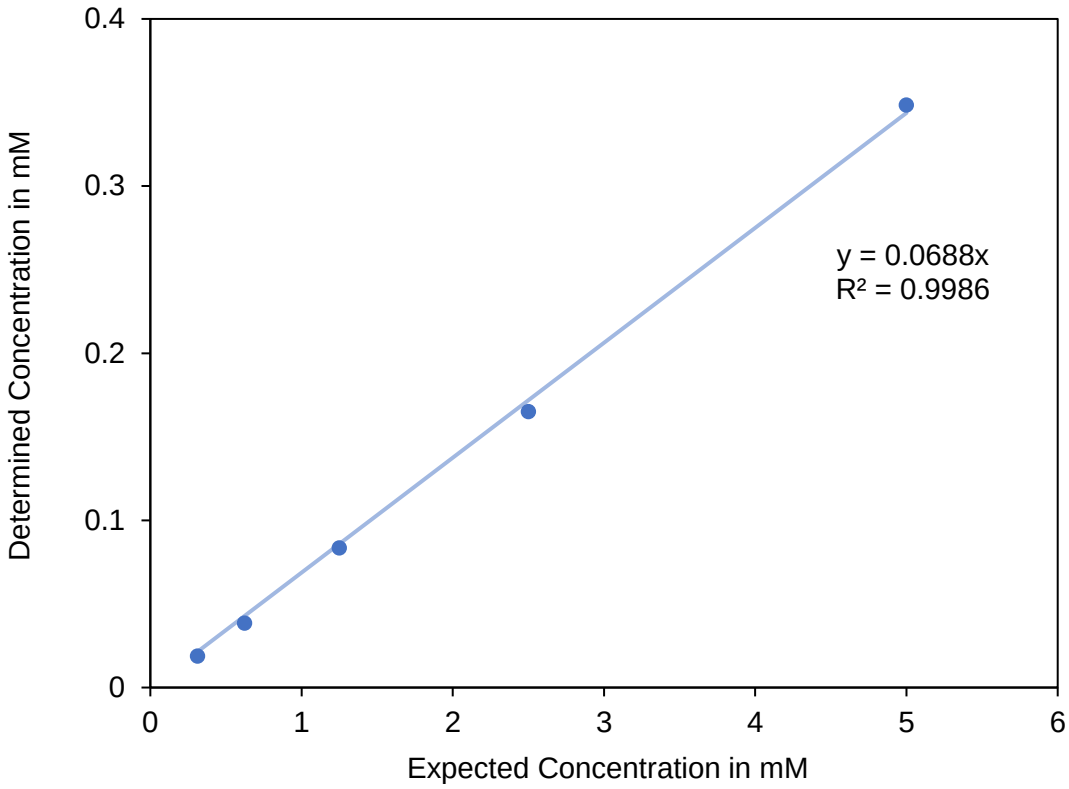

Figure 2-8: Ninhydrin calibration curve of leucine in Ethanol 60%, using the ninhydrin protocol from the Dawson publication.[29] Each point represents a single replicate.

A final test on reaction time in the conditions of 100 ^{o}C, in a water bath with primary amine octylamine at a constant aliquot concentration of 2.47 mM showed that 10 minutes gave maximal color production for the assay. Results are found in **Fig. 2-9**.

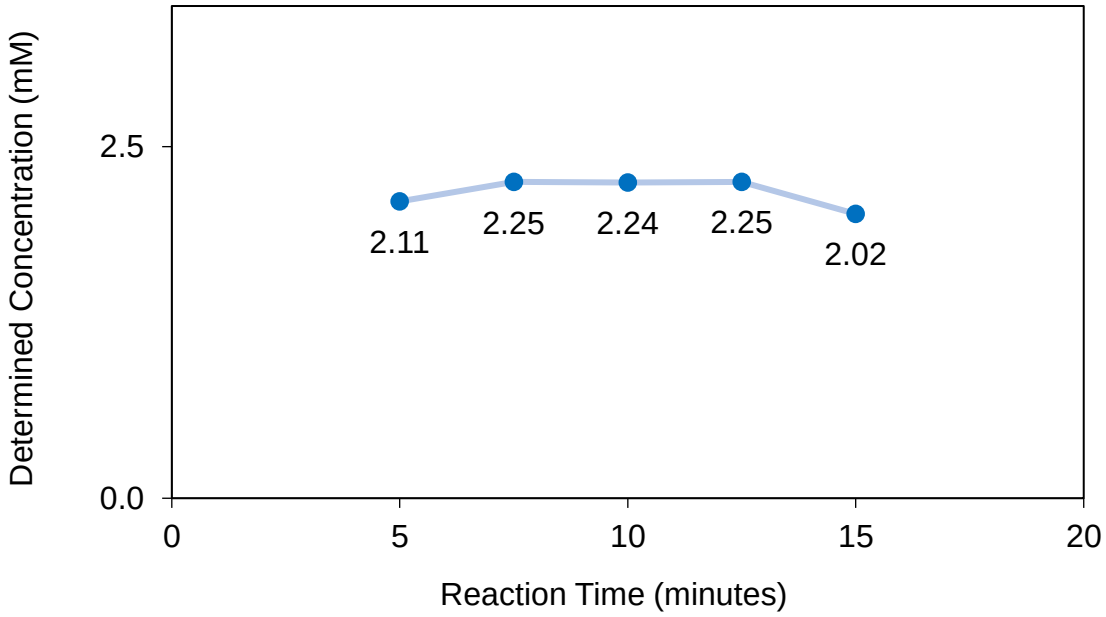

Figure 2-9: Ninhydrin reaction time kinetics with octylamine in ethanol 60%. A 2.47 mM aliquot was used. Each point represents a single replicate.

2.3.2 Ninhydrin Dye Stability

An experiment was performed to assess the stability of the colored dye generated from the ninhydrin reaction, Ruhemann's Purple. From a reaction with 50 nm aminated silica nanoparticles, the colored solution was capped and stored in the dark and re-measured over a span of an hour. The values from **Fig. 2-10** suggest that the dye is stable over the time period required to isolate the supernatant, dilute and measure the absorbance when the assay is used to measure amines on silica NPs.

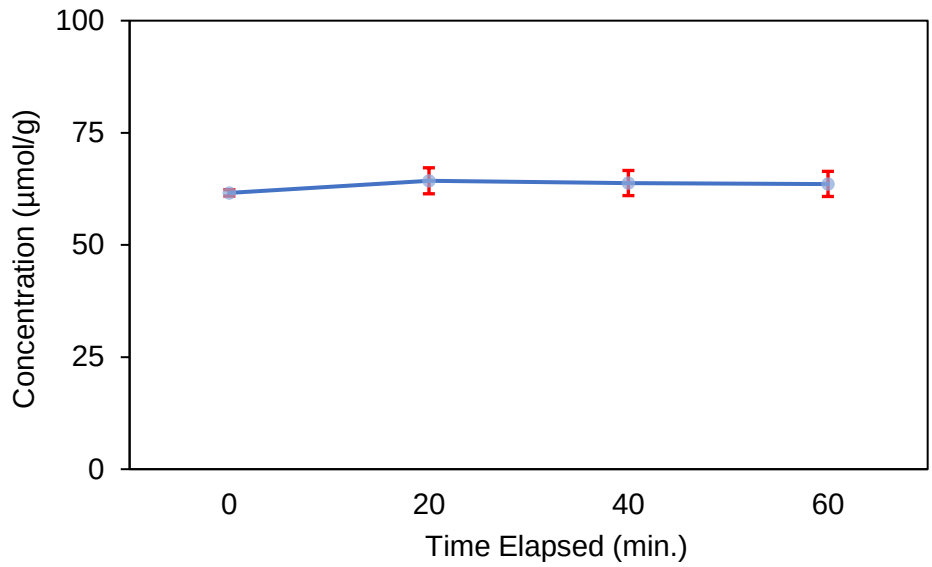

Figure 2-10: Stability of ninhydrin assay dye product over time. Data points represent the average of a triplicate, from the reaction with 50 nm aminated silica nanoparticles.

2.3.3 Effect of Solvent on Aminated Silica Nanoparticles Assayed by Ninhydrin

As a corollary to the study with primary amine standards, experiments were performed to study the effect of the reaction solvent on the output on aminated silica nanoparticles. It was found that the highest yield was in a mixture of ethanol and water, plateauing at roughly 50 to 80% EtOH/H_2O, which matches well with the range of maximal output found in tests on octylamine in varying mixtures of ethanol/H_2O (see **Fig. 2-11** and **2-12**).

Consequently, 60% EtOH/H_2O was used as the solvent system for the ninhydrin assay for measurement on commercial aminated silica nanoparticles. A correction

factor was used to account for the performance of ninhydrin with the primary amine standard, octylamine. It is the inverse slope of the linear regression in the calibration curve.

$$Concentration\ of\ NH_2\ on\ Silica\ Nanoparticles\left(\frac{\mu mol}{g}\right)$$

$$= \frac{\left(Absorbance_{sample} - Absorbance_{blank}\right) \times 10^6}{(21\,000\ M^{-1}cm^{-1})\left(Mass_{sample}\ in\ mg\right)} \times Correction\ Factor$$

$$Correction\ Factor = Slope\ of\ Octylamine\ Calibration\ Curve^{-1}$$

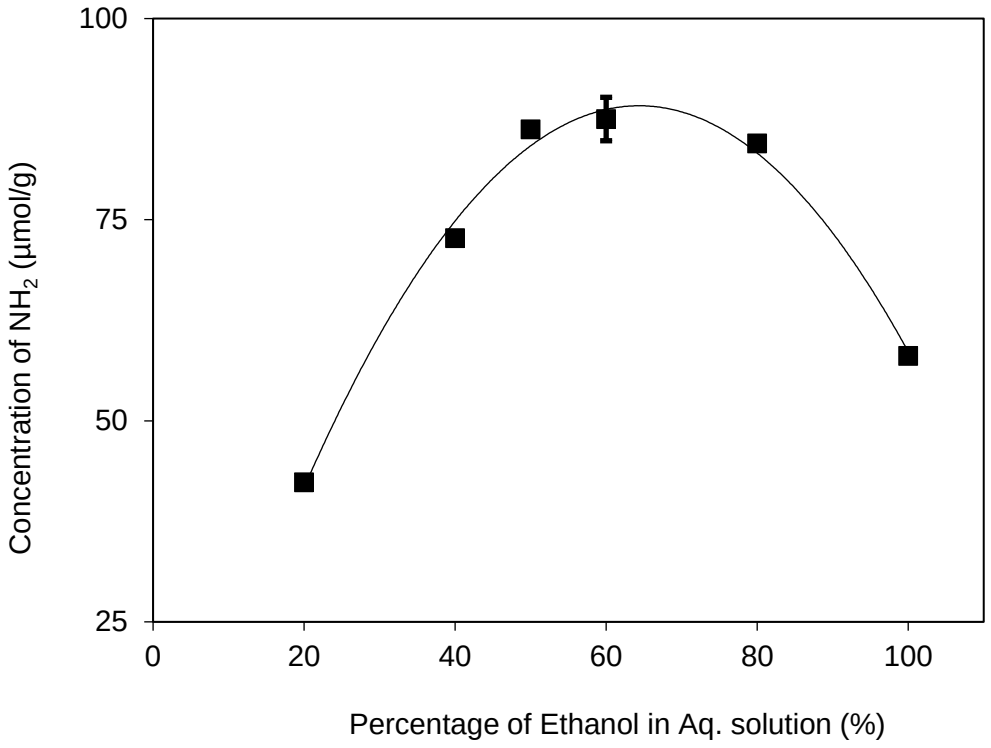

Figure 2-11: Varying percentage of ethanol in aqueous reaction solution and effects on determining surface amine concentration of amine functionalized silica nanoparticles by the ninhydrin assay. 50 nm Nanocomposix nanoparticles were used. n = 1 for all points except 60% with n = 3. A 2nd degree polynomial has been added for a guide.

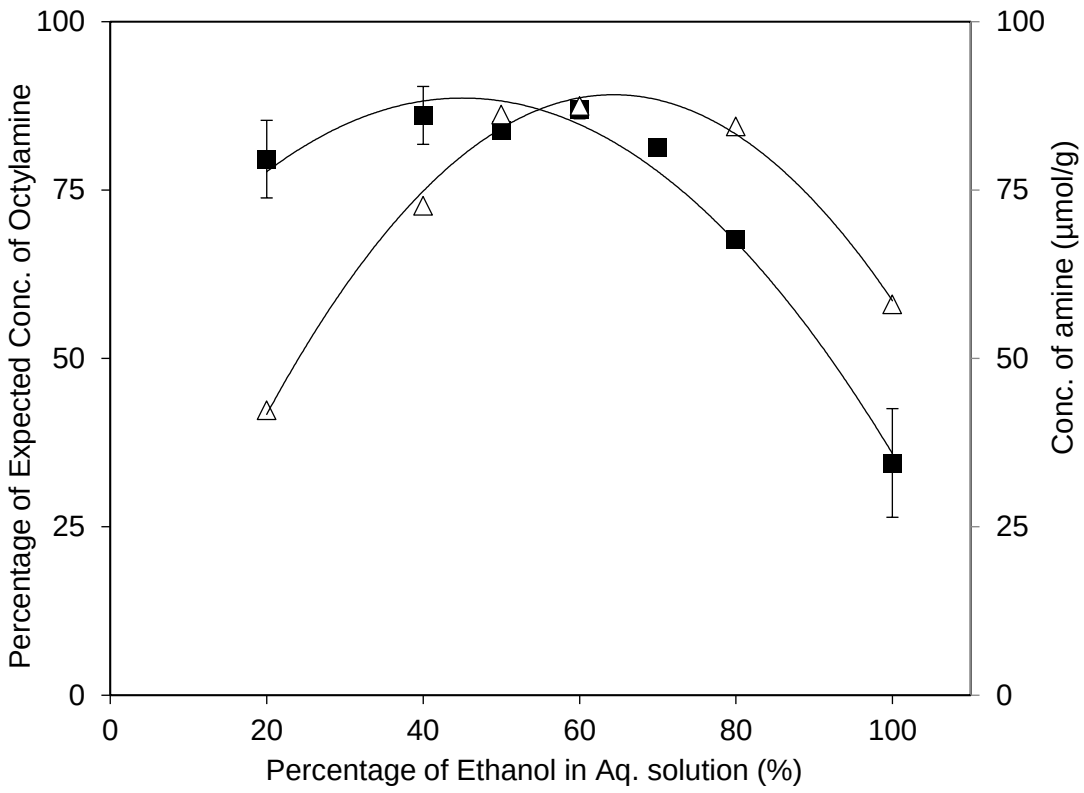

Figure 2-12: Varying percentage of ethanol in aqueous reaction solution and effects on determining concentration of primary amine calibrant octylamine (■) and surface amine concentration of NH_2 functionalized silica NP (△) by the ninhydrin assay. The figure has an overlay of Fig. 2-4. A 2nd degree polynomial has been added for a guide.

2.3.4 Calibration and Optimization Experiments for 4-nitrobenzaldehyde

The 4-NBA assay requires measurement of the free dye in solution (shown in **Fig. 2-13**) and does not require reaction with a primary amine standard for calibration.

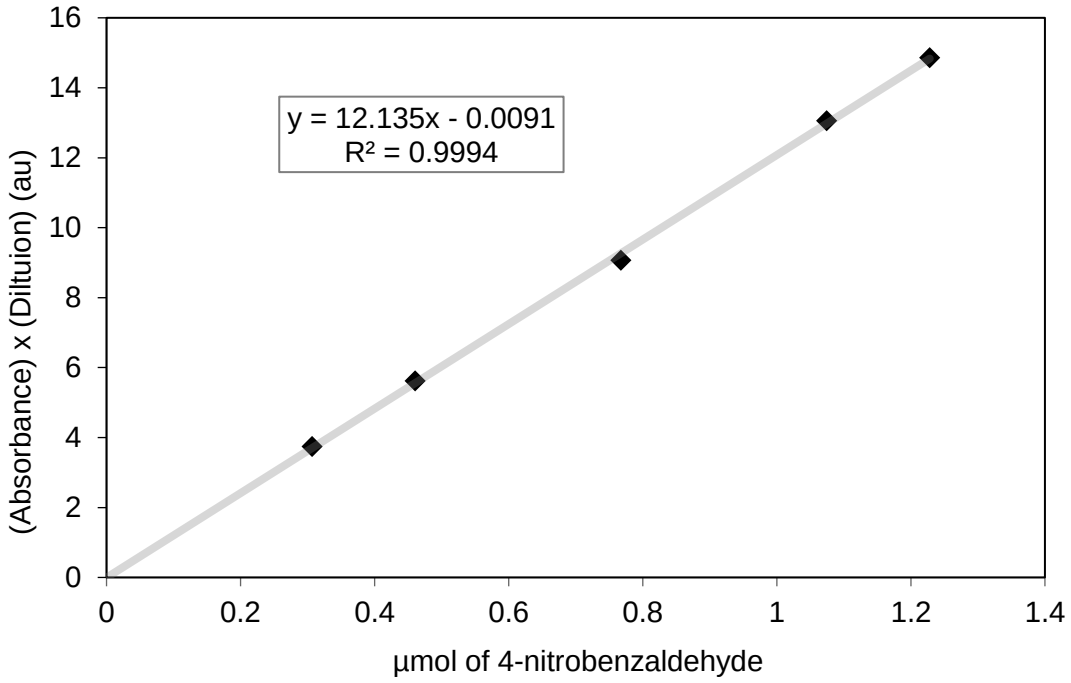

Figure 2-13: Calibration curve for 4-nitrobenzaldehyde in methanol/H_2O (hydrolysis solution).

A control experiment was performed to determine the number of rounds of purification and hydrolysis that were necessary for our protocol for silica NPs, as some literature examples have identified these washing steps as potential sources of error.[25] Incomplete purification would result in additional 4-nitrobenzaldehyde in the sample measured for absorbance. Incomplete hydrolysis would result in underestimation of the number of surface amine functional groups. Furthermore, it is safe to assume that non-

specific binding is dependent on surface chemistry and morphology, and therefore should be monitored carefully.

80 nm aminated silica nanoparticles (B2) were used for the experiment. Results (Fig. 2-14) indicated that at least four washes are necessary to release residual 4-nitrobenzaldehyde non-covalently bound to silica particles. For the hydrolysis and complete removal of the covalently bound dye, three washes are required, with the first done overnight.

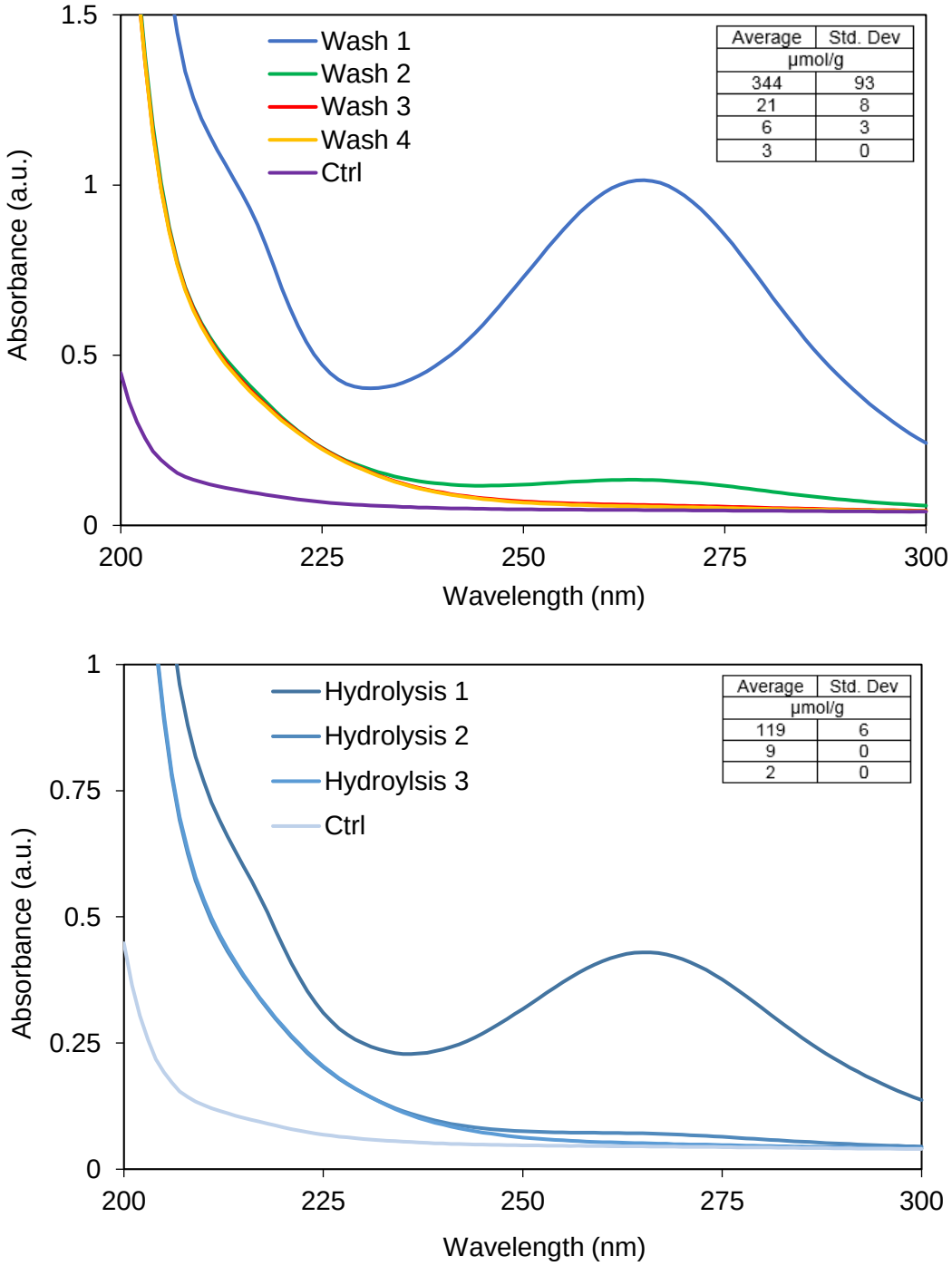

Figure 2-14: UV-visible spectra from the control experiment on the purification and hydrolysis of the 4-nitrobenzaldehyde dye on aminated silica nanoparticles (B2). Each trace represents the average of three replicates. The amine concentration for each wash or hydrolysis step is in the inset with the standard deviation for the triplicate measurements.

2.3.5 Physicochemical Characterization of Silica Nanoparticles

With respect to the physicochemical characterization of these nanoparticles, the commercial supplier provided a specification sheet with each commercial batch, which included particle size (diameter) from TEM, coefficient of variation and mass concentration. If the particles were supplied in ethanol as suspensions, which was the case for the smaller sizes (>50 nm) hydrodynamic diameter and zeta potential were also supplied. Relatively speaking, the amount of characterization we received from Nanocomposix was more comprehensive than other commercial suppliers we have worked with. We consistently found good agreement with the supplier when performing our own particle size measurements by DLS (refer to **Table 2-4 and 2-5** and **Table A-1** in the appendix). In addition, TEM imaging performed by other group members early in the project confirmed the shape and morphology of the particles.

As stressed in the introduction, nanomaterials are in a dynamic state, and may exhibit changes to their shape, size and morphology depending on their chemical environment. This was even reflected by the labels provided from the supplier, as they indicated a limited shelf-life for storage (12-16 months). As silica nanoparticles are known have limited stability in solution, we occasionally monitored the hydrodynamic diameter, zeta potential, and polydispersity of solutions prepared for analysis by the assays. For samples which arrived powdered and require dispersal, tests were performed with our bath sonicator to ensure the time we used resulted in a monodisperse solution that did not contain large aggregates. Aggregation or agglomeration of our sample would foreseeably reduce the total available surface area

and result in underestimating the number of surface functional groups present on our materials.

Table 2-4. Monitoring polydispersity of suspension of aminated silica nanoparticles stored and suspended in ethanol, and effects of bath sonication. Sample was B2, 100 nm. Stock bottle was measured as received, without previous use.

Duration of sonication	Hydrodynamic diameter (nm)	Polydispersity Index (PdI)
Stock (un-sonicated, as received)	135.5	0.05
5 min.	136.5	0.04
10 min.	136.5	0.07
15 min.	133.2	0.03
20 min.	135.2	0.04

Although the results from **Table 2-4** suggest that bath sonication is not required for samples kept in suspensions, results found in **Table 2-5**, show that not all samples exhibited the same aggregation behavior, as 100 nm aminated silica nanoparticles from different batches differed in polydispersity and hydrodynamic diameter during storage.

To prepare the silica nanoparticles in a suspension of ethanol 60%, those samples which were stored in ethanol had to be pelleted/centrifuged, so that the appropriate aliquot of ethanol could be removed and replaced with Milli-Q water. To ensure that the pelleting of the sample did not promote formation of aggregates, an additional test with bath sonication and polydispersity and hydrodynamic diameter was performed, which can be found in **Table 2-5**. Note the differences in **Table 2-4** and **2-5**

with respect to the hydrodynamic diameter and polydispersity of the sample in the stock bottle. While there is not an appreciable difference, we encountered multiple cases where the samples stored in solution did show visible signs of aggregation and DLS measurements were necessary to ensure that bath sonication restored mono-dispersity.

Table 2-5. Monitoring polydispersity of suspension of aminated silica nanoparticles stored and suspended in ethanol, and effects of solvent exchange procedure with bath sonication. Sample was B1, 100 nm.

Duration of sonication	Hydrodynamic diameter (nm)	Polydispersity Index (PdI)
From stock bottle (EtOH), 0 minutes	158	0.08
Solvent Exchanged, Re-dispersed in 60% EtOH, 5 minutes	140	0.02
15 minutes	136	0.03
30 minutes	137	0.02

2.3.6 Determination of Surface Amine Content on Silica Nanoparticles

We began testing of the colorimetric assays on aminated silica nanoparticles by first assessing the reproducibility of the assay on separate days (see **Fig. 2-15**). Each individual replicate and bar represent a separate aliquot of aminated silica which underwent reaction and analysis by UV-vis spectrophotometer. Each time the assays were performed, three replicates (triplicate) were prepared, which were exposed to the same reaction conditions. Each replicate (n = 1) represents its own reaction, production of colored dye, and measurement of amine quantification.

We can see measurements across 12 replicates, measured on 4 separate days, over a few weeks for ninhydrin, and 9 and 3 respectively for 4-NBA. The average amine concentration for this size and batch (100 nm, B1) was 202 ± 12 (µmol/g). The standard deviation as such is roughly 6%. For the example for the 4-nitrobenzaldehyde assay, 9 replicates are shown for 50 nm B3, with a determination of 53 ± 3 (µmol/g), and a deviation of 6%. Overall, the two colorimetric assays show comparable reproducibility, with the average standard deviation for all samples accounting for 6.3% and 6.2% of the measured amine concentration for ninhydrin and 4-NBA respectively.

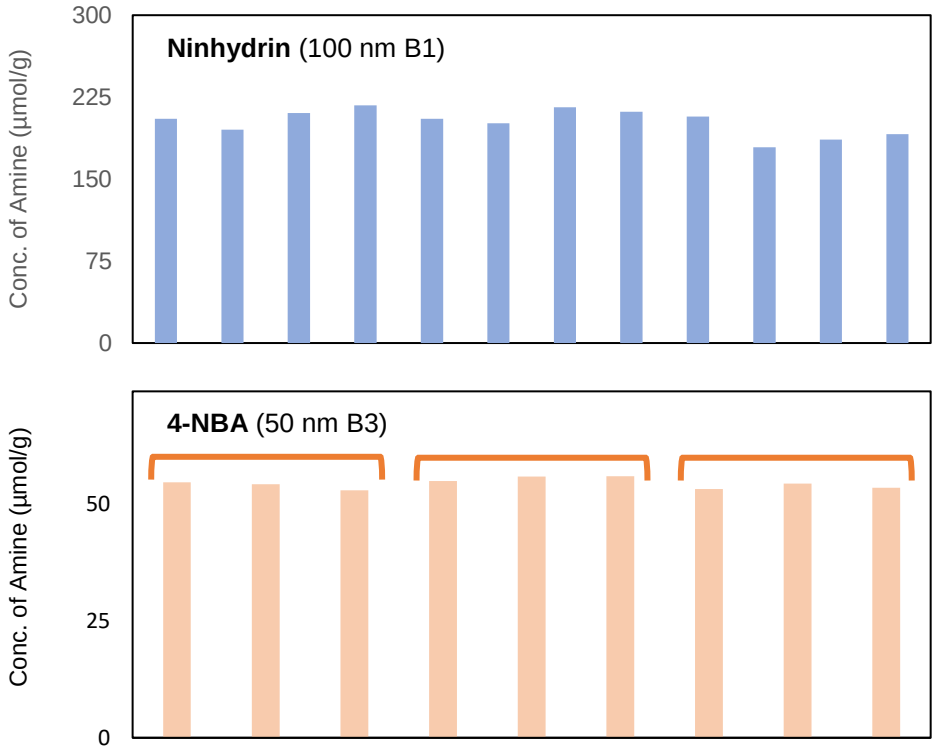

Figure 2-15: Bar graphs showing reproducibility and variance of individual batches of aminated silica nanoparticles in respective colorimetric assays. Each bar represents a single replicate (*n*). The average amine concentrations for the two silica samples are 202 ± 12 (µmol/g) and 53 ± 3 (µmol/g). For visual guide, brackets are inset on the 4-NBA graph to indicate the individual days the triplicates were performed.

Following tests which indicated the consistent and reproducible measurements with both assays, we sought to quantify surface amine groups on multiple batches of commercial silica nanoparticles, (Nanocomposix) for a range of sizes (20-120 nm).

Comparing measurements between batches revealed a large degree of variability in the surface amine concentration for some sizes of these commercial silica NPs. **Fig. 2-16** illustrates these differences across three particles sizes and three commercial batches. While the 80 nm nanoparticles have a similar surface amine

content after consideration of the standard deviation, both the 50 nm and 100 nm NPs show variable content. The greatest difference (nearly 4-fold) can be found in the first batch of the 50 nm NPs and the following preparations.

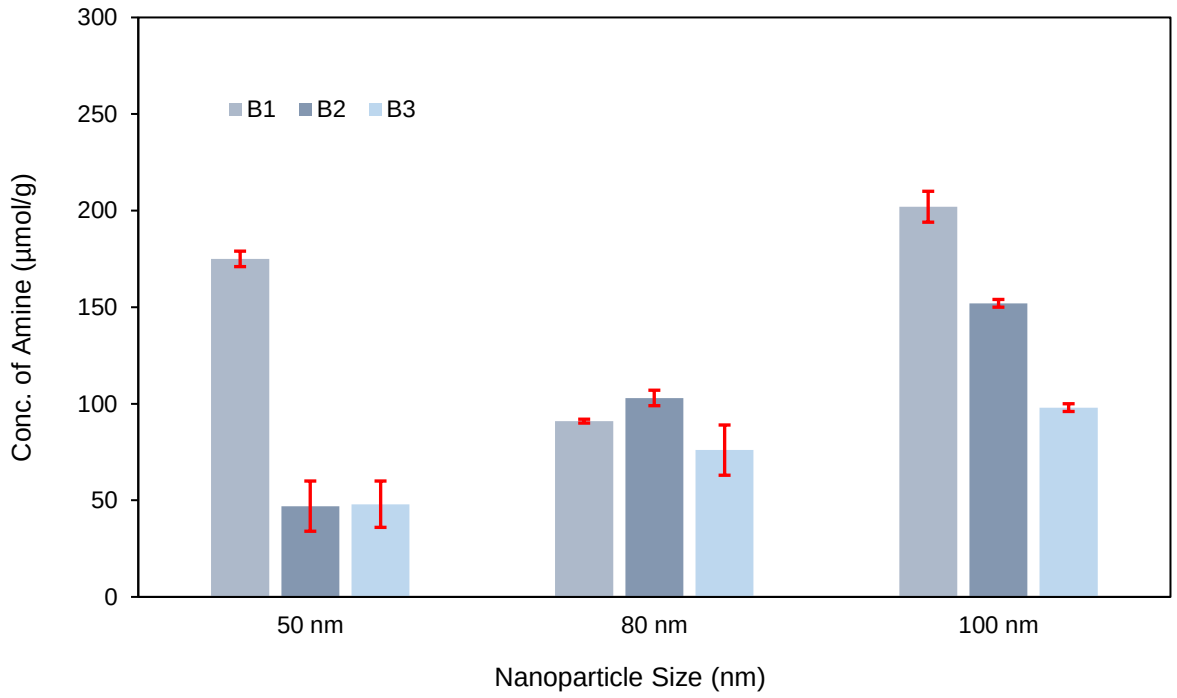

Figure 2-16: Bar graphs showing batch-to-batch inconsistencies in surface amine content of silica nanoparticles, quantified by the ninhydrin assay. Each bar represents an average of 3-9 replicates from a separate production batch; error bars represent standard deviation.

Table 2-6 shows the complete list of measurements on aminated silica nanoparticles across three separate commercial batches (B1-B3) by the two colorimetric assays.

Table 2-6. Determination of amine content for silica nanoparticles using ninhydrin and 4-nitrobenzaldehyde colorimetric assays.

Commercial Batch Number	Sample size	Ninhydrin		4-NBA (µmol/g)	
		n	(µmol/g)	*n*	(µmol/g)
B1	50 nm	6	175 ± 4	-	
	80 nm	9	91 ± 13		
	100 nm	12	202 ± 12		
B2	20 nm	6	317 ± 23	6	459 ± 5
	50 nm	9	47 ± 1	9	66 ± 12
	80 nm	9	103 ± 4	9	132 ± 15
	100 nm	9	152 ± 13	9	169 ± 15
	120 nm	6	117 ± 4	6	122 ± 2
B3	50 nm	3	48 ± 8	9	53 ± 3
	80 nm	3	76 ± 2	3	113 ± 4
	100 nm	3	98 ± 2	6	117 ± 1

2.3.7 Sensitivity and Limits of Detection

The two colorimetric assays are comparable in their sensitivities and limits of detection. For the assay conditions used (5 mg of silica nanoparticles per aliquot), the assays can detect amine concentrations as low as 1.5 µmol g^{-1} for ninhydrin and 2.5 µmol g^{-1} for the 4-NBA assay. These limits of detection were derived from the lowest concentration prepared in their respective calibration curves. In addition, these

concentrations were above the working range for UV-visible spectrophotometric measurements, generally cited as approximately 0.2 absorbance (63% transmittance).

2.4 Conclusion

A comprehensive study on two colorimetric assays was performed to adapt protocols for the quantification of amine groups on the surface of silica nanoparticles. For the ninhydrin assay, studies on the reaction conditions and standardization with primary amines revealed the influence of the solvent system on the quantitative output, as well as reaction time and temperature.

Although primary amine groups are widely used as anchor points for covalent bioconjugation of peptides, polysaccharides and lipids, a direct link between surface group content and subsequent derivatization is missing.[4,30] For this challenge to be met, validated and reproducible methods are required for surface analysis of nanomaterials. We found that across multiple sizes and production batches of commercial silica nanoparticles, surface amine content was highly variable.

Unpredictable changes to surface charge and hydrodynamic diameter can impede successful applications in biological systems, where the aggregation state and formation of the protein corona are of concern and can drastically alter the circulation characteristic and rates of clearance. Furthermore, studies on nanoparticle toxicology have repeatedly shown size dependant effects. For nanomaterials with variable changes to surface chemistry, their unexpected aggregation could prevent the accurate assessment of potentially impactful drug delivery systems. In applications where the

primary amine groups are meant to be sites for additional chemical derivatization and bioconjugation reactions, subsequent biological activities and performances may also fluctuate and change unexpectedly.

Thus, the results from the colorimetric assays on commercial silica reinforce the use of multiple methods to characterize and quantify surface functional group content to better understand the reactivity, accessibility and behavior of these materials.

2.5 References

(1) Shiota, S.; Yamamoto, S.; Shimomura, A.; Ojida, A.; Nishino, T.; Maruyama, T. Quantification of Amino Groups on Solid Surfaces Using Cleavable Fluorescent Compounds. *Langmuir* **2015**, *31* (32), 8824–8829. https://doi.org/10.1021/acs.langmuir.5b02548.

(2) Moser, M.; Nirmalananthan, N.; Behnke, T.; Geißler, D.; Resch-Genger, U. Multimodal Cleavable Reporters versus Conventional Labels for Optical Quantification of Accessible Amino and Carboxy Groups on Nano-and Microparticles. *Anal. Chem.* **2018**, *90* (9), 5887–5895. https://doi.org/10.1021/acs.analchem.8b00666.

(3) Poli, E.; Chaleix, V.; Damia, C.; Hjezi, Z.; Champion, E.; Sol, V. Efficient Quantification of Primary Amine Functions Grafted onto Apatite Ceramics by Using Two UV-Vis Spectrophotometric Methods. *Anal. Methods* **2014**, *6* (24), 9622–9627. https://doi.org/10.1039/C4AY02012J.

(4) Noel, S.; Liberelle, B.; Robitaille, L.; De Crescenzo, G. Quantification of Primary Amine Groups Available for Subsequent Biofunctionalization of Polymer Surfaces. *Bioconjug. Chem.* **2011**, *22* (8), 1690–1699. https://doi.org/10.1021/bc200259c.

(5) Kaiser, E.; Colescott, R. L.; Bossinger, C. D.; Cook, P. I. Color Test for Detection of Free Terminal Amino Groups in the Solid-Phase Synthesis of Peptides. *Anal. Biochem.* **1970**, *34* (2), 595–598. https://doi.org/10.1016/0003-2697(70)90146-6.

(6) Shah, A.; de Biasi, V.; Camilleri, P.; Rahman, S. S. Development of Colorimetric Method for the Detection of Amines Bound to Solid Support. *Anal. Commun.* **2002**, *34* (11), 325–328. https://doi.org/10.1039/a705630c.

(7) West, R. Siegfried Ruhemann and the Discovery of Ninhydrin. *J. Chem. Educ.* **2009**, *42* (7), 386. https://doi.org/10.1021/ed042p386.

(8) Friedman, M. Applications of the Ninhydrin Reaction for Analysis of Amino Acids, Peptides, and Proteins to Agricultural and Biomedical Sciences. *J. Agric. Food*

Chem. **2004**, *52* (3), 385–406. https://doi.org/10.1021/jf030490p.

(9) Curotto, E.; Aros, F. Quantitative Determination of Chitosan and the Percentage of Free Amino Groups. *Anal. Biochem.* **1993**, *211* (2), 240–241. https://doi.org/10.1006/abio.1993.1263.

(10) Prochazkova, S.; Vårum, K. M.; Ostgaard, K. Quantitative Determination of Chitosans by Ninhydrin. *Carbohydr. Polym.* **1999**, *38* (2), 115–122. https://doi.org/10.1016/S0144-8617(98)00108-8.

(11) Jarre, G.; Heyer, S.; Memmel, E.; Meinhardt, T.; Krueger, A. Synthesis of Nanodiamond Derivatives Carrying Amino Functions and Quantification by a Modified Kaiser Test. *Beilstein J. Org. Chem.* **2014**, *10*, 2729–2737. https://doi.org/10.3762/bjoc.10.288.

(12) Zhang, Y.; Chen, Y. Fmoc-Cl Fluorescent Determination for Amino Groups of Nanomaterial Science. *IET Nanobiotechnol* **2012**, *6* (2), 76–80. https://doi.org/10.1049/iet-nbt.2011.0027.

(13) Lu, H.-T. Synthesis and Characterization of Amino-Functionalized Silica Nanoparticles. *Colloid J.* **2013**, *75* (3), 311–318. https://doi.org/10.1134/S1061933X13030125.

(14) Soto-Cantu, E.; Cueto, R.; Koch, J.; Russo, P. S. Synthesis and Rapid Characterization of Amine-Functionalized Silica. *Langmuir* **2012**, *28* (13), 5562–5569. https://doi.org/10.1021/la204981b.

(15) Hristov, D. R.; Rocks, L.; Kelly, P. M.; Thomas, S. S.; Pitek, A. S.; Verderio, P.; Mahon, E.; Dawson, K. A. Tuning of Nanoparticle Biological Functionality through Controlled Surface Chemistry and Characterisation at the Bioconjugated Nanoparticle Surface. *Sci. Rep.* **2015**, *5* (August), 17040. https://doi.org/10.1038/srep17040.

(16) Friedman, M. Applications of the Ninhydrin Reaction for Analysis of Amino Acids, Peptides, and Proteins to Agricultural and Biomedical Sciences. *J. Agric. Food Chem.* **2004**, *52* (3), 385–406. https://doi.org/10.1021/jf030490p.

(17) Moore, B. Y. S.; Stein, H. Photometric Ninhydrin Method for Use in the Chromatography of Amino Acids. *J. Biol. Chem.* **1948**, No. 176, 367.

(18) TROLL, W.; CANNAN, R. K. A Modified Photometric Ninhydrin Method for the Analysis of Amino and Imino Acids. *J. Biol. Chem.* **1953**, *200* (2), 803–811.

(19) MOORE, S.; STEIN, W. H. A Modified Ninhydrin Reagent for the Photometric Determination of Amino Acids and Related Compounds. *J. Biol. Chem.* **1954**, *211* (2), 907–913.

(20) Moore, S. Amino Acid Analysis : Aqueous Dimethyl Sulfoxide As Solvent for the Ninhydrin Reaction. *J. Biol. Chem.* **1968**, *243* (23), 6281–6283.

(21) Moon, J. H.; Shin, J. W.; Kim, S. Y.; Park, J. W. Formation of Uniform Aminosilane Thin Layers: An Imine Formation to Measure Relative Surface Density of the Amine Group. *Langmuir* **1996**, *12* (20), 4621–4624. https://doi.org/10.1021/la9604339.

(22) van de Waterbeemd, M.; Sen, T.; Biagini, S.; Bruce, I. J. Surface Functionalisation of Magnetic Nanoparticles: Quantification of Surface to Bulk Amine Density. *Micro Nano Lett.* **2010**, *5* (5), 282–285. https://doi.org/10.1049/mnl.2010.0112.

(23) Sen, T.; Bruce, I. J. Surface Engineering of Nanoparticles in Suspension for Particle Based Bio-Sensing. *Sci. Rep.* **2012**, *2*, 1–6. https://doi.org/10.1038/srep00564.

(24) Rosenholm, J. M.; Lindén, M. Wet-Chemical Analysis of Surface Concentration of Accessible Groups on Different Amino-Functionalized Mesoporous SBA-15 Silicas. *Chem. Mater.* **2007**, *19* (20), 5023–5034. https://doi.org/10.1021/cm071289n.

(25) Ghasemi, M.; Minier, M.; Tatoulian, M.; Arefi-Khonsari, F. Determination of Amine and Aldehyde Surface Densities: Application to the Study of Aged Plasma Treated Polyethylene Films. *Langmuir* **2007**, *23* (23), 11554–11561. https://doi.org/10.1021/la701126t.

(26) Sarin, V. K.; Kent, S. B. H.; Tam, J. P.; Merrifield, R. B. Quantitative Monitoring of Solid-Phase Peptide Synthesis by the Ninhydrin Reaction. *Anal. Biochem.* **1981**, *117* (1), 147–157. https://doi.org/10.1016/0003-2697(81)90704-1.

(27) Iannazzo, D.; Piperno, A.; Ferlazzo, A.; Pistone, A.; Milone, C.; Lanza, M.; Cimino, F.; Speciale, A.; Trombetta, D.; Saija, A.; et al. Functionalization of Multi-Walled Carbon Nanotubes with Coumarin Derivatives and Their Biological Evaluation. *Org. Biomol. Chem.* **2012**, *10* (5), 1025. https://doi.org/10.1039/c1ob06598j.

(28) Jung, H.-S.; Moon, D.-S.; Lee, J.-K. Quantitative Analysis and Efficient Surface Modification of Silica Nanoparticles. *J. Nanomater.* **2012**, *2012*, 1–8. https://doi.org/10.1155/2012/593471.

(29) Hristov, D. R.; Rocks, L.; Kelly, P. M.; Thomas, S. S.; Pitek, A. S.; Verderio, P.; Mahon, E.; Dawson, K. A. Tuning of Nanoparticle Biological Functionality through Controlled Surface Chemistry and Characterisation at the Bioconjugated Nanoparticle Surface. *Sci. Rep.* **2015**, *5* (August), 17040. https://doi.org/10.1038/srep17040.

(30) Irena, G.; Jolanta, B.; Karolina, Z. Chemical Modification of Poly(Ethylene Terephthalate) and Immobilization of the Selected Enzymes on the Modified Film. *Appl. Surf. Sci.* **2009**, *255* (19), 8293–8298. https://doi.org/10.1016/j.apsusc.2009.05.126.

(31) Yemm, E. W.; Cocking, E. C.; Ricketts, R. E. The Determination of Amino-Acids with Ninhydrin. *Analyst* **1955**, *80* (948), 209–214. https://doi.org/10.1039/an9558000209.

Chapter 3: Solid-state NMR

The results of this chapter appear in the following publication. My contribution was in the design of the labelling reaction, preparing labelled samples, and performing/analyzing the NMR experiments. The quantitative solid-state NMR method for ^{19}F on silica nanoparticles used was established by Dr. Andreas Brinkmann (see reference 18).

Sun, Y.; Kunc, F.; Balhara, V.; Coleman, B.; Kodra, O.; Raza, M.; Chen, M.; Brinkmann, A.; Lopinski, G.; Johnston, L. Quantification of Amine Functional Groups on Silica Nanoparticles: A Multi-Method Approach. *Nanoscale Adv.* **2019**. https://doi.org/10.1039/C9NA00016J.

3.1 Background

Solid-state NMR (ss NMR) is a versatile characterization technique for the study of materials. Because of the various anisotropic interactions which arise from magnetic resonance in solids, a great deal of structural (such as orientation, geometry, spatial distances) and chemical (dynamics, diffusion, functionality) information can be acquired. **Figure 3-1** illustrates how this valuable information originates from the fundamental interactions that can be observed in solid-state NMR experimentation.

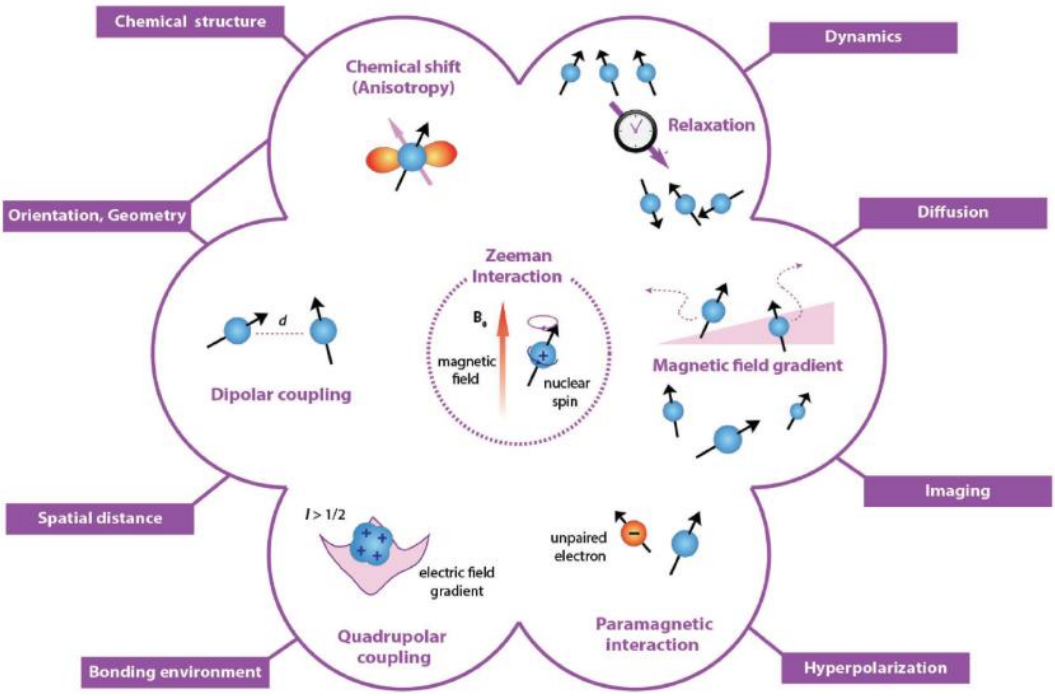

Figure 3-1: A graphical representation of the fundamental nuclear interactions and phenomena found in NMR experiments. The useful chemical information that can be retrieved from these interactions surround the perimeter of the graphic. Image from reference (1).

Unfortunately, isolating these interactions from one another is often non-trivial. Solid-state NMR studies on powdered samples result in a wide spectral line-shape corresponding to the distribution of randomly oriented crystallites (shown in **Fig. 3-2**) in the presence of the applied magnetic field (B_o). The broad features are a consequence of multiple interactions superimposed and overlapping one another. In the context of nanomaterial characterization, similar spectral profiles come about from other non-uniformities. Different levels of structure (such as core/shell), and distributions of chemical species orientations similarly give rise to a broad, complex spectrum. Technical and theoretical advances in the last 25 years have made some of these interactions accessible through the development of multi-dimensional experimental techniques and pulse schemes.[2]

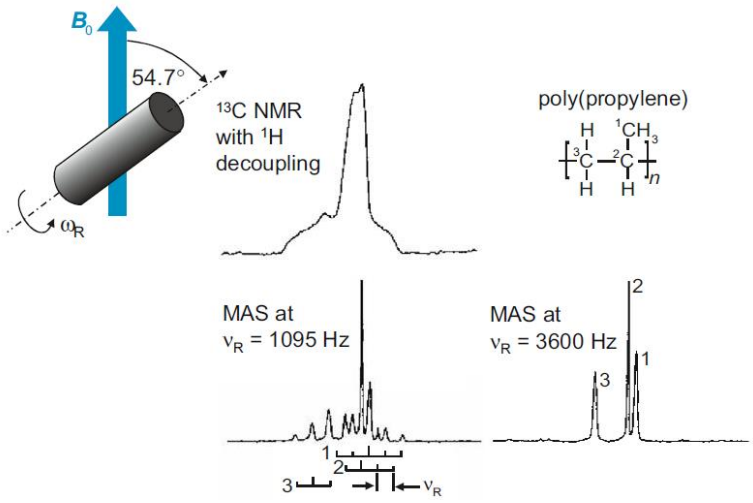

Figure 3-2: Examples of the broad powder pattern from overlapping anisotropic interactions found in NMR on solids. MAS techniques can be applied to suppress some of these interactions and retrieve isotropic chemical shifts and additional information. Image from reference (3).

One popular method to suppress some of these anisotropic effects is with magic angle spinning (MAS). MAS is commonly used to deconvolute spectra from chemical shielding, heteronuclear dipolar, antisymmetric J-coupling and 1st order quadrupolar interactions. What essentially remains are the isotropic chemical shifts, which match the sharp line-shapes found in solution-state NMR.

MAS suppresses angular-dependent NMR interactions by satisfying the 2nd order Legendre Polynomial which appears in the expanded Hamiltonian operators for J (scalar), dipolar, and quadrupolar coupling. This is done by rapidly rotating the sample rotor at an angle of 54.7° (with respect to B_o, the applied magnetic field). where the angle dependent term $3\cos\theta = 1$ which time-averages to equal 0. Consequently, the broad 'powder pattern' collapses to form sharp peaks provided the sample is rotated fast enough. Depending on the rotation speed, spinning sidebands (refer to Fig. 3-2 for example) may remain which are separated from the isotropic resonance frequency by multiples of $n\ \omega_R$, where $\omega_R = 2\pi\ \nu_L$ and ν_L is the Larmor frequency (or resonance frequency).

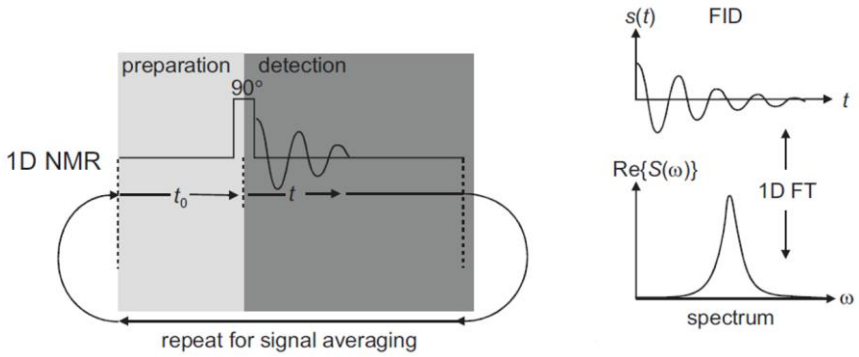

Figure 3-3: Pulse diagram for a typical one-dimensional NMR experiment. Adapted from reference (4).

Most one-dimensional NMR experiments can be divided two stages: preparation and detection (see Fig. 3-3). During the preparation stage, nuclei can relax to their equilibrium state, which is followed by the radiofrequency pulse inducing nuclear spins to flip to the excited state, and then a detection period whereby spin-lattice T_1 and spin-spin T_2 relaxation pathways proceed, and the decaying signal is collected as the system equilibrates.

$$P = \frac{N_\alpha - N_\beta}{N_\alpha + N_\beta} = tanh\left(\frac{\gamma \hbar B_0}{2k_B T}\right)$$

The equation above is for the Boltzmann factor. The α and β refer to the possible eigenstates for a spin 1/2 nucleus in an applied magnetic field. The Boltzmann factor describes the thermodynamic distribution of spins in non-degenerate energy levels. The differences in the populations of the spin states ($N_{\alpha,\beta}$), divided by the sum is shown to be dependent on the magnetogyric ratio γ, B_0 for the strength of applied magnetic field, and T for temperature in Kelvin (disregarding the constants). For standard NMR experiments, the primary determinant of polarization of spins (and thus NMR-active nuclei) will be the magnetogyric ratio, and where possible, the most powerful magnet (B_0). Advanced sensitivity enhancement methods exploit the temperature of the experiment (cryogenic temperatures), as well as different approaches to polarization (exogenous agents).

3.1.1 Applications for the Study of Functionalized Nanomaterials

In the last 20 years, solid-state NMR has shown itself to be an indispensable technique for the characterization and analysis of functionalized nanomaterials. In the case of nanoscale silica, it has been used in the study of mesoporous silica nanoparticles for applications in carbon capturing and as heterogeneous catalysts.[5–7] Surface functionalization of these materials is frequently performed as it can significantly improve their catalytic activity and performance.[8–11] As touched on the introduction, solid-state NMR is often used to assess total functional group content, since it cannot discriminate between surface and embedded species. With respect to the study of mesoporous materials, typically the chemical species of interest are located below the surface, coating the interior of the pores. Consequently, these groups can be challenging to probe and access through conventional spectrophotometric techniques. For example, UV-visible and fluorescent assays can struggle to successfully label these groups owing to their steric crowding and inaccessibility. With NMR-based techniques, regardless of the location of the chemical moiety, their magnetic resonance signatures will be detected and measured.

Notable contributions have come from researchers from the University of Iowa and the *Ames Laboratory, Department of Energy*.[12–15] An excellent example appears in a publication from 2003 by Huh et al.[12] In this work, researchers utilized a range of organofunctional silanes to prepare functionalized mesoporous silica by the co-condensation approach. The materials were then characterized by MAS solid-state NMR techniques to determine the reference chemical shifts as well as quantify the number of functional groups, which can be found in **Fig. 3-4**. The example is one of

many studies which exploit MAS as a means to retrieve meaningful chemical shifts for identification and quantification of chemical species or functional groups.

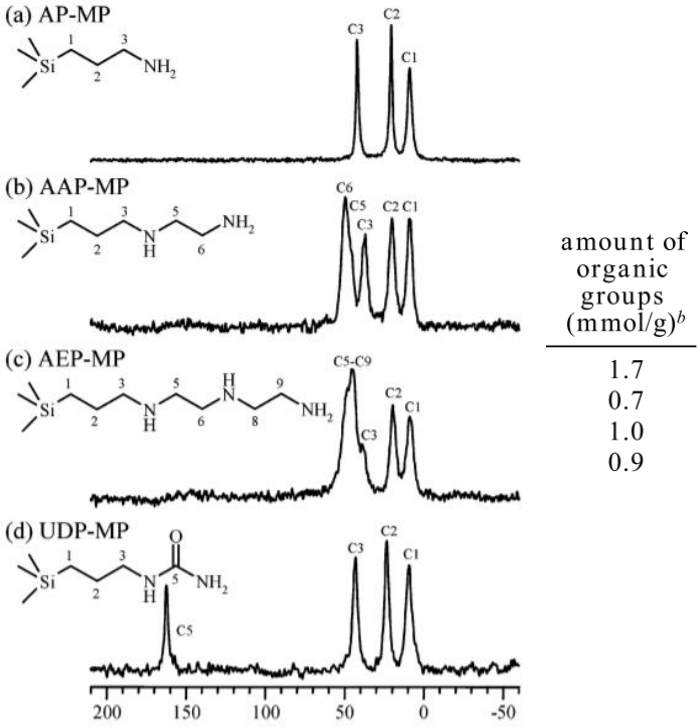

Figure 3-4: Solid-state NMR utilized to compare the various isotropic chemical shifts of organofunctional silanes on mesoporous silica. Cross-polarization ^{1}H – ^{13}C MAS techniques were used, with spectra and corresponding quantification. Note that in the absence of MAS the individual peaks would broaden into an envelope or 'powder pattern' (12).

Another early example from 2007 demonstrates the use of MAS ss NMR to monitor the various modes of binding of silanols to water within mesoporous silica. As shown in **Fig. 3-5**, various structures are seen with their reference chemical shifts. Hydration and rehydration cycles are often involved in thermal treatment of mesoporous silicas to remove defects and templating molecules used to fabricate the pores. This

study showed the ability of solid-state NMR to monitor the presence of moisture and monitor the treatment and processing of these materials.

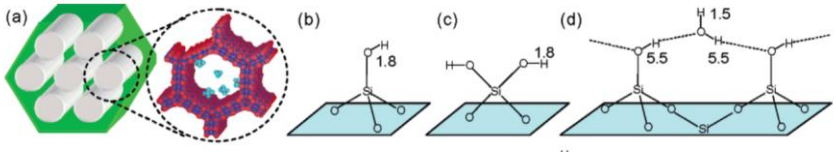

Figure 3-5: Various modes of binding of water to silanols within nanoscale mesoporous silica (MCM-41) as identified by solid-state NMR spectroscopy. a) shows an overview of the silanols studied, while b-d) shows the various structures and corresponding chemical shifts. Image adapted from reference (13).

Recent work from Pruski and Rossini is focused on the implementation of dynamic nuclear polarization-enhanced multi-dimensional solid-state NMR spectroscopy. Their studies have been key in building understanding of the different surface structures which result from various synthetic pathways in nanoscale silica and other nanomaterials. Rossini stresses the ability of DNP and solid-state NMR to scrutinize surface sites on colloidal semiconductor nanoparticles can support the development of successful applications in photovoltaics, lighting and display technologies.[16] The central concept behind DNP is the transfer of polarization from unpaired electrons (radicals from polarizing agents) to nuclear spins to drastically increase the sensitivity of NMR.

Poor sensitivity is ubiquitous in all forms of NMR experimentation. It remains a sizeable issue in the study of organic functional groups, surface-bound and otherwise. In general, these chemical groups make up only a small fraction of the total sample, and in cases where controlled surface functionalization is desired, their concentration may

approach limits of detection and quantification in standard NMR methods. In the context of nanoscale silica, this issue is compounded by low gyromagnetic sensitivities of the nuclei of interest.

$^{1}H = 267.5$	$^{29}Si = -53.2$
$^{14}N = 19.3$	$^{15}N = -27.1$
$^{13}C = 67.3$	

Gyromagnetic ratio in units of 10^6 rad s^{-1} T^{-1}

As a result, many contemporary examples of applications of solid-state NMR for the characterization of functionalized nanomaterial depend on sensitivity enhancement techniques such as DNP, which can be costly and complex, requiring specialized instrumentation hardware. Furthermore, they require the addition of exogenous agents (polarization agents) and additives. Consequently, the nanomaterials studied are not strictly pristine and in their native state.

An alternative approach to analyzing endogenous nuclei in materials is to chemically label the surface groups. In the cases where organic moieties present on the surface are used for further surface derivatization (i.e. NH_2, COOH), the use of probes or labels can also provide estimates for reactive surface groups, giving a better estimate of expected yields of conjugation reactions. A detailed review on molecular sensing in NMR effectively summarized the ability of these sensors to “expand the scope” and address the limitations in conventional NMR methods.[17] Fluorine-based labels (as well as ^{31}P and ^{129}Xe) were highlighted as ideal nuclei for sensors, as their resonances are well-resolved, allowing for straightforward identification of molecules in various chemical environments. Additionally, fluorine’s gyromagnetic sensitivity is high, comparable to

hydrogen's, making it an ideal nucleus for study. ($^{19}F = 251.6 \approx {}^{1}H = 267.5$, units 10^6 rad s^{-1} T^{-1}). Development of fluorine-based probes can extend well into bioapplications involving MR imaging, as the review notes that the low likelihood of exogenous xenon and organofluorine compounds in the body reduces background. The review stresses the potential of these sensors as effective and simple alternatives for the study of NMR-inactive or insensitive materials for a broad range of bioapplications.

Although labelling with probes is one convenient way to address the issue of sensitivity, it also restricts the nuclei measured to those labelled on the surface. Consequently, those groups which may be present within pores, or deeper within the silica network will not be detected. Furthermore, as with all labelling-based approaches, it is likely there will be differences in reactivity and accessibility of those groups on the surface, owing to the various orientations and configurations of silane monolayers. A work-around to this limitation is to exploit the fluorine labelling by performing surface analysis with X-ray photoelectron spectroscopy (XPS). XPS can compare the fluorine signal with other elements such as carbon and nitrogen to validate the coupling yield of our fluorine tag. Thus, developing an effective fluorine-labelling technique for use with quantitative solid-state NMR was essential to provide the means to enable additional analysis by XPS, and a way to investigate and assess the accessibility and reactivity of surface amine groups on silica.

3.2 Experimental

3,5-bistrifluoromethylbenzaldehyde (BTFBA)-conjugated silica NPs were prepared by adding 5 mL of 10 mg/mL anhydrous ethanol dispersion to a scintillation vial with a magnetic stir bar and adding an excess of BTFBA (~ 100-fold). The solution was stirred overnight at room temperature.

The solution was then divided into four microcentrifuge tubes (2 mL) for high-speed centrifugation (20 minutes, 14K RPM) of the nanoparticles into a pellet. The excess BTFBA in ethanol was carefully pipetted off, and additional anhydrous ethanol (1.5 mL) was added to allow for purification and removal of residual reagent. The particles were re-dispersed by ultrasonic bath (>5 minutes) and then pelleted back down. This process was repeated three times for a total of four purification cycles.

To prepare dry particles for solid-state NMR measurement, the dispersions were centrifuged at 14K RPM for 20 min, the supernatants were carefully pipetted off, and the remaining solvent in the sample was removed by freeze-drying overnight.

A Bruker 200 MHz Avance solid state NMR spectrometer equipped with a 3.2 mm Bruker double resonance probe-head and magic-angle spinning at a frequency of 18 kHz were used for all experiments. Silica NPs (typically 7-9 mg) were placed in Bruker zirconia sample rotors which were weighed on a microgram scale, alongside two additional spacers (delrin) and the Vespel drive tip.

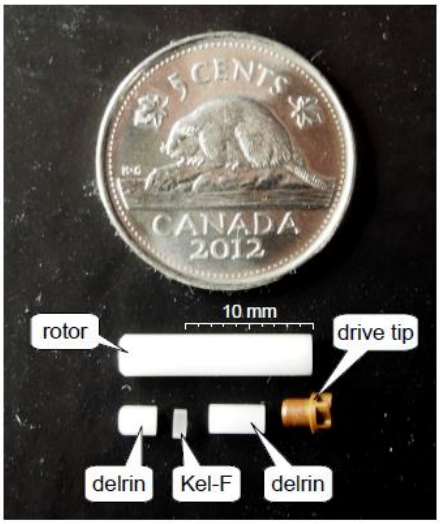

The probe was manually tuned prior to every measurement utilizing the ‘wobb’ function for ^{13}C and ^{19}F nuclei. Quantitative NMR measurements were performed with an external calibrant, 3,5-bis-(trifluoromethyl)-benzoic acid (BTFMBA), which was measured either before or after each analyte measurement on consecutive days.

We employed the ERETIC (Electronic REference To access In vivo Concentrations) and EASY (Elimination of Artifacts in NMR Spectroscopy) methods.[17, 18] A relaxation delay of 20.89 s and a spectral width of 100 kHz were used for all experiments. We co-added 3328 individual transients with 4096 complex data points and identical receiver gain. The 90º pulse was optimized prior to each experiment, typically found between 2.3 and 2.5 µs.

After measurements were performed, the rotor assemblies were carefully cleaned first by mechanically removing the nanoparticles with a screw tool, flushed extensively with acetone, methanol and ethanol, and dried for ~3 hours in an 80ºC oven.

NMR signals were processed by complex Fourier transform, with spectral phasing (0^{th} and 1^{st} order). Baselines around peaks were individually corrected (as well as spinning sidebands) using a polynomial function.

With the processed NMR spectra, quantification of fluorine content and thus amine content was determined using equation (1) for mass fraction (purity) of the analyte BTFBA. The quantification method is thoroughly detailed in a publication in *Metroglia* by Brinkmann, Raza and Melanson:[18]

$$\omega_{ana} = \frac{I_{ana}}{I_{cal}} \frac{I_{cal}^{E}}{I_{ana}^{E}} \frac{P_{cal}}{P_{ana}} \frac{\omega_{cal} m_{cal}}{M_{cal}} \frac{M_{ana}}{m_{ana}}$$

$$= \underbrace{\left(\frac{I_{ana}}{I_{ana}^{E} P_{ana}} \frac{M_{ana}}{m_{ana}} \right)}_{I_{ana}^{norm}} \times \underbrace{\left(\frac{I_{cal}}{I_{cal}^{E} P_{cal}} \frac{M_{cal}}{m_{cal}} \right)^{-1}}_{I_{cal}^{norm}}$$

$$= I_{ana}^{norm} / I_{cal}^{norm},$$

where subscripts “ana” and “cal” refer to analyte and calibrant, respectively. I and I^{E} refer to the integrated intensity of the NMR resonance line and the ERETIC signal, respectively. m and M refer to mass and molar mass, respectively. P refers to the number of nuclei which contribute to the NMR resonance line (which is 6 in respect to the 6 fluorine nuclei in both the calibrant as well as the fluorine label). ω_{ana} and ω_{cal} refer to the mass fraction purity. The second line of the equation above is a grouping of terms to arrive at normalized molar intensities (I_{ana}^{norm} and I_{cal}^{norm}).

Rearrangement of equation (1) to arrive at concentration in units of (µmol/g):

$$c_{ana} = \left(\frac{I_{ana}}{I_{ana}^{E} P_{ana}} \Big/ \frac{I_{cal}}{I_{cal}^{E} P_{cal}} \right) \times \left(\frac{\omega_{cal} m_{cal}}{M_{cal}} / m_{ana} \right)$$

3.3 Results and Discussion

3.3.1 BTFBA Labelling of Aminated Silica Nanoparticles

Reaction with primary amines with 3,5-bistrifluoromethylbenzaldehyde (BTFBA) was motivated by previous works in our group involving labelling of aminated silica nanoparticles with trifluoroacetyl groups by reaction with trifluoroacetic acid (TFAA). Initial results indicated a high coupling yield, which was consistent with colorimetric assay results at the time. However, additional trials and repeats of the reaction yielded secondary and competing reactions which prevented quantification of the primary CF_3 peak in solid-state ^{19}F NMR spectra.

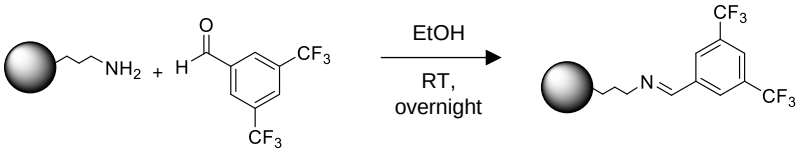

3,5-bistrifluoromethyl-benzaldehyde

The reaction scheme for BTFBA with aminated silica adapted reaction conditions from a publication by Macosko and others, who used the reaction for the quantification of aminated polymer groups in solution ^{19}F NMR.[19] The BTFBA label introduces two CF_3 groups for an improvement of sensitivity from the single CF_3 group in the trifluoro acetyl functionality. The amine group is converted to an imine. It is expected that the strongly

electronegative F atoms in BTFBA improve the electrophilicity of the aldehyde in comparison to 4-nitrobenzaldeyhde, due to the electron density withdrawn from the benzene ring. This is interesting to note when comparing the performance and coupling yields of the two labelling strategies.

Test reactions began with stirring aminated silica NPs overnight at a large excess of BTFBA (100-fold), which were comparable to the reaction conditions from the optimized 4-NBA assay. Multiple rounds of purification which required centrifugation and re-dispersion by bath sonication were done in accordance with the tests and optimization from the assay. Samples were freeze-dried overnight to ensure residual solvent would not interfere with solid-state NMR (MAS) measurements. Care was taken to ensure the sample was thoroughly dried as small imbalances in weight from a damp sample can result in costly damage to the probe at the high spinning frequencies required for the experiment (18 kHz).

3.3.2 Solid-state NMR Measurements on BTFBA-labelled Silica

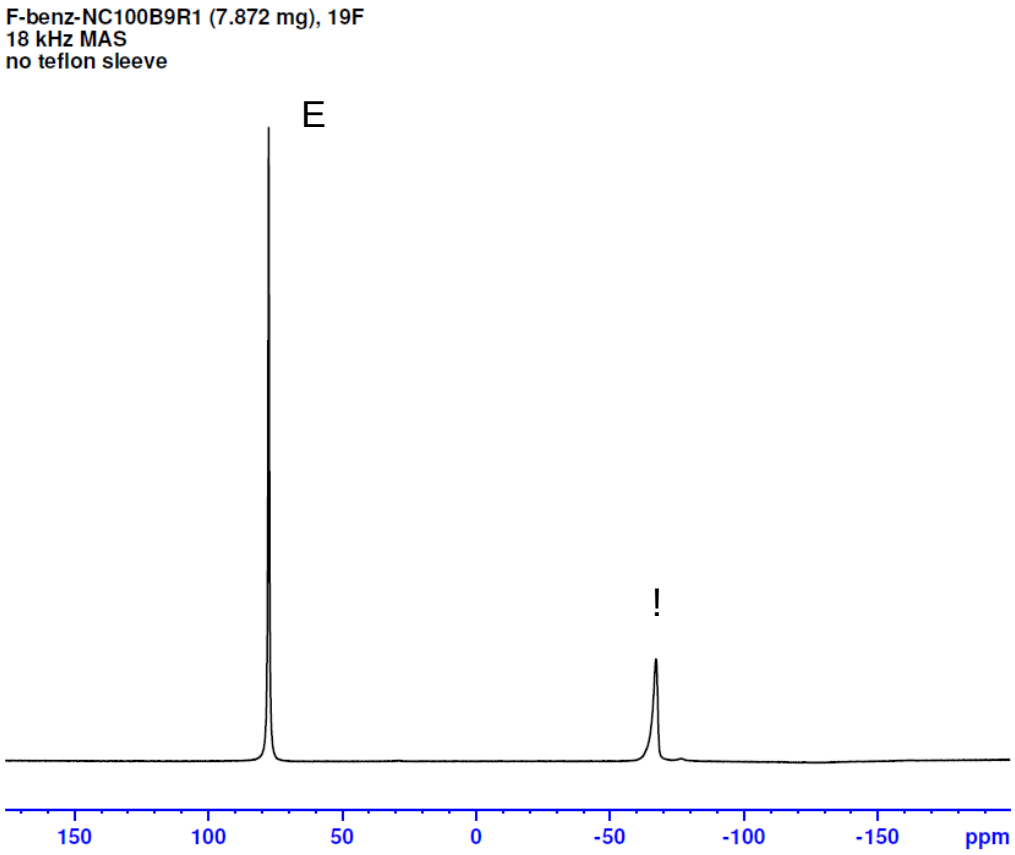

Figure 3-6*:* Representative Solid-state ^{19}F NMR MAS spectrum of BTFBA-labelled aminated silica nanoparticles (100 nm). (E) denotes the ERETIC signal which is electronically synthesized, while (!) denotes the peak attributed to the labelled CF_3 groups.

In **Fig. 3-6**, we can see a representative spectrum of BTFBA labelled aminated silica nanoparticles. The ERETIC signal (E) is the intense, sharp signal downfield from the peak corresponding to the analyte. The ERETIC method enables quantitative NMR without the use of internal standards, which is crucial when as much sample as possible is desired in the rotor to maximize signal. Having to divide the rotor for both internal standard and analyte would sacrifice at least half of the signal to noise. Centered roughly

at -65 ppm is the signal attributed to the rotor sample, within the characteristic range of CF_3 functionality. The spinning side-bands are not visible at this magnification.

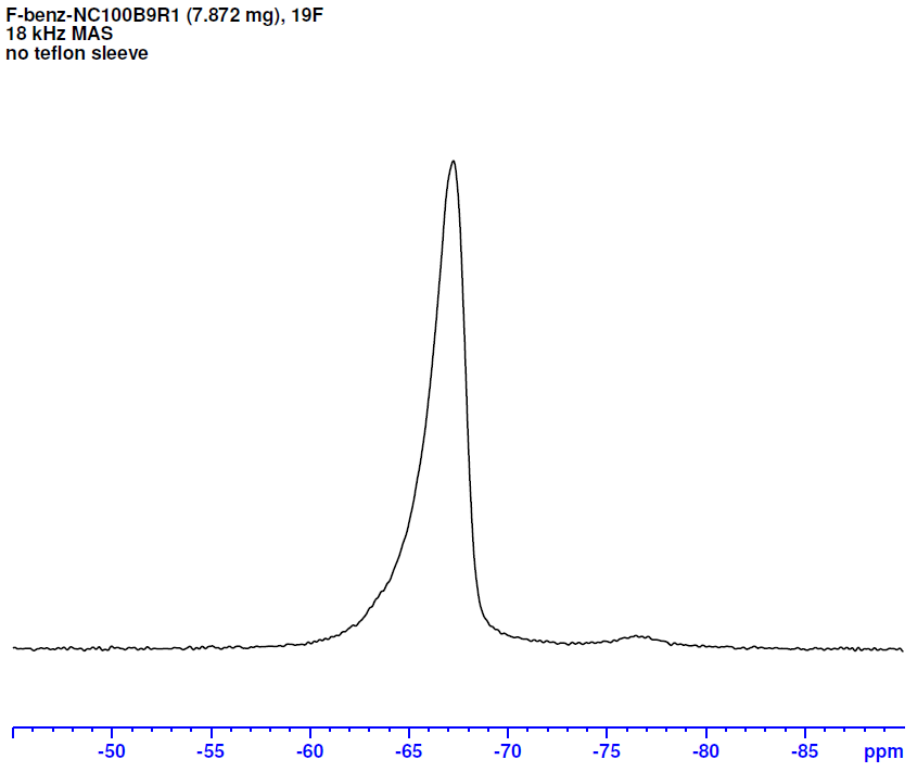

Figure 3-7*:* Solid-state ^{19}F NMR MAS spectrum of BTFBA-labelled aminated silica nanoparticles (100 nm). Zoomed in image of primary peak corresponds with previous spectrum.

Fig. 3-7 shows a magnified view of the CF_3 peak of the same sample shown in Fig. 8. Note the presence of a small feature upfield (approximately -77 ppm). Experiments were carried out to address the source of this additional peak which are explored in the following section "*Investigation of Impurity Peaks*".

3.3.3 Solid-State Quantitative ^{19}F NMR Experimentation

Quantitative NMR of BTFBA-labelled silica was performed with an external calibrant, 3,5-bis-(trifluoromethyl)-benzoic acid (BTFMBA). A representative spectrum is shown in **Fig. 3-8**. Tests were performed to study the stability and reproducibility of measurements with the external calibrant over a series of days.

Solid-state NMR instrumentation can be highly sensitive to temperature, humidity and in general perturbances from the laboratory environment. For our instrument, it was found that measurements of the standard were stable for multiple days.

For best practices, we elected to measure analytes within one to two days of measurement of the standard. In addition to the external calibrant BTFMBA, a synthesized reference signal was generated according to the ERETIC method, which serves as another reference value.[20] Ideally, an internal standard is combined with the analyte. However, considerations for matching the longitudinal relaxation time (T_1) for the two chemical species make choosing an internal standard non-trivial. Additionally, as previously stated, signal-to-noise and sensitivity of the technique, which are challenging to manage with a restricted rotor size, would be sacrificed to make space for the inclusion of a standard. The ERETIC method addresses this issue by generating a pseudo-FID that can be readily integrated and positioned outside the range of expected peaks attributed to analytes of interest. An FID or free induction decay is the signal that results from transverse magnetization, and is Fourier transformed to yield NMR spectra.

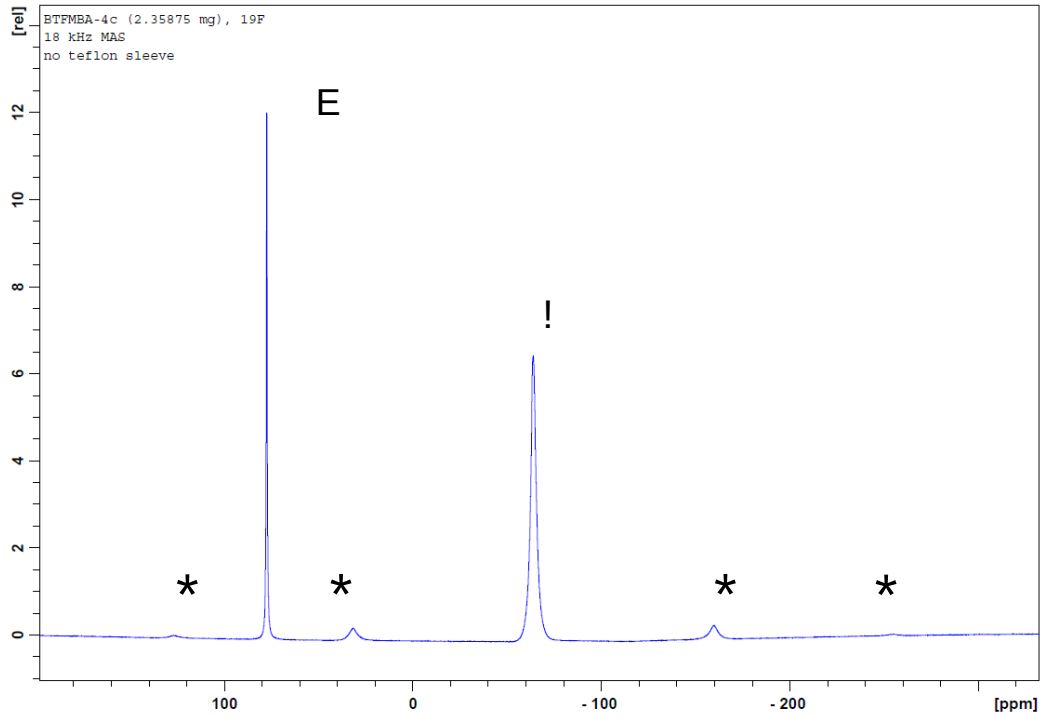

Figure 3-8*:* Representative Solid-state ^{19}F NMR MAS spectrum of external calibrant BTFMBA-4c. (E) denotes the ERETIC signal which is electronically synthesized, (!) denotes the peak attributed to the labelled CF_3 groups, and (*) denotes the spinning side-bands.

The experimental parameters (3328 individual transients recorded for every sample) were chosen for practical reasons, allowing for samples to be measured overnight.

To address the significant background that results from Teflon-coated parts in the solid-state NMR hardware and assembly, we applied the EASY method. Specifics on the pulse sequence can be found in a pair of publications detailing the method by Jaeger and Hemmann.[21,22]

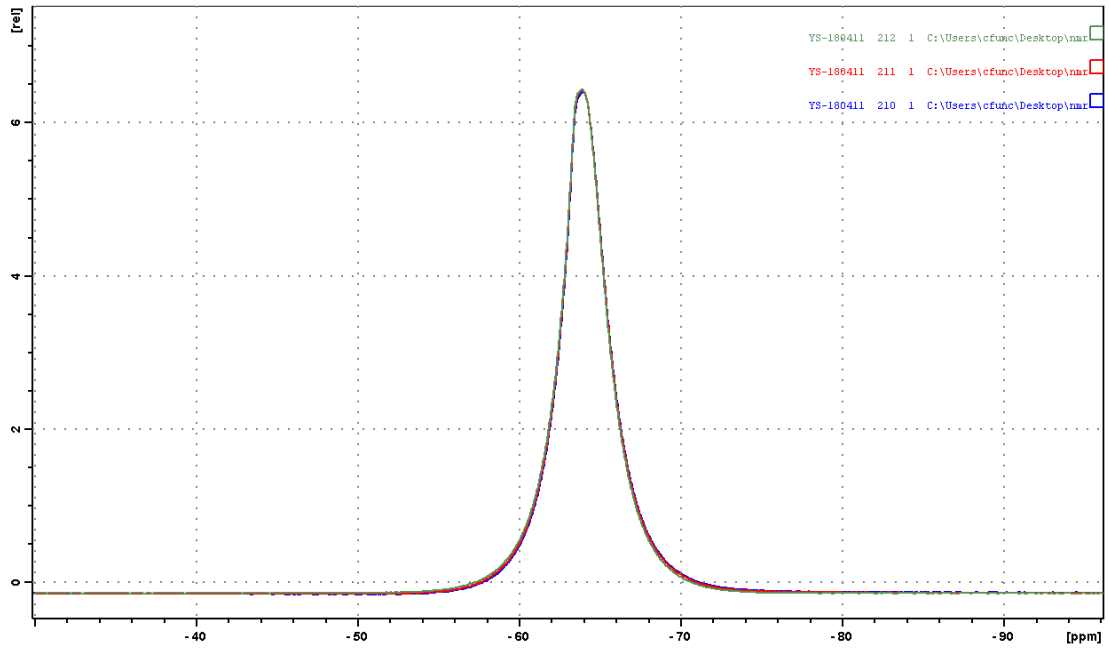

Figure 3-9*:* Solid-state ^{19}F NMR MAS spectrum of external calibrant BTFMBA-4c recorded over three days. Green, red and blue traces are measurements recorded on consecutive days.

The spectrum above shows the primary CF_3 peak of the external standard BTFMBA, measured across three consecutive days shown in the overlaid traces (in green, red and blue). The results point to the reproducibility and stability of the measurements over the course of multiple days.

3.3.4 Investigation of Impurity Peaks

An experiment was performed to address the presence of two secondary peaks that are upfield from the primary peak attributed to the CF_3 groups (located approximately -78 ppm and -82). To ascertain whether they originated from the reaction, we utilized a non-aminated (bare) sample as a control.

Bare silica nanoparticles (possessing only surface silanols) were subjected to BTFBA labelling reaction conditions, with the expectation that the absence of primary amine groups would prevent reaction, covalent bonding and assess whether non-specific binding of the BTFBA reagent was taking place. We can see in **Fig. 3-10**, that the bare silica NP successfully reproduced the secondary peaks. **Fig. 3-10** also visualizes the comparable amounts of fluorine content attributed to the secondary peak between the bare silica NP control and the amounts found in a similarly sized aminated silica NP.

This result suggests this peak is not caused by a side product in the reaction with amines which would interfere with determining functional group concentration. Possible options include that the broader peak at -78 ppm is an impurity within the reagent (96.5% purity via GC, Sigma Aldrich). Meanwhile, the sharper peak at -82 ppm is likely due to unremoved solvent from incomplete drying, as sharp features such as these are typically found with solution NMR spectra.

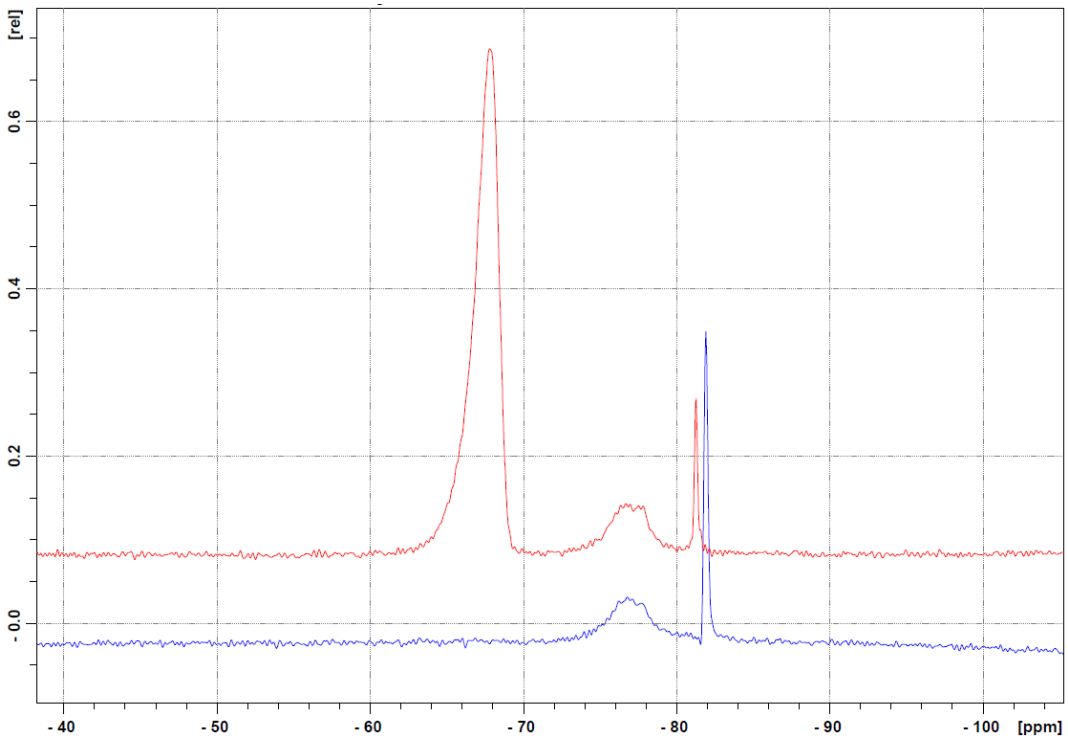

Figure 3-10*:* Solid-state ^{19}F NMR spectrum of BTFBA-labelled aminated silica nanoparticles (50 nm, red trace) and bare silica nanoparticles (50 nm, blue trace) which have been exposed to the same reaction conditions. The overlay serves to ascertain whether the impurity peaks (-78 and -82 ppm) are products of the reaction.

In **Table 3-1**, the impurity is assumed to contain (2 × CF_3) per molecule, and the corresponding amine quantification is shown of the integrated area of the peaks.

Table 3-1. Quantification of impurity peaks in comparison study.

Sample ID	Primary Peak (-68 ppm)	Secondary Peaks (-78 to -82 ppm)
50 nm bare silica NP control	-	4.65 µmol/g
50 nm NH_2 silica NP	40.3 µmol/g	6.50 µmol/g

Since the second peak is spaced sufficiently and does not overlap or interfere with quantification with the primary CF_3 peak, it was not included in determinations of primary amine concentration on the silica nanoparticles. Across the various particle sizes, it was found that the area of this secondary peak remained relatively stable and was not related to the area of the primary peak/concentration of primary amine in the sample. This is also consistent with this peak being due to an impurity in the reagent.

This is shown clearly in the case of one of the highest loadings of amine, in the 20 nm sample (spectrum in **Figure 3-11**). Amine concentration was determined as 379 µmol/g from the primary peak area integration. The secondary peak corresponding amine concentration was 6.71 µmol/g, which is again consistent with amounts found in the control experiment.

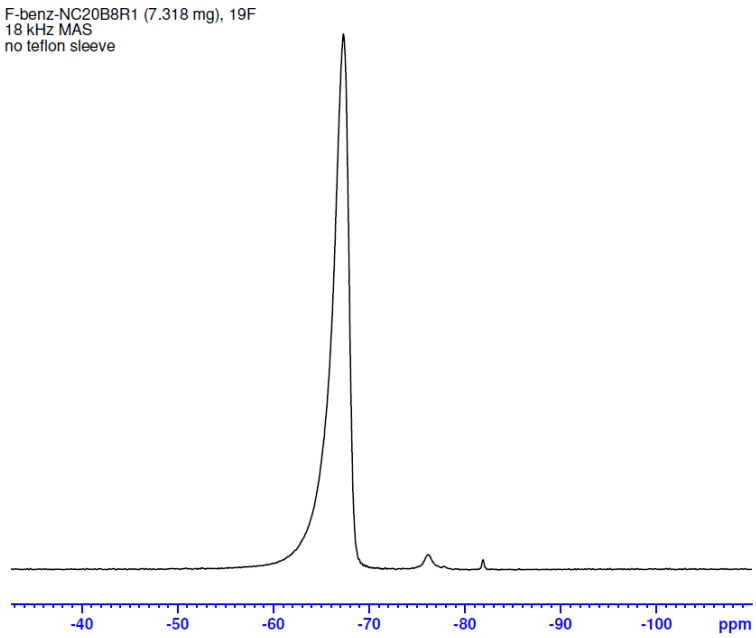

Figure 3-11: BTFBA labelled NH_2 silica nanoparticles, 20 nm. Primary CF_3 peak is shown, alongside secondary impurity peak. Amine concentration is 379 µmol/g and 6.71 µmol/g respectively.

3.3.5 Repeatability of BTFBA-labelling and Solid State NMR Method

We used a series of NPs studied by colorimetric assays for BTFBA-labeling and analysis by solid-state ^{19}F qNMR and XPS (Ch. 4). A range of particle sizes (20 to 100 nm) were selected, and each were analyzed by the two colorimetric assays, BTFBA labelled and quantified by solid-state NMR spectroscopy, and further evaluated by X-ray Photoelectron Spectroscopy (XPS) for additional compositional information.

As shown in the following table, the reaction with BTFBA was performed two times on the same batch of nanoparticles to study the reproducibility of the reaction conditions (noted as 1st and 2nd Replicates). We were pleased to see that the BTFBA labelling reaction was reproducible and yielded determinations with low variance.

Table 3-2. Surface amine quantification of silica nanoparticles by BTFBA labelling and solid-state ^{19}F NMR.

Sample	1st Replicate	2nd Replicate	Average[a] (µmol/g)
20 nm, B2	379	382	380 ± 1
50 nm, B3	39.9	40.3	40.1 ± 0.2
80 nm, B3	112	106	109 ± 3
100 nm, B3	131	119	125 ± 6

[a] Averages are based on replicate experiments for two independently prepared BTFBA-labelled samples for each NP size.

Centered roughly at -65 ppm is the signal attributed to the rotor sample, within the characteristic range of CF_3 functionality. The spinning side-bands are not visible at this magnification.

3.3.6 Comparison with Colorimetric Assays

A comparison of the two assays, the ^{19}F ss NMR approach and total amine content from solution-state qNMR is shown in **Fig. 3-12**. A table with the individual values for comparison is provided below for reference on reproducibility of the assays and NMR methods.

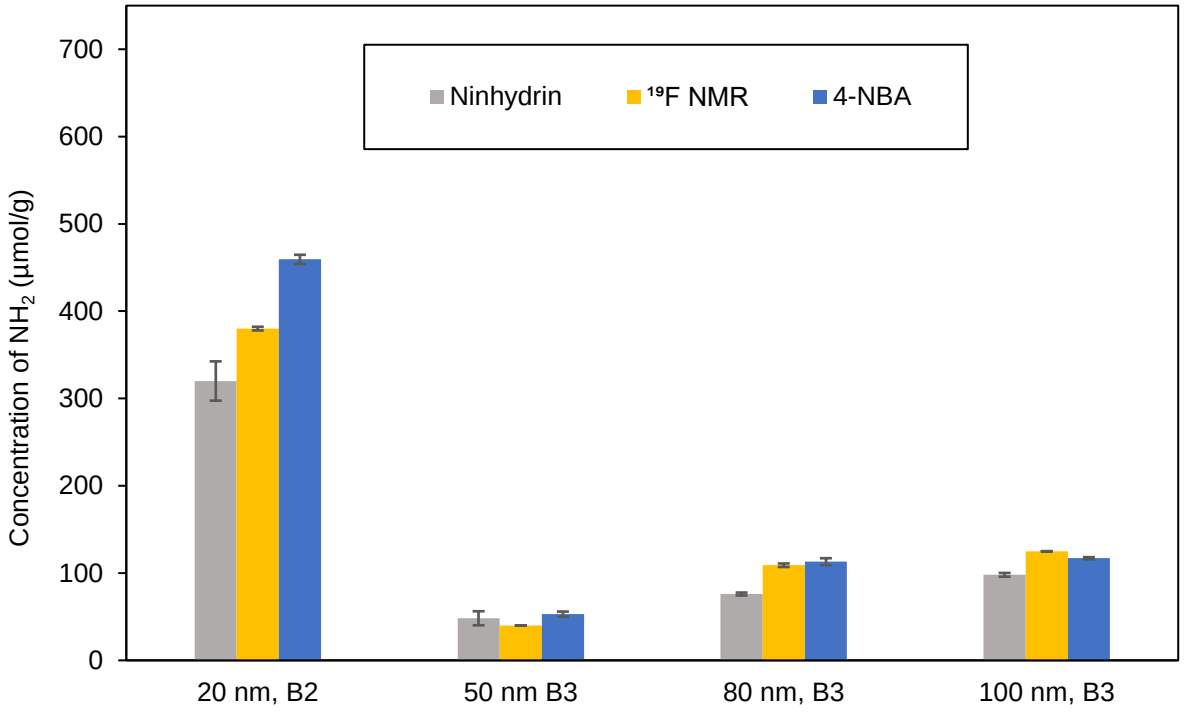

Figure 3-12: Comparison of colorimetric assays Ninhydrin and 4-NBA with BTFBA labelling and solid-state ^{19}F NMR method. Number of replicates ranging from 6-9 in the two assays, while BTFBA labelling is an average of two.

Table 3-3. Amine quantification by Ninhydrin, 4-Nitrobenzaldehyde, and Solid-state ^{19}F qNMR on a series of aminated silica nanoparticles. Number of replicates ranging from 6-9 in the two assays, while BTFBA labelling is an average of two. Values correspond to **Fig. 3-12**.

	Ninhydrin assay (*µmol/g)*	4-Nitrobenzaldehyde assay (*µmol/g)*	^{19}F ss NMR (*µmol/g)*
20 nm, B2	320 ± 20	459 ± 5	380 ± 1
50 nm, B3	48 ± 8	53 ± 3	40.1 ± 0.2
80 nm, B3	76 ± 2	113 ± 4	109 ± 3
100 nm, B3	98 ± 2	117 ± 1	125 ± 6

The determinations of surface amine content by solid-state NMR and BTFBA labelling are in good agreement with the results obtained for the ninhydrin and 4-NBA assays.

Notably, the two aldehyde-based assays both report higher surface amines in comparison to the ninhydrin assay. While we expected the ninhydrin assay to have a higher coupling efficacy due to its unique dye production mechanism, it appears that steric hindrance plays a lesser role in the reactivity of the assays in our case. In two sizes, 80 and 100 nm, the aldehyde-based assays are nearly matched. In the 20 nm, the differences in the coupling/labelling are much more pronounced, with an apparent gap in the amine determinations.

The solid-state NMR method also compares well in sensitivity, as the given conditions (3328 co-added transients) provide a limit of quantification of 3 µmol of

amine/g of silica (see the average of LOQ in **Table 3-4**), which is well below the concentrations found in any of our commercial samples.

Table 3-4. Signal-to-noise for BTFBA-labelled aminated silica nanoparticles measured by the solid-state qNMR method, organized by individual replicates. Limit of detection (LOD) is the mass required for a signal to noise ratio of 3, while limit of quantification (LOQ) is mass required for a signal to noise ratio of 10 for the given experimental conditions.

	S/N (per µmol NH_2/g silica)	LOD (µmol NH_2/g silica)	LOQ (µmol NH_2/g silica)
20 nm Rep 1	1014.26	1.121	3.737
50 nm Rep 1	150.67	0.794	2.648
80 nm Rep 1	419.84	0.800	2.668
100 nm Rep 1	320.58	1.226	4.086

	S/N (per µmol NH_2/g silica)	LOD (µmol NH_2/g silica)	LOQ (µmol NH_2/g silica)
20 nm Rep 2	1157.22	0.990	3.301
50 nm Rep 2	171.87	0.703	2.345
80 nm Rep 2	359.99	0.883	2.945
100 nm Rep 2	367.71	0.971	3.236

Average	-	0.9362 ±0.1764	3.121 ±0.5879

Note that the method's signal to noise encompasses multiple sensitivity contributions, such as the fluorine nuclei's magnetic resonance properties, the amount of BTFBA labelled onto the sample, the amount of sample which will fit into the rotor,

and the number of transients which are co-added. Therefore, the signal to noise can increase and decrease depending on conditions selected such as total experimental time, and instrumental considerations, such as strength of magnetic field and rotor size and type.

3.4 Conclusion

The combined BTFBA labelling and ^{19}F solid-state NMR quantification approach is non-destructive, demonstrates good reproducibility and helps to address concerns and limitations in the colorimetric assays. Since both colorimetric assays are performed in solution and elevated temperatures, nanoparticle stability and aggregation state are a concern during the measurement. Although the BTFBA labelling reaction does occur in solution, the rest of the method involves the handling of dry nanoparticles and does not involve these issues.

Furthermore, the protocol establishes a straightforward chemistry that can be extended to introducing other functionalities, potentially useful for deeper studies on surface structure on silica. Chemical derivatization can be useful for both homonuclear and heteronuclear correlation spectroscopic methods, which have been previously used effectively to study spatial distribution of silanols within nanoscale silica.[23] The high coupling yield of the reaction and its adaptation for surface quantification of chemical groups on silica nanoparticles is an advancement towards a highly reliable and traceable method, necessary for the design of reference materials and standards.[24]

3.5 References

(1) Marchetti, A.; Chen, J.; Pang, Z.; Li, S.; Ling, D.; Deng, F.; Kong, X. Understanding Surface and Interfacial Chemistry in Functional Nanomaterials via Solid-State NMR. *Adv. Mater.* **2017**, *29* (14). https://doi.org/10.1002/adma.201605895.

(2) Baccile, N. *Application of Advanced Solid-State NMR Techniques to the Characterization of Nanomaterials: A Focus on Interfaces and Structure*; 2010. https://doi.org/10.1002/9783527630530.ch6.

(3) Blümich, B. *Essential NMR: For Scientists and Engineers*; 2005. https://doi.org/10.1007/b138660.

(4) Levitt, M. . *Spin Dynamics: Basics of Nuclear Magnetic Resonance*; 2000. https://doi.org/10.1002/cmr.a.20130.

(5) Slowing, I. I.; Trewyn, B. G.; Giri, S.; Lin, V. S.-Y. Mesoporous Silica Nanoparticles for Drug Delivery and Biosensing Applications. *Adv. Funct. Mater.* **2007**, *17* (8), 1225–1236. https://doi.org/10.1002/adfm.200601191.

(6) Popat, A.; Hartono, S. B.; Stahr, F.; Liu, J.; Qiao, S. Z.; Lu, G. Q. Mesoporous Silica Nanoparticles for Bioadsorption, Enzyme Immobilisation, and Delivery Carriers. *Nanoscale* **2011**, *3* (7), 2801–2818. https://doi.org/10.1039/c1nr10224a.

(7) Slowing, I. I.; Vivero-Escoto, J. L.; Trewyn, B. G.; Lin, V. S. Y. Mesoporous Silica Nanoparticles: Structural Design and Applications. *J. Mater. Chem.* **2010**, *20* (37), 7924–7937. https://doi.org/10.1039/c0jm00554a.

(8) Trewyn, B. G.; Slowing, I. I.; Giri, S.; Chen, H.; Lin, V. S. Synthesis and Functionalization of a Mesoporous Silica Nanoparticle Based on the Sol–Gel Process and Applications in Controlled Release. *Acc. Chem. Res.* **2007**, *40* (9), 846–853. https://doi.org/10.1021/ar600032u.

(9) Liu, J.; Feng, X.; Fryxell, G. E.; Wang, L. Q.; Kim, A. Y.; Gong, M. Hybrid Mesoporous Materials with Functionalized Monolayers. *Adv. Mater.* **1998**, *10* (2),

161–165. https://doi.org/10.1002/(SICI)1521-4095(199801)10:2<161::AID-ADMA161>3.0.CO;2-Q.

(10) Luechinger, M.; Prins, R.; Pirngruber, G. D. Functionalization of Silica Surfaces with Mixtures of 3-Aminopropyl and Methyl Groups. *Microporous Mesoporous Mater.* **2005**, *85* (1–2), 111–118. https://doi.org/10.1016/j.micromeso.2005.05.031.

(11) Heydari-Gorji, A.; Belmabkhout, Y.; Sayari, A. Polyethylenimine-Impregnated Mesoporous Silica: Effect of Amine Loading and Surface Alkyl Chains on CO2 Adsorption. *Langmuir* **2011**, *27* (20), 12411–12416. https://doi.org/10.1021/la202972t.

(12) Huh, S.; Wiench, J. W.; Yoo, J. C.; Pruski, M.; Lin, V. S. Y. Organic Functionalization and Morphology Control of Mesoporous Silicas via a Co-Condensation Synthesis Method. *Chem. Mater.* **2003**, *15* (22), 4247–4256. https://doi.org/10.1021/cm0210041.

(13) Trébosc, J.; Wiench, J. W.; Huh, S.; Lin, V. S. Y.; Pruski, M. Solid-State MMR Study of MCM-41-Type Mesoporous Silica Nanoparticles. *J. Am. Chem. Soc.* **2005**, *127* (9), 3057–3068. https://doi.org/10.1021/ja043567e.

(14) Mao, K.; Kobayashi, T.; Wiench, J. W.; Chen, H. T.; Tsai, C. H.; Lin, V. S. Y.; Pruski, M. Conformations of Silica-Bound (Pentafluorophenyl)Propyl Groups Determined by Solid-State NMR Spectroscopy and Theoretical Calculations. *J. Am. Chem. Soc.* **2010**, *132* (35), 12452–12457. https://doi.org/10.1021/ja105007b.

(15) Kobayashi, T.; Singappuli-Arachchige, D.; Slowing, I. I.; Pruski, M. Spatial Distribution of Organic Functional Groups Supported on Mesoporous Silica Nanoparticles (2): A Study By1H Triple-Quantum Fast-MAS Solid-State NMR. *Phys. Chem. Chem. Phys.* **2018**, *20* (34), 22203–22209. https://doi.org/10.1039/c8cp04425b.

(16) Rossini, A. J. Materials Characterization by Dynamic Nuclear Polarization-

Enhanced Solid-State NMR Spectroscopy. *J. Phys. Chem. Lett.* **2018**, *9* (17), 5150–5159. https://doi.org/10.1021/acs.jpclett.8b01891.

(17) Xu, Z.; Liu, C.; Zhao, S.; Chen, S.; Zhao, Y. Molecular Sensors for NMR-Based Detection. *Chem. Rev.* **2019**, *119* (1), 195–230. https://doi.org/10.1021/acs.chemrev.8b00202.

(18) Brinkmann, A.; Raza, M.; Melanson, J. E. Metrologically Traceable Quantification of Trifluoroacetic Acid Content in Peptide Reference Materials by 19 F Solid-State NMR. *Metrologia* **2019**, *56* (2), 024002. https://doi.org/10.1088/1681-7575/ab04e3.

(19) Ji, S.; Hoye, T. R.; Macosko, C. W. Primary Amine (-NH 2) Quantification in Polymers: Functionality by 19F NMR Spectroscopy. *Macromolecules* **2005**, *38* (11), 4679–4686. https://doi.org/10.1021/ma050178b.

(20) Akoka, S.; Barantin, L.; Trierweiler, M.; Cnrs, L. U. Concentration Measurement by Proton NMR Using the ERETIC Method. **1999**, *71* (95), 2554–2557. https://doi.org/10.1021/ac981422i.

(21) Jaeger, C.; Hemmann, F. EASY : A Simple Tool for Simultaneously Removing Background , Deadtime and Acoustic Ringing in Quantitative NMR Spectroscopy . Part II : Improved Ringing Suppression , Application to Quadrupolar Nuclei , Cross Polarisation and 2D NMR . *Solid State Nucl. Magn. Reson.* **2014**, *63–64*, 13–19. https://doi.org/10.1016/j.ssnmr.2014.08.001.

(22) Jaeger, C.; Hemmann, F. EASY : A Simple Tool for Simultaneously Removing Background , Deadtime and Acoustic Ringing in Quantitative NMR Spectroscopy — Part I : Basic Principle and Applications. *Solid State Nucl. Magn. Reson.* **2014**, *57–58*, 22–28. https://doi.org/10.1016/j.ssnmr.2013.11.002.

(23) Lee, D.; Monin, G.; Duong, N. T.; Lopez, I. Z.; Bardet, M.; Mareau, V.; Gonon, L.; De Paëpe, G. Untangling the Condensation Network of Organosiloxanes on Nanoparticles Using 2D29Si-29Si Solid-State NMR Enhanced by Dynamic Nuclear Polarization. *J. Am. Chem. Soc.* **2014**, *136* (39), 13781–13788.

https://doi.org/10.1021/ja506688m.

(24) Hennig, A.; Dietrich, P. M.; Hemmann, F.; Thiele, T.; Borcherding, H.; Hoffmann, A.; Schedler, U.; Jäger, C.; Resch-Genger, U.; Unger, W. E. S. En Route to Traceable Reference Standards for Surface Group Quantifications by XPS, NMR and Fluorescence Spectroscopy. *Analyst* **2015**, *140* (6), 1804–1808. https://doi.org/10.1039/c4an02248c.

Chapter 4: X-Ray Photoelectron Spectroscopy

The results in this chapter appear in the following publication. Maohui Chen assisted in the optimization of the sample preparation and Oltion Kodra performed the XPS measurements. My contribution was in the preparation of samples and analysis of XPS data with the supervision of Dr. Lopinski.

Sun, Y.; Kunc, F.; Balhara, V.; Coleman, B.; Kodra, O.; Raza, M.; Chen, M.; Brinkmann, A.; Lopinski, G.; Johnston, L. Quantification of Amine Functional Groups on Silica Nanoparticles: A Multi-Method Approach. *Nanoscale Adv.* **2019**. https://doi.org/10.1039/C9NA00016J.

4.1. Background

X-ray Photoelectron Spectroscopy (XPS) is one of the most frequently used spectroscopy techniques for the study of functionalized surfaces and thin films. Also known as electron spectroscopy for chemical analysis (ECSA), it is a semi-quantitative technique for chemical analysis of materials based on the photoelectric effect. It is commonly used to determine surface elemental composition through fingerprinting of unique photoemission peaks, provide information on the local chemical environment (i.e. chemical shift), and semi-quantitatively determine the concentration of surface chemical species.

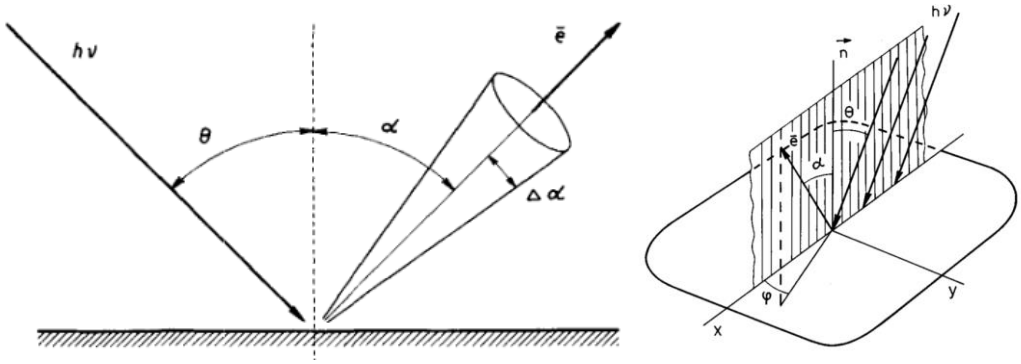

Figure 4-1: Schematic outlines of the configuration of an XPS experiment. On the right, the shaded plane indicates the incident X-ray plane. Images from references (1,2)

Principally, XPS involves the irradiation of a solid sample (i.e. nanomaterial) by monochromatic x-rays to achieve ionization of a core-level electron and photoemission. A simplified, general scheme is shown in **Fig. 4-2**. Koopman's theorem relates orbital energies (ε) to the ionization energy (E_i) of the residing electrons. The photoemitted electron possesses a distinct kinetic energy (E_k) that corresponds to the specific element's unique set of core level binding energies (E_b) and is attenuated by the work

function (ϕ). The work function is commonly broken down into contributions from the spectrometer and the surface potential of the material. XPS instruments contain spherical or hemispherical energy analyzers, which measure a distribution of electrons with respective E_k's to generate a photoemission spectrum.

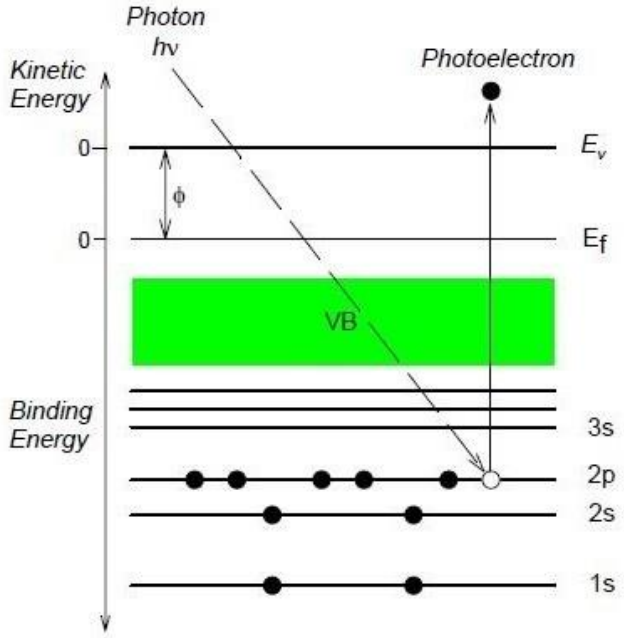

Figure 4-2: Photoemission energy diagram.

$$E_i = -\varepsilon$$

$$h\nu = E_b + \frac{1}{2}mv^2 + \phi$$

$$h\nu = E_b + E_k + \phi$$

$$E_b = h\nu - E_k + \phi$$

Distinct chemical environments and bonding states give rise to unique binding energies, allowing for identification of atomic compositions, functional groups and oxidation state. Fine structure, which can be studied from high-resolution spectra of

regions of interest, allows for deeper chemical analyses. Spin-orbit-splitting (SOS) effects result in the presence of doublets with specific structure and area ratios. Magnetic moment of the spin (s) and orbital angular momentum (l) when coupled result in total angular momentum (j).

$$j = l + s$$

Ionization and successful detection of photoemitted electrons is highly dependent on the inelastic mean free path (IMFP, λ). The sampling depth and sensitivity of XPS is not restricted by the penetration depth of the x-rays (which can typically extend well past 1 mm), but rather the escape depth of the photoelectrons. Secondary scattering effects which are inelastic in nature prevent the escape of electrons without energy loss, which result in reduced E_k. The attenuation length, described in the wavelengths (λ) of the electrons is described by the Beer-Lambert Law: $I(x)$, and the probability of the finding an electron at depth (x) in the material:

$$I(x) = I_o e^{-x/\lambda}$$
$$P(x) = I/I_o = e^{-x/\lambda}$$

Where $I_o$is the intensity of the emitted electron, and I is the intensity of the escape electron.

The exponential relationship shows that the sampling depth of XPS is restricted to 3λ, where 95% of all electrons are scattered by the time they reach the surface. Since typical wavelengths of an Al Kα x-ray source range from 1 to 3.5 nm, the often cited 3-10 nm sampling depth results from the 3λ term. This explains the inherent surface-sensitivity of XPS.

For semi-quantitative elemental analysis of surfaces, it is possible to integrate the photoemission peak areas to determine stoichiometry, providing information relating to relative amounts of chemical species. One of the primary challenges in this endeavor is addressing the large, inelastic, step-like background which is characteristic to XPS spectra. Typically, background subtraction requires a decision between linear, or Shirley and Tougaard algorithm methods.

Linear background subtractions are suitable when there is little variation in the shape and structure of the background over the width of the peak. However, in instances where the peak of interest spans a background which is changing or stepwise, the integral or Shirley algorithm is more accurate for corrections. The final choice for background subtraction is the Tougaard algorithm, which addresses the inelastic electron scattering by using an energy loss cross-section, most frequently the "universal cross-section", which is a general-use parameter and carries with it a broad approximation.[3,4]

In a comparative study of the techniques by Lahtinen et al., they noted that frequently, none of the methods is sufficient or correct for all cases, and that an analysis of relative uncertainties is recommended.[5] This underscores the reputation of XPS as a "semi-quantitative" technique, as a significant amount of variability can arise from background contributions and subsequent analysis.

A visualization of linear and Shirley, a popular fitting algorithm, methods for background subtraction is shown in **Fig. 4-3.**

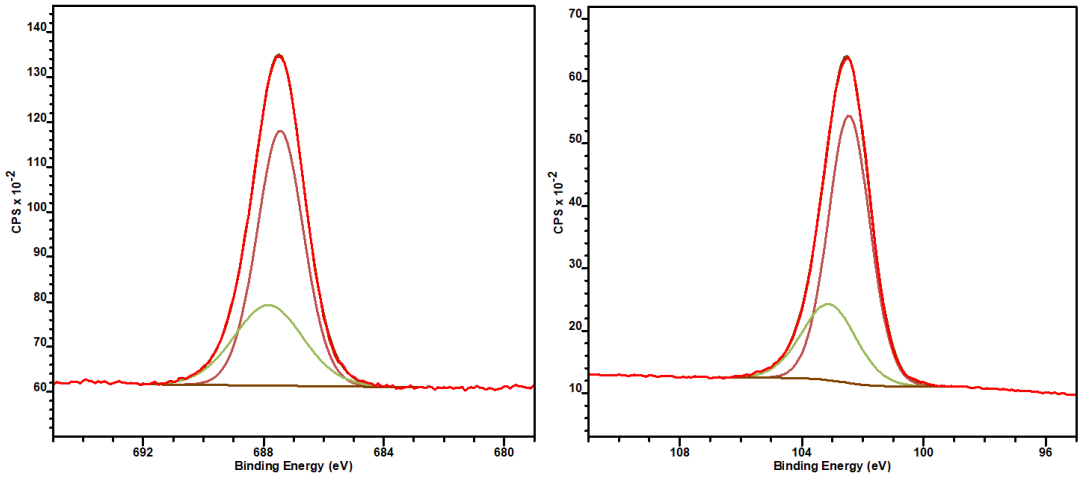

Figure 4-3: Comparison of background subtraction techniques. (Left) is the flourine 1s core-level photoemission peak with a linear background. (Right) is a comparison with silicon 2p peak, with a Shirley background subtraction. The additional overlapping peaks represent the two fitted components to the peak.

4.1.1 XPS for the Study of Functionalized Nanomaterials

In the last 20 years, as novel applications have shifted from studies of thin films towards complex nanostructures, XPS has remained a relevant and popular method of surface characterization. The technique's ability to rapidly assess the overall surface composition while still providing detail on local chemical environment make it well-suited to tackle emerging challenges in nanomaterials characterization.

In a comprehensive review published in 2013, Baer and others stressed "inadequate and incomplete characterization" plaguing studies and reports on the behaviors and properties of nanomaterials.[6] They cited the appropriate application of traditional spectroscopic methods such as XPS as a means to address these outstanding issues in nanomaterial research. Key examples include the instability of

nanomaterials in aqueous environments and solution, which showcases XPS' ability to assess formal oxidation state, which revealed the degradation and oxidization of ceria nanoparticles.[7] Furthermore, XPS's capability of broadly scanning for elemental composition extends its use in alerting researchers to the presence of contaminants. In a case where Cu-based particles were surface contaminated by a thin layer of fluorine, likely from PTFE products and their breakdown, the authors stressed the importance of preventing the fouling of surfaces by common labware materials.[6] Effective and wide-ranging characterization of nanomaterials is critical, especially when samples are meant to be the subject of toxicological studies.

In respect to the study of surface functional groups, XPS is often enabled by chemical derivatization, sometimes referred to as "derivatization XPS" or "CD-XPS". Coupling with UV-Vis/fluorescence spectrometry techniques is also commonplace.[8–12] The sampling depth and surface sensitivity of the technique are ideal for the characterization and detection of surface functionalized nanomaterials.[13]

However, applying XPS quantitatively to study the surface of nanomaterials is a complex challenge, made more difficult when addressing nanoparticles with spherical curvature and complex morphologies.[14] Typically in quantitative XPS, experimental variables such as analyzer efficiency, inelastic mean free path, and atomic concentration of elements are addressed using sensitivity factors (or relative sensitivity factors, RSF). In this work, quantitative measurements implemented the Kratos Axis library of sensitivity factors integrated in the analysis software (CasaXPS) which accounts for the performance and efficiency of our instrument. For more physically realistic and accurate calculations, geometric considerations and modelling are the next

step, especially in complex, non-uniform nanomaterials. Assumptions made on structural homogeneity and distribution of atoms in relative sensitivity factors fall short in cases of layered, porous and surface coated materials.

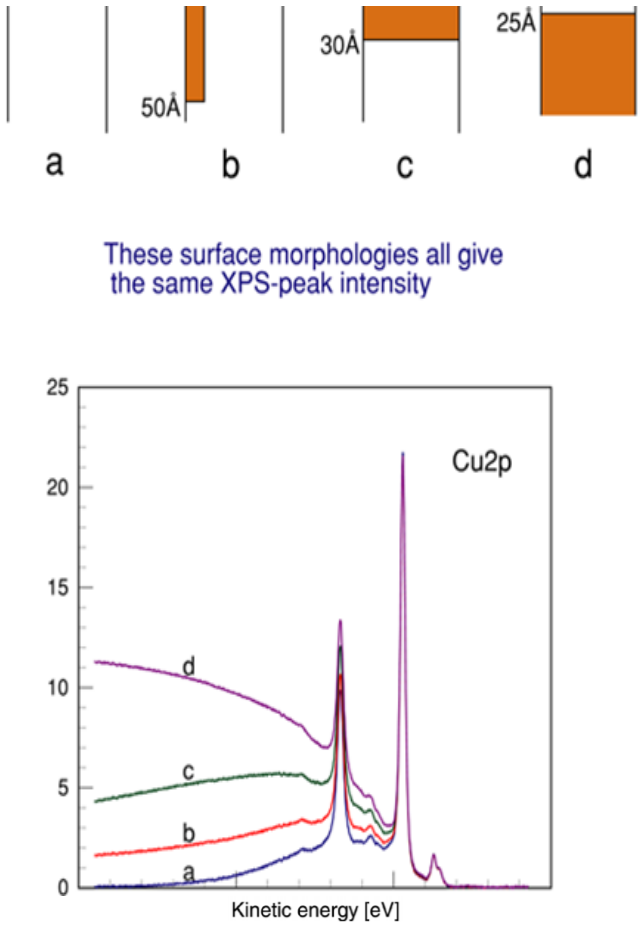

Figure 4-4: Simulated XPS spectra depicting how the different surface morphologies in examples (a-d) affect the peak intensities and background. Note the effects in the background signal. Image adapted from the QUASES User Manual (15).

As shown in the example in **Fig. 4-4**, the peak intensity of the Cu 2p doublet remains the same throughout all four surface distributions of copper, despite there being distinct differences in what would qualify as surface copper content between the examples (a-d). At lower binding energies, there are notable changes in the background

intensity indicating greater inelastic scattering and attenuation of electrons. This case study emphasizes the uncertainties and errors that can emerge in the analysis of surface species that may appear in complex and non-uniform materials. Quantitative integration of the photoemission peak of interest can clearly depend on a host of variables.

A good demonstration of XPS used for surface quantification on nanomaterials came from Hennig et al., who combined XPS with ^{19}F NMR for the study of polymer particles (PMMA core with a shell of PAA), which were surface fluorinated with 2,2,2-trifluoroethylamine (TFEA).[10] As shown in **Fig. 4-5**, the authors demonstrate XPS' ability to detect and quantify the chemical derivatization with TFEA in C 1s photoemission spectra. Although the agreement of the two methods was good in most cases, there were instances where relative error in quantification of the fluorine label was quite high (28% difference).

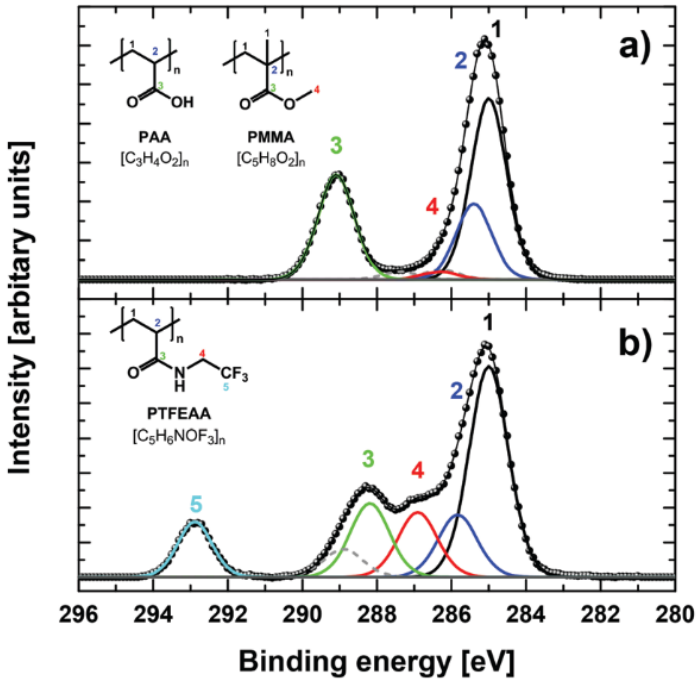

Figure 4-5. Carbon 1s spectra of polymer particles prepared by Hennig et al., who utilize XPS to monitor surface labelling with TFEA. a) shows the polymer particles prior, and b) after reaction.

The authors attributed these differences limitations to their XPS quantification method, as well as the intermediary thickness of the surface PAA layer and the depth restriction of XPS.

An example of interest for the study of silica surfaces came from Fischer et al., who utilized XPS to monitor the surface modification of silane films with a fluorescent label.[9] "Dual-modes" of analysis by fluorescence and XPS was enabled by the boron-dipyrromethene (BODIPY) fluorescent dye which also contained aromatic CF_3 groups. Various amino-functionalized SAMs were prepared with different silane coupling agents, which were then labelled and studied by the two characterization techniques. Although their work did not involve challenges associated with XPS analysis on nanoparticles,

they clearly demonstrated the potential of the technique in their approach. Excellent agreement was found between the two methods, as shown in **Fig. 4-6**, which compared the amino fraction of the films determined by XPS and fluorescence.

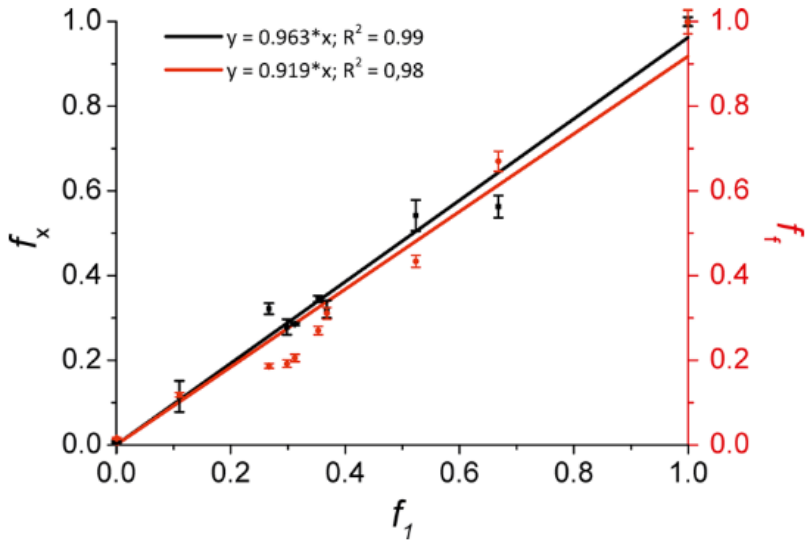

Figure 4-6. Amino fraction determined by XPS and fluorescence, in black and red axes respectively.

Shard and Castner have made significant contributions towards developing approaches to address non-uniform shell thicknesses and composition for applications of XPS on surfaces of nanoparticles. Their publications explore XPS as a method to determine surface *structure* as opposed to composition, by quantifying photoemission peaks which are attributable either to core or shell elements.[16–19] Thus, effective modeling of the structure and shape of nanoparticles, however simplified, is integral to the applicability and relevance of their methods.

There are now a variety of analytical codes which can help account for variations in size, shape, multi-layers and overlayers.[19] For example, the most recent version of

Simulation of Electron Spectra for Surface Analysis (SESSA), developed by the National Institute of Standards (NIST) was first demonstrated to effectively model experimental data with alkylated gold nanoparticles.[18] Along with other software packages such as QUASES-Tougaard, there are an increasing number of sophisticated options to help approximate and address specific challenges in surface analysis of nanomaterials with XPS.

XPS remains one of the most frequently used instrumental methods for its versatility, offering information on surface chemistry, environment, and even morphology and structure. While software techniques continuously refine and improve to allow for more accurate quantitative approaches, XPS can still provide detailed chemical information in a semi-quantitative manner.

We sought to apply XPS for the surface analysis of our silica nanoparticles before and after chemical modification with BTFBA. Following the example set forth by Hennig and others, the extent of surface functionalization with the fluorine label could then be determined by integration of photoemission spectra. The resulting coupling yields will help validate the surface quantification methods outlined in the previous chapters (colorimetric assays and solid-state NMR).

As previously mentioned, accessibility and reactivity of the surface functional groups may reduce the ability of labelling-based approaches. As a label-free technique, XPS can play a crucial role in helping us determine whether we are accounting for all chemical groups on the surface, or in fact, only those which are available for surface modification.

4.2 Experimental

XPS measurements on functionalized nanoparticles spin-coated onto gold were acquired by a Kratos Analytical Axis Ultra DLD spectrometer with monochromatized Al Kα X-rays. Au substrates (Arandee, Germany, 12 x 12 mm) were rinsed with dichloromethane, isopropyl alcohol, Milli-Q H_2O and then Piranha cleaned (3:1, H_2SO_4:H_2O_2) for two minutes. After extensive rinsing with water (>1 L) to remove residual Piranha and solvent, substrates were then dried with N_2 and ozone treated for 30 minutes.

The series of aminated silica nanoparticles which were BTFBA-labelled and studied by colorimetric assays and solid-state ^{19}F qNMR were the principal samples of interest, alongside their non-labelled forms which were used as controls. Nanoparticle suspensions (5 mg/mL) were prepared in methanol via bath sonication for 30 minutes and briefly sonicated prior to spin-coating on cleaned Au substrate. Spin coating was performed 3 times using 50 µL volumes to ensure sufficient coverage (each coating programmed to first 12 s 500 rpm, and 2 min. at 2000 rpm).

AFM imaging was performed to ensure even coverage; examples shown below in **Fig. 4-7**. Images were recorded with a NanoWizard II BioAFM (JPK Instruments, Germany) mounted on an Olympus IX91 inverted microscope (Olympus Corporation, Japan, and operating in tapping mode with a XSC11 (42 N/m) cantilever.

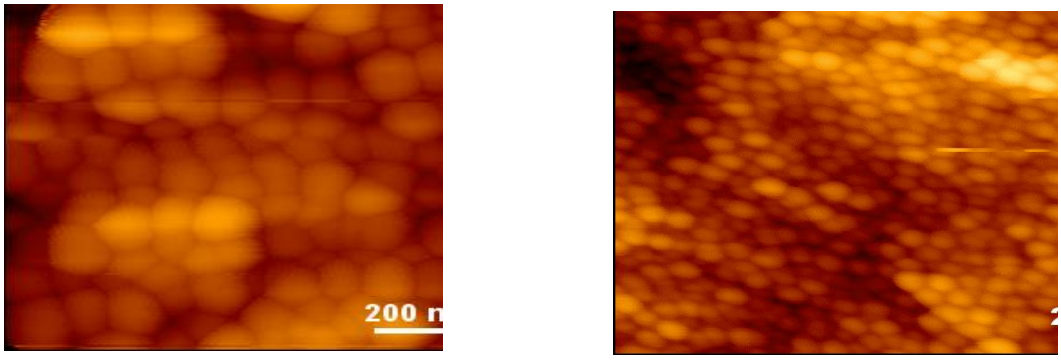

Figure 4-7: AFM images of 100 nm and 50 nm BTFBA-labelled NH_2 silica nanoparticles deposited on Au substrates on the left and right respectively.

XPS measurement scans were performed on three spots on each sample. Survey scans were measured to determine relative elemental composition and assess potential contaminants. High resolution spectra in regions which corresponded to core level transitions for relevant elements (C 1s, O 1s, N 1s, F 1s, Si 2p, Au 4f) in the sample were also acquired.

For quantitative analysis of the high-resolution spectra, CasaXPS analysis software and relative sensitivity factors (Kratos) were used. Peak integration was done with Shirley method for background subtraction for Au4f, Si2p, O1s, and linear background was chosen for N1s and F1s peaks. This was justified by the overall shape of the background, and whether it had a step-like structure, as opposed to a linear form. In the figure shown below, a high-resolution spectrum shows the position of the photoemission peak centered on a step-like background (note the differences in intensity between the two ends of the peak).

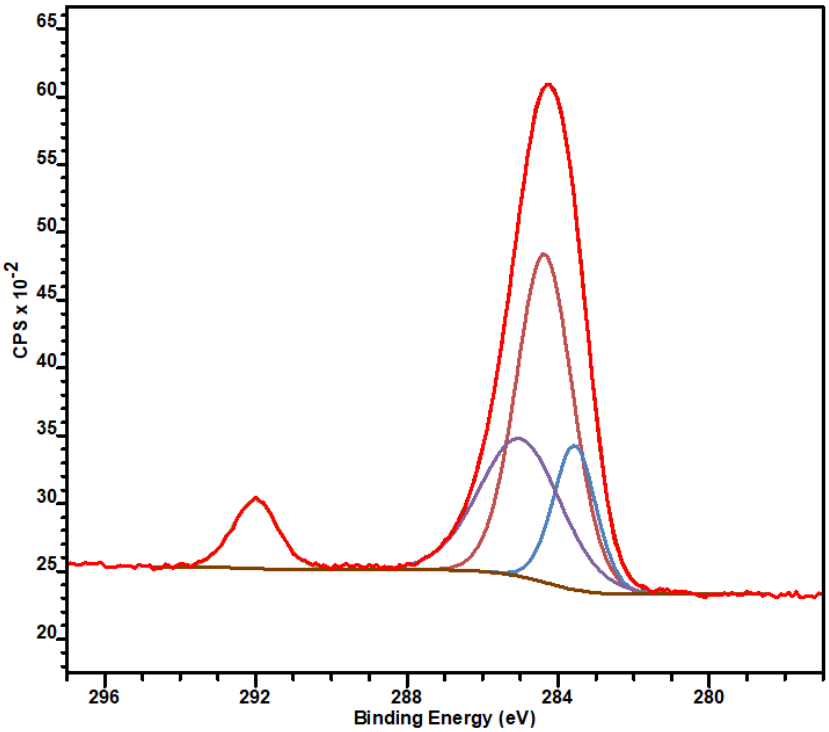

Figure 4-8: High-resolution spectrum of Si 2p showing an example of the Shirley background correction method, as well as the peak deconvolution for integration.

Additionally, considerations between choosing the area of the fitted component and total peak area lead us to choose the latter for peak quantification. A comparison of the two methods is shown in the following figure.

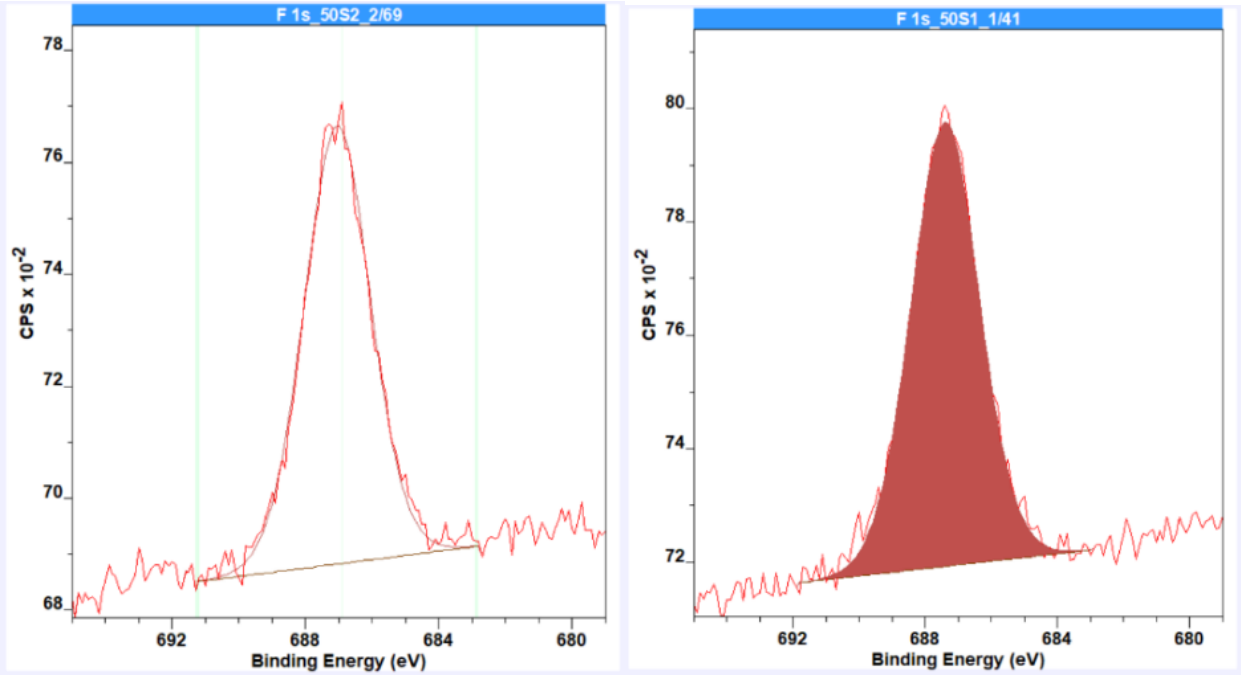

Figure 4-9: Comparison between (left) integration of total area and (right) fitted component.

4.3 Results and Discussion

4.3.1 Control Experiments

A series of control experiments were performed to study and determine the elemental composition of the bare gold substrate and aminated silica nanoparticles which were used for BTFBA labelling. It was necessary to quantify the levels of contamination for relevant elements such as nitrogen and fluorine that could not be removed though the cleaning process. Typically, multiple samples were measured by the XPS instrument in a series. BTFBA-labelled silica nanoparticles spin-coated onto gold were measured alongside bare gold substrate to ensure sets of experiments did not involve use of contaminated substrates. Some preliminary work was also done with

AFM imaging to optimize the spin-coating settings to ensure even coverage of the substrate with the particles.

The following spectra are representative of the measurements performed on a range of sizes of commercial aminated silica which appear in the following **Table 4-1** and **4-2**.

As shown in **Figure 4-10**, the survey spectrum (A) and high-resolution spectra indicate strong Au signals and the absence of silicon, as expected with the Au substrates prior to spin-coating of silica nanoparticles. In (C) and (D) we can see the presence of low levels of nitrogen and fluorine contamination of the surface.

Figure 4-11 depicts spectra of gold spin-coated aminated silica nanoparticles prior to their labelling with BTFBA. As expected, silicon and nitrogen elemental content increase, and the gold signal decreases accordingly. The amount of fluorine remains comparable to the concentrations seen in the non-spin coated gold substrate. This suggests that the aminated silica nanoparticle control does not contain appreciable surface fluorine content, and that the gold substrate is responsible for most of the fluorine contamination. This is important to address given the general use of PTFE (Teflon) in chemical laboratories, which would interfere with quantitative measurement of fluorine content.

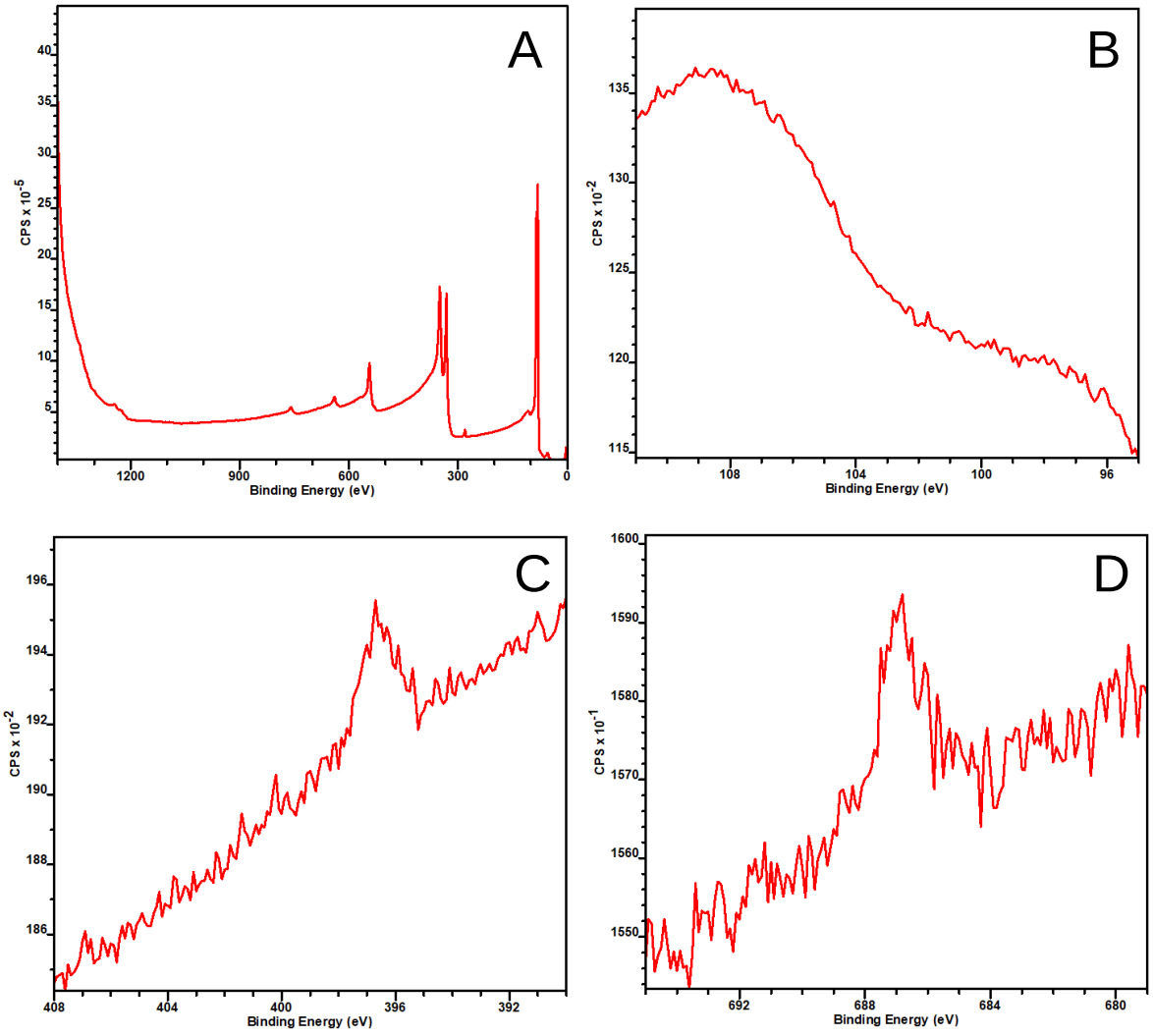

Figure 4-10: (A) XPS survey spectrum of bare gold substrate cleaned for coating with silica nanoparticles. (B - D) High resolution spectra for silicon, nitrogen and fluorine.

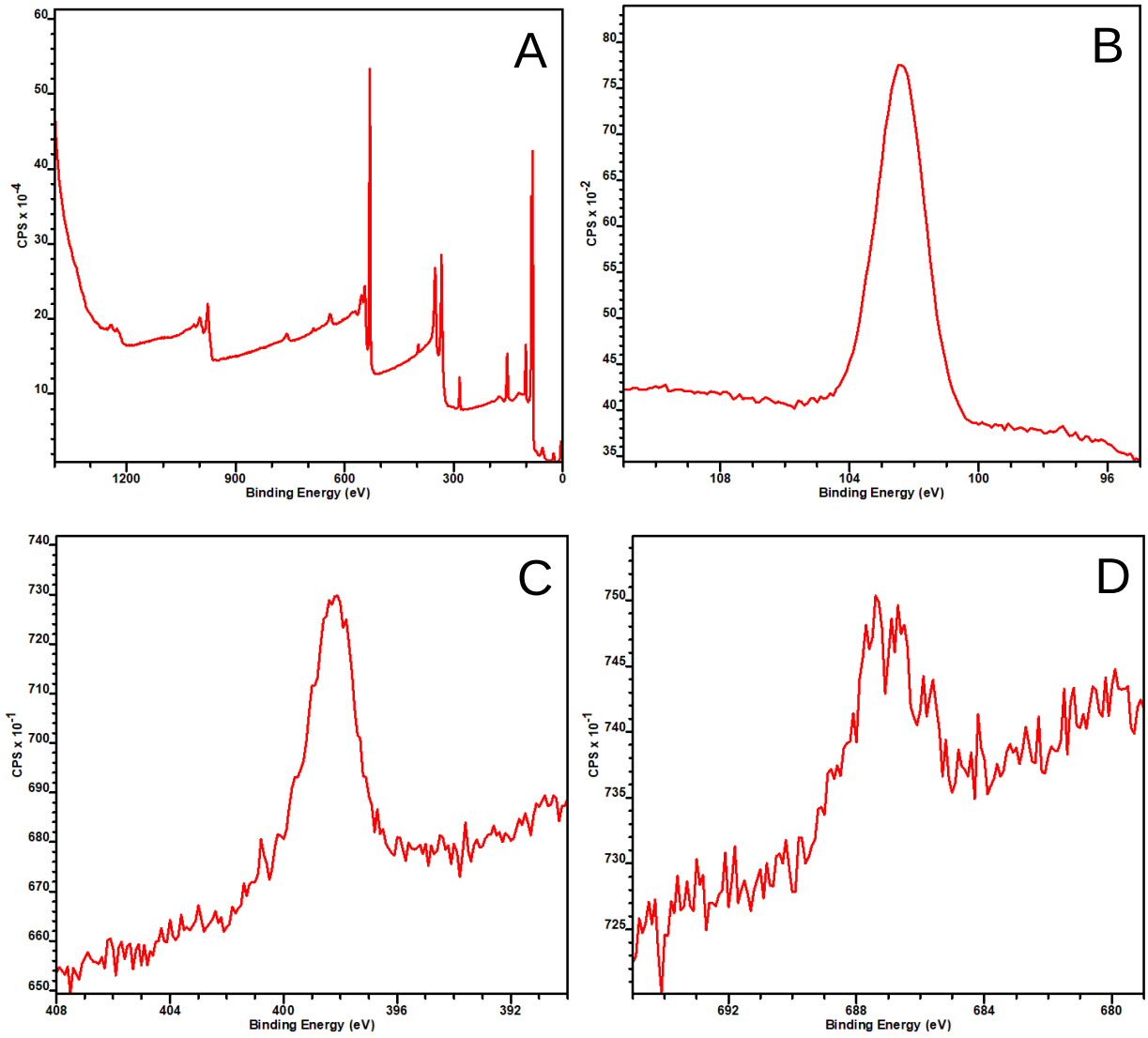

Figure 4-11: (A) XPS survey spectrum of aminated silica nanoparticles (100 nm) spin-coated onto gold substrate. (B - D) High resolution spectra for silicon, nitrogen and fluorine.

The final set of XPS spectra shown in **Fig. 4-12** and **4-13** represents the same commercial batch of 100 nm aminated silica nanoparticles which have been BTFBA-conjugated and spin-coated onto gold. Note the significant increase of fluorine content which indicates successful labelling of BTFBA in the high-resolution spectrum in (D).

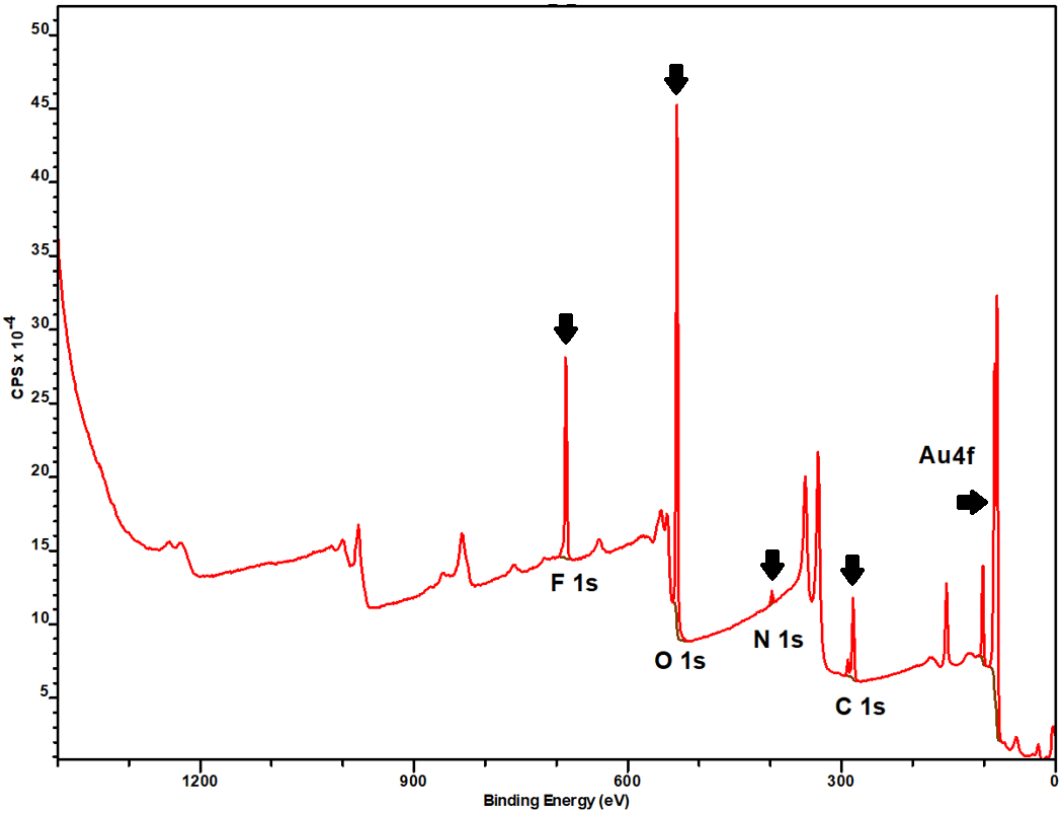

Figure 4-12: An example of a survey spectrum of a BTFBA-labelled aminated silica nanoparticle (100 nm). The F 1s (687 eV), O 1s (531 eV), N 1s (398 eV), C 1s (284 eV), and Au 4f (82 eV) regions are labelled.

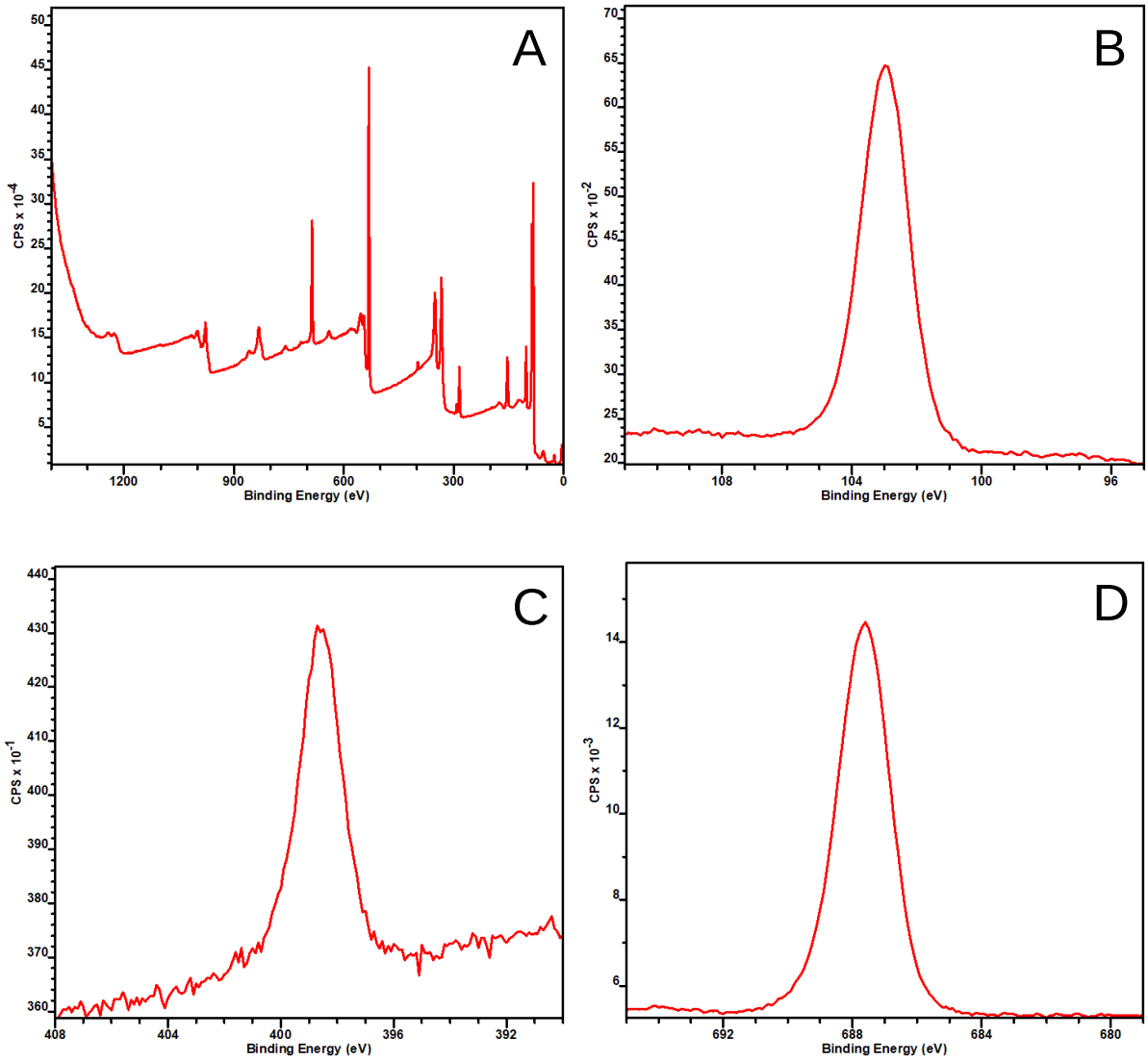

Figure 4-13: (A) XPS survey spectrum of BTFBA-labelled aminated silica nanoparticles (100 nm) spin-coated onto gold substrate. (B - D) High resolution spectra for silicon, nitrogen and fluorine.

Elemental ratios which are particularly relevant and provide feedback on the success and quality of the sample preparation are those involving Si, Au, C, and O. Si/O can be related to bulk silicate structures (SiO_2), and therefore should approximate 0.5, which is seen in **Table 4-1**. Au/Au (control) and Si/Au for example, can elucidate the degree of coverage of the silica nanoparticle suspension onto the gold substrate. The

first column of the table, Au/Au (control), compares the gold signal of samples with BTFBA-labelled particles with the clean gold substrate control. A lower value therefore corresponds to greater attenuation of the Au signal, which is principally determined by coverage by silica particles. This is further shown in the Si/Au ratios which match relatively well with the gold ratios. Although the total amount of coverage does not need to be stable for the results to be usable/valid, it is preferable to maintain a constant coverage of the substrate where possible.

Table 4-1. Additional relative atomic compositions relevant to sample preparation of BTFBA-labelled aminated silica samples. Au (control) annotates the bare, non-coated gold substrate control.

	Au/Au (control)	**Si/Au**
20 R1	0.03	1.51
20 R2	0.02	1.47
50 R1	0.21	0.26
50 R2	0.19	0.24
80 R1	0.35	0.08
80 R2	0.25	0.12
100 R1	0.19	0.16
100 R2	0.25	0.11

The N/C ratio, found in **Table 4-2**, is another useful ratio to monitor the prevalence of carbon contamination in the sample. Ideally, this value should remain constant, as our samples should approximate stoichiometric ratios of carbon and nitrogen according to the APTES functional group (1 nitrogen atom to every 3 carbon).

The differing values found in the non-BTFBA labelled aminated silica controls in Table 1 point to the potential amount of carbon contamination that limits the use of carbon as a useful element for study.

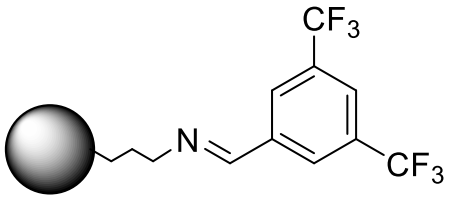

Monitoring the F/Si ratio of the non-BTFBA labelled aminated silica controls is important to assess possible contamination by Teflon-coated or other fluorinated materials. We can see in **Table 4-2** that the controls show very low amounts, suggesting that fluorine contamination was not an issue in our work.

4.3.2 BTFBA-labelled Silica Nanoparticles

Aminated silica nanoparticles between sizes of 20 to 100 nm were BTFBA-labelled, prepared for XPS analysis and measurements were performed to determine relative atomic compositions. As the elements surveyed were C, O, N, F, Si and Au, their relative ratios provide considerable information regarding deposition of the nanoparticles, and crucially, the extent of BTFBA labelling. The spectra in **Figure 4-10, 4-11, 4-12,** and **4-13** are representative of the spectra collected for the range of particle sizes. It should be stressed that XPS was not implemented to perform absolute measurements, which would require a given mass and monolayer coverage of particles.

Table 4-2. Relative atomic compositions obtained from quantitative analysis of XPS data for aminated silica samples before and after modification with BTFBA. The naming of T1 and T2 correspond to the R1 and R2 used elsewhere.

	n	Si/O	N/Si	F/Si	N/C	F/N	CF3/Ctot
20 nm, B2 T1	6	0.53 ± 0.01	0.075 ± 0.003	0.42 ± 0.01	0.077 ± 0.002	5.7 ± 0.3	0.086 ± 0.004
20 nm, B2 T2	6	0.54 ± 0.01	0.074 ± 0.001	0.43 ± 0.01	0.077 ± 0.001	5.9 ± 0.1	0.091 ± 0.004
50 nm, B3 T1	3	0.45 ± 0.01	0.027 ± 0.005	0.052 ± 0.003	0.035 ± 0.005	2.0 ± 0.3	
50 nm, B3 T2	6	0.44 ± 0.01	0.028 ± 0.003	0.065 ± 0.004	0.027 ± 0.001	2.3 ± 0.2	
80 nm, B3 T1	3	0.45 ± 0.02	0.085 ± 0.017	0.47 ± 0.02	0.065 ± 0.002	5.7 ± 0.9	0.082 ± 0.013
80 nm, B3 T2	3	0.48 ± 0.01	0.070 ± 0.001	0.41 ± 0.01	0.069 ± 0.002	5.8 ± 0.3	0.086 ± 0.006
100 nm, B3 T1	3	0.49 ± 0.01	0.095 ± 0.001	0.63 ± 0.01	0.077 ± 0.001	6.6 ± 0.2	0.127 ± 0.002
100 nm, B3 T2	3	0.49 ± 0.01	0.098 ± 0.009	0.47 ± 0.01	0.075 ± 0.003	4.9 ± 0.6	0.080 ± 0.008
50 nm, B2	3	0.46 ± 0.01	0.019 ± 0.001	0.004 ± 0.001	0.031 ± 0.001	0.21 ± 0.03	
80 nm, B3	3	0.46 ± 0.01	0.063 ± 0.005	0.011 ± 0.001	0.098 ± 0.002	0.18 ± 0.03	
100 nm, B3	3	0.45 ± 0.01	0.101 ± 0.006	0.017 ± 0.002	0.116 ± 0.003	0.16 ± 0.04	

The most relevant ratios for evaluating BTFBA labelling efficiency are naturally those involving F and N. The N/Si ratios are useful for a measurement for relative surface amine content and track well with the determinations of amine content by the qNMR technique and the colorimetric assays. Similarly, the F/Si ratios also match well with the solid-state ^{19}F NMR measurements. In respect to reproducibility, both ratios are relatively consistent between runs of BTFBA-labelling. However, there are cases in both ratios where the standard deviations are rather high, approaching 20% for the case of the 80 nm particles for N/Si, and 100 nm particles for F/Si.

In the case of the 80 nm particles, the uncertainty between measurements can be primarily attributed to the relatively weak N1s signal. As shown in the survey spectrum for the aminated and BTFBA-labelled silica nanoparticles, the photoemission peak is relatively small feature against the high background in the 350 to 500 eV region.

The resulting signal-to-noise is poor, especially in comparison to other core level peaks. Additionally, it has been reported in the literature that the N1s peak is especially prone to degradation and a loss of intensity and total peak area during data acquisition.[20]

For the 100 nm particles, the solid-state ^{19}F NMR reports a percent difference of 9.6% between the two trials (131 and 119 µmol/g). However, the difference between the F/Si ratio is 29.1%, which may point to the level of uncertainty of the XPS technique.

With BTFBA labelled materials, the F/N and N/C ratio are important measurements which should point to the efficiency of the coupling between BTFBA and the surface amine groups. For complete binding, the expected ratios are (6:1, 2×CF_3 to NH_2) and (1:13, NH_2 to C) respectively. The F/N ratios for the 20, 80 and 100 nm particles suggest near complete surface conjugation of the detected amine groups, where calculated yields are in the range of >95%. In the case of the 50 nm particle, the yield shown decreases to 33-38%. This calculation diverges from the determination provided by the solid-state ^{19}F NMR, although both indicate lower than complete surface labelling by BTFBA.

CF_3 groups also exhibit a significant chemical shift in XPS spectra, seen in **Fig. 4-14**. The strongly electronegative fluorine atoms withdraw charge and introduce a greater positive character on the carbon atoms, resulting in higher characteristic binding energies.

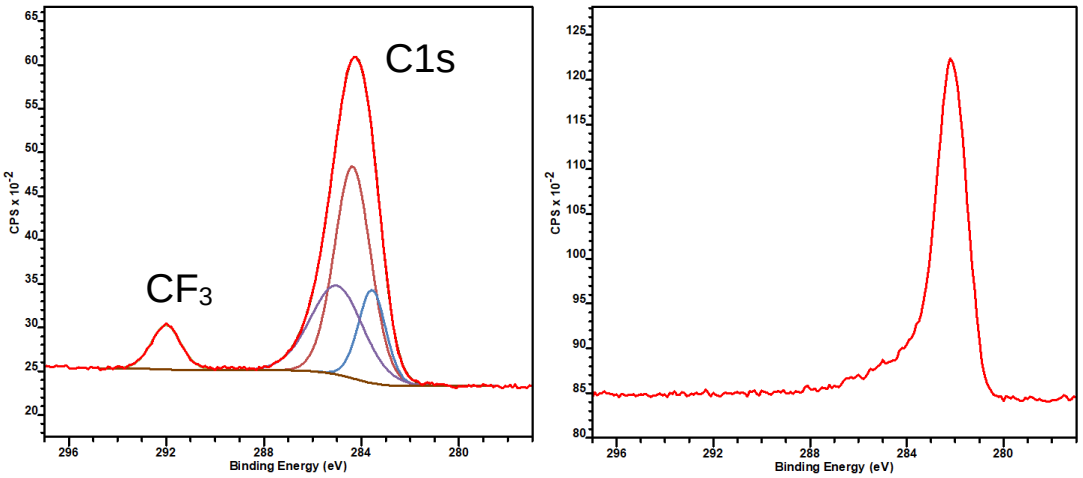

Figure 4-14: (Left) Carbon 1s photoemission peaks from BTFBA-labelled aminated silica nanoparticles. (Right) Carbon contamination of bare gold-substrate in high-resolution C1s peak.

Calculation of the peak areas of CF_3 compared to the total C1s peak yielded ratios that were well below the ratio expected (0.17). Unfortunately, these values do not match well with the yields determined by the other spectroscopic methods or the F/N ratio. Again, it is likely due to surface carbon contamination to the C 1s peak, which is shown to be significant in the control spectrum on the bare gold substrate.

The XPS results on surface atomic compositions are the most useful when providing additional detail on results gathered from the other techniques. One of the remaining questions with our surface quantification techniques comes from the issue of accessibility and reactivity of the amine groups. For now, we depend on XPS as the main technique to investigate this issue through the elemental ratios. While the F/N ratio reinforces the notion of high coupling yields via the BTFBA labelling technique, and therefore the quantification by the chemical assays, it is necessary to continue to explore this measurement, potentially with carefully loaded and controlled surface

functionalized silica. For a set of particles which have a predetermined surface coverage of amine groups, where the total and surface amine content are in good agreement, it would be highly beneficial to perform XPS analyses to confirm the reliability of this measurand.

4.4 Conclusion

Following the steps of previous works which propose combined surface analytical techniques implementing XPS,[9] we found the chemical information provided by XPS very useful in validating our multi-method approach for the detection and quantification of surface amine groups. On a range of aminated silica nanoparticles, XPS suggests that the determinations from the colorimetric assays and solid-state NMR approach represent good to excellent coupling efficiency. In some cases, measured elemental ratios point to near complete binding of surface amines. Cases where the measured content were anomalous may indicate the limitations of our method, which does not account for our materials geometric profile and surface structure.

4.5 References

(1) Jablonski, A. Escape Depth of Photoelectrons. *Surf. Interface Anal.* **1994**, *21* (11), 758–763. https://doi.org/10.1002/sia.740211104.

(2) Jablonski, A.; Tilinin, I.; Powell, C. Mean Escape Depth of Signal Photoelectrons from Amorphous and Polycrystalline Solids. *Phys. Rev. B - Condens. Matter Mater. Phys.* **1996**, *54* (15), 10927–10937. https://doi.org/10.1103/PhysRevB.54.10927.

(3) Fairley, N. Peak Fitting in XPS. *Casaxps.Com* **2006**, 1–29.

(4) Tougaard, S. Quantitative Analysis of the Inelastic Background in Surface Electron Spectroscopy. *Surf. Interface Anal.* **1988**, *11* (9), 453–472. https://doi.org/10.1002/sia.740110902.

(5) Aronniemi, M.; Sainio, J.; Lahtinen, J. Chemical State Quantification of Iron and Chromium Oxides Using XPS: The Effect of the Background Subtraction Method. *Surf. Sci.* **2005**, *578* (1–3), 108–123. https://doi.org/10.1016/j.susc.2005.01.019.

(6) Thevuthasan, S.; Kuchibhatla, S. V. N. T.; Karakoti, A.; Baer, D. R.; Wang, H.; Elder, A.; Mueller, K.; Lai, J.; Baisch, B. L.; Moon, D.; et al. Surface Characterization of Nanomaterials and Nanoparticles: Important Needs and Challenging Opportunities. *J. Vac. Sci. Technol. A Vacuum, Surfaces, Film.* **2013**, *31* (5), 050820. https://doi.org/10.1116/1.4818423.

(7) Kuchibhatla, S. V. N. T.; Karakoti, A. S.; Baer, D. R.; Samudrala, S.; Engelhard, M. H.; Amonette, J. E.; Thevuthasan, S.; Seal, S. Influence of Aging and Environment on Nanoparticle Chemistry: Implication to Confinement Effects in Nanoceria. *J. Phys. Chem. C* **2012**, *116* (26), 14108–14114. https://doi.org/10.1021/jp300725s.

(8) Ederer, J.; Janoš, P.; Ecorchard, P.; Tolasz, J.; Štengl, V.; Beneš, H.; Perchacz, M.; Pop-Georgievski, O. Determination of Amino Groups on Functionalized Graphene Oxide for Polyurethane Nanomaterials: XPS Quantitation vs.

Functional Speciation. *RSC Adv.* **2017**, *7* (21), 12464–12473. https://doi.org/10.1039/c6ra28745j.

(9) Fischer, T.; Dietrich, P. M.; Streeck, C.; Ray, S.; Nutsch, A.; Shard, A.; Beckhoff, B.; Unger, W. E. S.; Rurack, K. Quantification of Variable Functional-Group Densities of Mixed-Silane Monolayers on Surfaces via a Dual-Mode Fluorescence and XPS Label. *Anal. Chem.* **2015**, *87* (5), 2685–2692. https://doi.org/10.1021/ac503850f.

(10) Hennig, A.; Dietrich, P. M.; Hemmann, F.; Thiele, T.; Borcherding, H.; Hoffmann, A.; Schedler, U.; Jäger, C.; Resch-Genger, U.; Unger, W. E. S. En Route to Traceable Reference Standards for Surface Group Quantifications by XPS, NMR and Fluorescence Spectroscopy. *Analyst* **2015**, *140* (6), 1804–1808. https://doi.org/10.1039/c4an02248c.

(11) Huimin Sui; Lei Chen; Xiao Xia Han; Xiaolei Zhang; Xiaolei Wang; Bing Zhao. Quantitative Determination of Total Amino Acids Based on SERS and Ninhydrin Derivatization. *Anal. Sci.* **2017**, *33* (March). https://doi.org/10.2116/analsci.33.53.

(12) Yegen, E.; Lippitz, A.; Treu, D.; Unger, W. E. S. Derivatization of Amino Groups by Pentafluorobenzaldehyde (PFB) as Observed by XPS and NEXAFS Spectroscopy on Spin Coated 4,4-Methylenebis(2,6- Diethylaniline) Films. *Surf. Interface Anal.* **2008**, *40* (3–4), 176–179. https://doi.org/10.1002/sia.2685.

(13) Wallart, X.; De Villeneuve, C. H.; Allongue, P. Truly Quantitative XPS Characterization of Organic Monolayers on Silicon: Study of Alkyl and Alkoxy Monolayers on H-Si(111). *J. Am. Chem. Soc.* **2005**, *127* (21), 7871–7878. https://doi.org/10.1021/ja0430797.

(14) Mohai, M. XPS MultiQuant: Multimodel XPS Quantification Software. *Surf. Interface Anal.* **2004**, *36* (8), 828–832. https://doi.org/10.1002/sia.1775.

(15) QUASES Tougaard Inc. QUASES-Tougaard 5.1.

(16) Powell, C. J.; Werner, W. S. M.; Kalbe, H.; Shard, A. G.; Castner, D. G. Comparisons of Analytical Approaches for Determining Shell Thicknesses of

Core-Shell Nanoparticles by X-Ray Photoelectron Spectroscopy. *J. Phys. Chem. C* **2018**, *122* (7), 4073–4082. https://doi.org/10.1021/acs.jpcc.7b12070.

(17) Shard, A. G. A Straightforward Method for Interpreting XPS Data from Core-Shell Nanoparticles. *J. Phys. Chem. C* **2012**, *116* (31), 16806–16813. https://doi.org/10.1021/jp305267d.

(18) Chudzicki, M.; Werner, W. S. M.; Shard, A. G.; Wang, Y. C.; Castner, D. G.; Powell, C. J. Evaluating the Internal Structure of Core-Shell Nanoparticles Using X-Ray Photoelectron Intensities and Simulated Spectra. *J. Phys. Chem. C* **2015**, *119* (31), 17687–17696. https://doi.org/10.1021/acs.jpcc.5b04517.

(19) Wang, Y. C.; Engelhard, M. H.; Baer, D. R.; Castner, D. G. Quantifying the Impact of Nanoparticle Coatings and Nonuniformities on XPS Analysis: Gold/Silver Core-Shell Nanoparticles. *Anal. Chem.* **2016**, *88* (7), 3917–3925. https://doi.org/10.1021/acs.analchem.6b00100.

(20) Gamage McEvoy, J.; Thibault, Y. Impact of Crystal Chemistry Properties on the Collector-Mineral Interactions Observed for REE Orthophosphates and Oxides. *Appl. Surf. Sci.* **2019**, *466* (October 2018), 970–981. https://doi.org/10.1016/j.apsusc.2018.10.103.

Chapter 5. Comparison of Quantification Techniques for Surface Amine Groups on Silica Nanoparticles

The results in this chapter are the focus of the first publication. My contribution in this section was in preparation and principal analysis of the various silica nanoparticles. Dr. Gregory Lopinski assisted in the XPS data analysis.

1. Sun, Y.; Kunc, F.; Balhara, V.; Coleman, B.; Kodra, O.; Raza, M.; Chen, M.; Brinkmann, A.; Lopinski, G.; Johnston, L. Quantification of Amine Functional Groups on Silica Nanoparticles: A Multi-Method Approach. *Nanoscale Adv.* **2019**. https://doi.org/10.1039/C9NA00016J.

5.1 Background

To critically assess the determinations of surface amine content from the various methods developed herein, it is crucial to address the fundamental differences in how they probe the surface of the silica nanoparticles. It should be again stressed that a fraction of the amine functional groups on the surface may have less reactivity or accessibility. The potential causes for this subset of groups are as follows:

For one, controlled fabrication of silane monolayers is a challenging task, as silanes may readily form areas or domains of multilayer configuration, as touched on in the introductory chapter.

In addition, functionalized silica nanoparticles which are synthesized or fabricated by co-condensation may inherently possess a significant fraction of groups which are embedded within the silica matrix below the surface layer. This is highly relevant as many mesoporous silica nanoparticles adopt this approach. For particles which are functionalized post-synthetically, multilayers or surface coatings may be intentionally grown to a certain thickness to achieve a desired particle diameter and size or to achieve a protective shell around the particle. This is illustrated below:

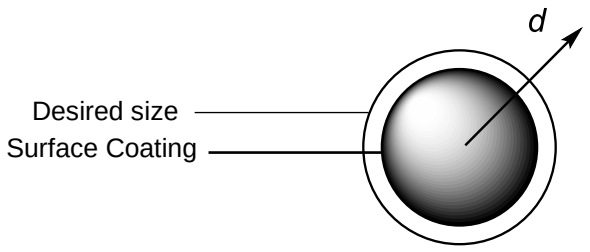

Attachment (via condensation) of organofunctional silanes onto silica surfaces can occur between any of the three substituents (ethoxy- in the scheme below) of the

headgroup. Consequently, silane coupling agents may bind in a multitude of orientations and geometries, depending on the number of siloxane bonds formed with the nanoparticle's surface.

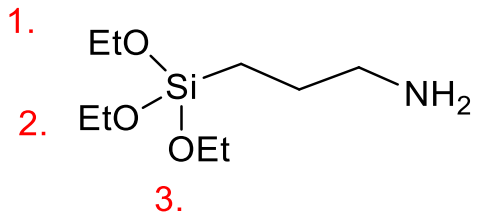

Silane surfaces should also not be considered inert and passivated, particularly when they are suspended in aqueous solutions and polar solvents. They are in a dynamic state, where groups may be readily hydrolyzed and re-arranged in different configurations. This is a major issue in some commercial applications, where certain functional silane coatings have been shown to be sensitive to elevated temperature and humidity.[1] A publication from our group studied the stability of functionalized silica coatings in respect to the effect of temperature on various degrees of functionalization and silane chain-lengths.[2]

The silica nanoparticles studied here have all been functionalized with APTES, a silane that presents some challenges. As previously mentioned, this reagent has the potential to self-polymerize and form oligomers. This has been considered a possible reason that some APTES coatings proceed by "island-type" growth, which is illustrated as "model 1" in **Fig. 5-1**.[3] This in turn, may influence both co-condensation and post-synthetic surface functionalization approaches.

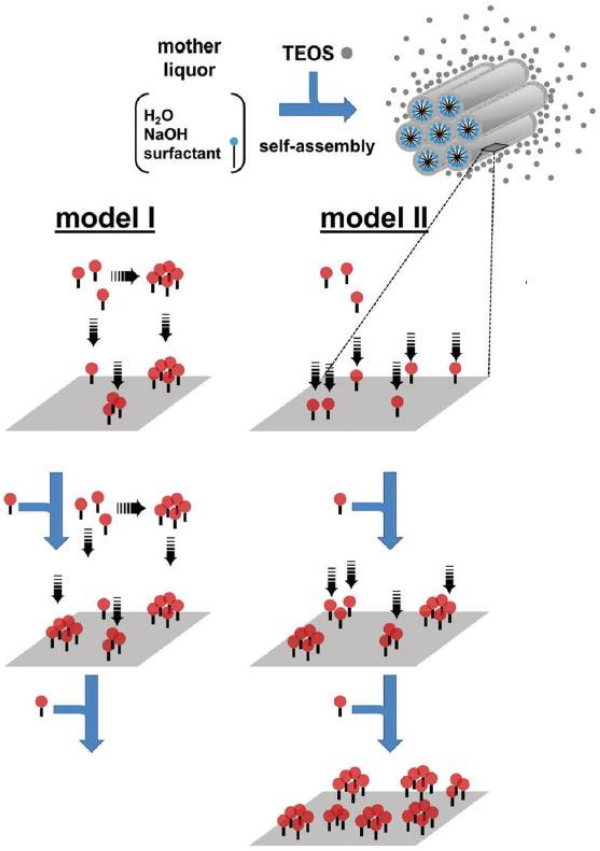

Figure 5-1: A simplified scheme depicting two different processes which give rise to heterogeneous domains or clusters of functionalities on mesoporous silica. Model 1 represents growth through an “island-type process”. Model 2 depicts preferential attachment of individual monomers to these domains. The scheme was adapted from reference.[3]

APTES’s primary amine functionality may also ‘compete’ with alkoxy headgroups for the surface silanols which otherwise present possible sites for grafting. They have the capability to participate in H-bonding to various degrees, depending on their protonation state.[4] This can be seen in the scheme shown in **Fig. 5-2**.

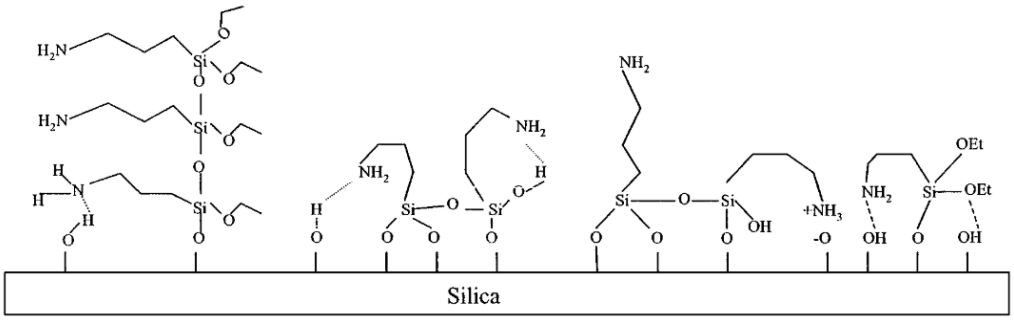

Figure 5-2: Scheme of various competing interactions between the primary amine moiety of APTES and desired attachment of the alkoxy head group. Image from reference.[4]

5.2 Results and Discussion

The two colorimetric assays are both restricted by the reactivity and accessibility of surface amine groups. They cannot detect and quantify groups embedded below the surface since steric hindrance restricts their reaction and yield. The solid-state ^{19}F NMR technique will also be affected by reactivity and accessibility of groups due to its reliance on BTFBA labelling to provide a magnetic resonance signal for quantification. On the other hand, XPS can provide surface analysis on BTFBA-labelled silica. We can use the elemental ratios to determine coupling yields of amine groups found within the depth probed by XPS (≈10 nm). Unfortunately, limitations of XPS in accounting for structure and geometry of nanoparticles and their surfaces introduces uncertainty into our result.

Therefore, we compared our ensemble of surface-specific techniques with another method which determines total functional group content. This allowed us to

study and account for the differences between reactive and non-reactive groups (which may be located on the surface or otherwise).

A solution-state ^{1}H NMR method which requires complete dissolution of silica nanoparticles was developed by our group.[2] By suspending the particles in strong base (0.4 M) and exposing them to high temperature (45 ^{o}C), the silica matrix will rapidly hydrolyze and dissolve in a few hours. This yields the bulk as silicic acid and importantly, the functional groups as monomers in solution, which can be analyzed by ^{1}H qNMR with addition of standard. As with other methods which determine total amine content and are destructive in nature, the solution-state NMR approach cannot distinguish between groups which have been liberated from the surface and those from the interior of the particle.

Previous work from our group has used qNMR to quantify the amine content in the same silica nanoparticles that have been examined using surface sensitive techniques. Of the techniques which provide direct quantification of surface amine content (which excludes XPS), we expected the total amine content to either be the highest determination of the four or match the highest determination between the label-based approaches.

In **Fig. 5-3**, we can see a comparison graph which shows the amine concentration determined by each of the techniques for 4 different sizes of silica nanoparticles. In most cases, the colorimetric assays are in agreement with one another. Looking closer, the 4-NBA assay and BTFBA-labelled silica quantified by solid-state NMR are typically closer in value, while the ninhydrin assay estimates lower surface amine content. This is unexpected, as ninhydrin's mechanism for dye

production relies on chemical reaction at the surface, which in theory should reduce the influence of steric crowding.

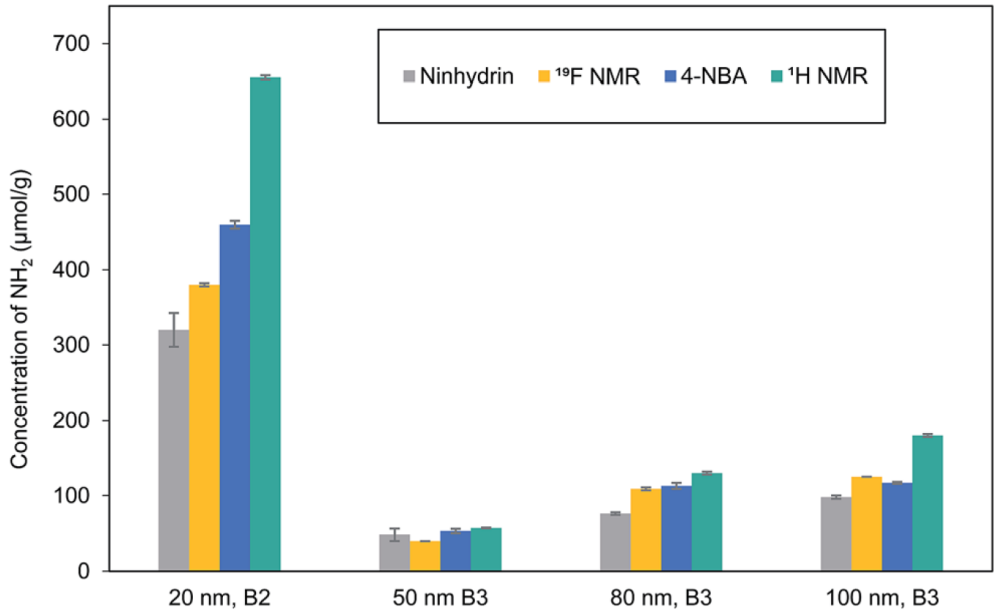

Figure 5-3: Comparison between surface quantification methods and determination of total functional group content by solution-state ^{1}H qNMR. The corresponding values are shown in Table 1.

Table 5-1 shows the determination of amine content with ninhydrin, 4-NBA and the solution state ^{1}H qNMR method. Two additional ratios are provided: the accessible/total amine, and the fractional monolayer coverage. The accessible to total amine ratio is obtained from the 4-NBA assay and qNMR determinations. It is interesting to see the different cases of very high to complete agreement of the accessible and total amine content (such as in the 50 nm and 80 nm B3 in **Fig. 5-3**) and those lower, at ≈ 0.70 and lower (such as in the 20 nm, B2 and 100 nm, B3 in **Fig. 5-3**).

Table 5-1. Results from determination of amine content with ninhydrin and 4-NBA colorimetric assay, and the ^{1}H qNMR approach.

Sample ID	Ninhydrin Assay (μmol g^{-1})	4-NBA Assay (μmol g^{-1})	^{19}F qNMR (μmol g^{-1})	Accessible/ Total Amine	Fractional Monolayer Coverage
20 nm B2	320 ± 20	459 ± 5	655 ± 3	0.70	0.71
50 nm B1	121 ± 3		215 ± 2		
50 nm B2	47± 1	66 ± 12	64 ± 1	1.03	0.18
50 nm B3	48 ± 8	53 ± 3	57 ± 1	0.93	0.16
80 nm B1	18 ± 2				
80 nm B2	103 ± 4	132 ± 15	145 ± 3	0.91	0.63
80 nm B3	76 ± 2	113 ± 4	130 ± 2	0.87	0.56
100 nm B1	91 ± 5				
100 nm B2	152 ± 13	169 ± 15	186 ± 1	0.91	1.03
100 nm B3	98 ± 2	117 ± 1	180 ± 2	0.64	1.02
120 nm B2	117 ± 4	122 ± 2	179 ± 3	0.68	1.19

There are some relevant examples from the literature on polymer and clay NPs which have shown a wide range of coupling efficiency with probes with respect to total functional group content.[5–9] Various assays and labelling approaches which depend on covalent modification and electrostatic binding have performed poorly when compared to total functional group content methods such as conductometric titrations and NMR-based approaches.[6,9,10]

The fractional monolayer coverage ratio is also important to consider. The estimate for a monolayer coverage comes the total amine content from qNMR and from the assumption of (4 aminopropyl siloxanes/nm^2)[11] and using the surface area from the mean TEM diameter from these NPs. In units of μmol g^{-1} they are 920 (20 nm), 360 (50

nm), 230 (80 nm), 180 (100 nm) and 150 (120 nm). Across the various samples, we can see that even with the highest projections provided by the ^{1}H qNMR method, most samples do not possess a functionalized monolayer.

The plots shown in **Fig. 5-4** and corresponding values in **Table 5-2** also use fractional monolayer estimates to study the correlation of the F/Si and N/Si ratios from XPS with the estimates from the NMR techniques. Both plots show good agreement of the methods, which demonstrates their collective ability to assess amine content, and in respect to the BTFBA-labelled silica, fluorine.

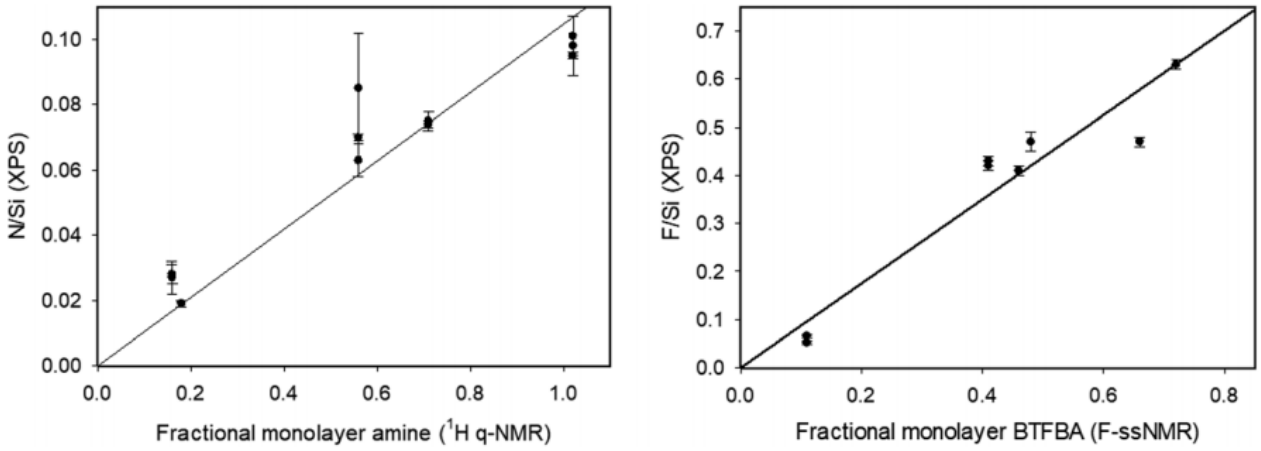

Figure 5-4: Correlation plots of fractional monolayer coverage with ^{1}H qNMR and ^{19}F ssNMR and XPS N/Si and F/Si ratios.

Table 5-2. Quantification of amine content determined by each method with standard deviation for the BTFBA-labelled series of silica nanoparticles.

(µmol/g)	Ninhydrin	^{19}F NMR	4-NBA	^{1}H NMR	Fractional Monolayer Coverage
20 nm	320 ± 23	380 ± 1	459 ± 5	655 ± 3	0.41
50 nm	48 ± 8	40 ± 0.2	53 ± 3	57 ± 1	0.11
80 nm	76 ± 2	109 ± 3	113 ± 4	130 ± 2	0.47
100 nm	98 ± 2	125 ± 6	117 ± 1	180 ± 2	0.69

We can refer to the XPS elemental ratios to ascertain whether this differences in total and surface amine is attributable to groups near the surface (within 10 nm of the depth profile) or those located further below. The XPS analysis for the BTFBA-labelled particles is shown in **Table 5-3**. The F/N ratios show that labelling of surface amines was close to full coupling efficiency, within the XPS depth profile. This suggests that the difference between the total vs. surface amine determination can be primarily attributed to amines beneath the surface.

Table 5-3. XPS elemental ratios on coupling efficiency of BTFBA-labelling on aminated silica nanoparticles.

	20 nm	50 nm	80 nm	100 nm	*100% Coupling*
F:N	5.8 ± 0.1	2.1 ± 0.2	5.8 ± 0.1	5.8 ± 1.0	**6.0** (6:1)
N:C	0.077 ± 0.001	0.031 ± 0.005	0.067 ± 0.003	0.076 ± 0.001	**0.083** (1:12)

The results from our multi-method study show that the commercially-sourced aminated silica nanoparticles may contain a significant fraction of amine groups which are inaccessible to the probes or reagents used here. This fraction would otherwise remain undetected in the absence of applying an additional method for determining total functional group content. We believe this underscores the importance of employing multiple approaches for the characterization and quantification of surface functionalized nanomaterials. Although these embedded groups do not provide reactive sites for bioconjugation and chemical derivatization, they may still influence other properties of properties and behaviors of these nanomaterials.

Since reactivity of these functional groups depends on steric hindrance of the colorimetric dyes and fluorinated probe, other smaller probes may still access and detect these FGs. For example, conductometric titrations utilize the smallest sized reporters (H^+/OH^-) to probe surface groups via their acid/base properties, and are believed to yield the highest possible determination for accessible functional group content.[9] Conversely, the groups which are detected by titration, and undetected by larger dyes may affect surface chemistry by influencing zeta-potential, and acid/base properties of the nanomaterial.

Embedding functional groups below the surface may also alter the ordering and structure of the silica matrix, introducing defect sites. Silica coatings are widely used to improve thermal stability of other nanomaterials such as gold and metal oxides. To these ends, there is evidence that the ordering and packing of silane monolayers influences their thermal stability.[12]

One widely cited advantage of using nanoscale silica in the design of drug delivery systems is their biocompatibility. A recent study investigated the potential influence of different surface amine densities on the toxicology of silica nanoparticles.[13] The results showed that at a specific minimum APTES loading the biocompatibility of the NPs was significantly improved in comparison to bare, non-functionalized silica. The authors added that the "…chemical composition of the core material…but also the number of surface exposed amino groups, seem to be critical to determine the ultimate toxicity of NPs." Thus, it is essential for studies of this kind to critically assess the location and origin of the functional groups, and to employ a combination of surface and total functional group content determination methods.

Lastly, it is unclear what effects these embedded groups may have on the toxicology and behavior of these nanomaterials in bioapplications. This is concerning, as nanoscale silica is widely used for its excellent biodegradability. For functionalized materials which contain a large fraction of inaccessible groups, there may be unexpected immunological responses and interactions which occur as these chemical species are released during particle dissolution.

To help interpret our findings, we can look to other similar studies, with two relevant examples on mesoporous silica. Ritter and Brühwiler used two fluorescent label

approaches, one which used covalent modification and release, and another which analyzed dissolved particles.[14] They found a significant fraction of inaccessible groups, likely located within the micropores of their material. In a work by Rosenholm and Liden, they found that the 4-NBA assay determined much lower amine content in comparison to quantification from thermogravimetric analysis, which again suggests a large fraction of groups internalized within pores.[15] These two studies are consistent and expected given the large internal surface area of mesoporous silica.

On that note, it is important to mention studies where the porosity of non-mesoporous silica nanoparticles has been established, and even exploited to yield hollowed structures.[16,17] These works postulate that silica nanoparticles formed by the Stöber process may contain small pores which may result from base-catalyzed etching and other processes. This is yet another potential cause for the formation of a significant fraction of inaccessible functional groups in silica nanoparticles.

5.3 Concluding Remarks

This work involved the development and application of multiple quantification techniques for the analysis of amine functionalized silica nanoparticles. The two colorimetric assays, ninhydrin and 4-NBA serve to provide a rapid and convenient option for the routine analysis of amine functionalized silica. The BTFBA-labelling approach allows for quantification by solid-state ^{19}F NMR, which is non-destructive and provides characterization of samples in their native state. Additionally, BTFBA-labelled silica can be analyzed by X-ray photoelectron spectroscopy, which provided us deeper

surface-specific analysis of our silica particles and information regarding coupling yields. We evaluated and demonstrated the high efficacy of our surface analysis approaches, as the various techniques provide mutual method validation. In addition, their respective limitations with regards to accessibility and reactivity of surface groups were thoroughly discussed as the focus of this final chapter.

The sensitivities of the various methods of characterization also differ. The ^{1}H qNMR method has an estimated limit of detection of 10 µmol g^{-1} while the ^{19}F qNMR method is approximately a factor of three higher. The two NMR methods are also considerably different in their convenience as the former requires a relatively straightforward protocol for particle dissolution and is faster to perform measurements (less than an hour). The solid-state NMR method requires an involved particle-labelling procedure, and measurements require multiple days. The assays in comparison, are the quickest and easiest to perform and are the most sensitive, with limits of detection an order of magnitude lower than the ^{1}H qNMR method.

All together our multi-method approach when used in conjunction with total amine content determinations such as the solution-state ^{1}H NMR technique, can provide a more comprehensive evaluation of chemical group functionality, surface-bound and otherwise. This is an important development for the study of functionalized nanomaterials, as it is still uncommon to find multiple characterization and quantification techniques used in the literature. We hope the ensemble of methods presented herein may serve as a useful option for the study of amine functionalized materials and advance their development in important applications which are wide-ranging in scope.

5.4 References

(1) Okhrimenko, D. V.; Budi, A.; Ceccato, M.; Cárdenas, M.; Johansson, D. B.; Lybye, D.; Bechgaard, K.; Andersson, M. P.; Stipp, S. L. S. Hydrolytic Stability of 3-Aminopropylsilane Coupling Agent on Silica and Silicate Surfaces at Elevated Temperatures. *ACS Appl. Mater. Interfaces* **2017**, *9* (9), 8344–8353. https://doi.org/10.1021/acsami.6b14343.

(2) Kunc, F.; Balhara, V.; Brinkmann, A.; Sun, Y.; Leek, D. M.; Johnston, L. J. Quantification and Stability Determination of Surface Amine Groups on Silica Nanoparticles Using Solution NMR. *Anal. Chem.* **2018**. https://doi.org/10.1021/acs.analchem.8b02803.

(3) Kobayashi, T.; Singappuli-Arachchige, D.; Slowing, I. I.; Pruski, M. Spatial Distribution of Organic Functional Groups Supported on Mesoporous Silica Nanoparticles (2): A Study By1H Triple-Quantum Fast-MAS Solid-State NMR. *Phys. Chem. Chem. Phys.* **2018**, *20* (34), 22203–22209. https://doi.org/10.1039/c8cp04425b.

(4) White, L.; Tripp, C. Reaction of (3-Aminopropyl)Dimethylethoxysilane with Amine Catalysts on Silica Surfaces. *J. Colloid Interface Sci.* **2000**, *232* (2), 400–407. https://doi.org/10.1006/jcis.2000.7224.

(5) Hennig, A.; Dietrich, P. M.; Hemmann, F.; Thiele, T.; Borcherding, H.; Hoffmann, A.; Schedler, U.; Jäger, C.; Resch-Genger, U.; Unger, W. E. S. En Route to Traceable Reference Standards for Surface Group Quantifications by XPS, NMR and Fluorescence Spectroscopy. *Analyst* **2015**, *140* (6), 1804–1808. https://doi.org/10.1039/c4an02248c.

(6) Hennig, A.; Borcherding, H.; Jaeger, C.; Hatami, S.; Würth, C.; Hoffmann, A.; Hoffmann, K.; Thiele, T.; Schedler, U.; Resch-Genger, U. Scope and Limitations of Surface Functional Group Quantification Methods: Exploratory Study with Poly(Acrylic Acid)-Grafted Micro- and Nanoparticles. *J. Am. Chem. Soc.* **2012**,

134 (19), 8268–8276. https://doi.org/10.1021/ja302649g.

(7) Hennig, A.; Hoffmann, A.; Borcherding, H.; Thiele, T.; Schedler, U.; Resch-Genger, U. Simple Colorimetric Method for Quantification of Surface Carboxy Groups on Polymer Particles. *Anal. Chem.* **2011**, *83* (12), 4970–4974. https://doi.org/10.1021/ac2007619.

(8) Moser, M.; Schneider, R.; Behnke, T.; Schneider, T.; Falkenhagen, J.; Resch-Genger, U. Ellman's and Aldrithiol Assay as Versatile and Complementary Tools for the Quantification of Thiol Groups and Ligands on Nanomaterials. *Anal. Chem.* **2016**, *88* (17), 8624–8631. https://doi.org/10.1021/acs.analchem.6b01798.

(9) Moser, M.; Nirmalananthan, N.; Behnke, T.; Geißler, D.; Resch-Genger, U. Multimodal Cleavable Reporters versus Conventional Labels for Optical Quantification of Accessible Amino and Carboxy Groups on Nano-and Microparticles. *Anal. Chem.* **2018**, *90* (9), 5887–5895. https://doi.org/10.1021/acs.analchem.8b00666.

(10) Hennig, A.; Dietrich, P. M.; Hemmann, F.; Thiele, T.; Borcherding, H.; Hoffmann, A.; Schedler, U.; Jäger, C.; Resch-Genger, U.; Unger, W. E. S. En Route to Traceable Reference Standards for Surface Group Quantifications by XPS, NMR and Fluorescence Spectroscopy. *Analyst* **2015**, *140* (6), 1804–1808. https://doi.org/10.1039/c4an02248c.

(11) Zhuravlev, L. T. Concentration of Hydroxyl Groups on the Surface of Amorphous Silicas. *Langmuir* **1987**, *3* (3), 316–318. https://doi.org/10.1021/la00075a004.

(12) H. E. Bergna, W. O. R.; Bergna, H. E.; Roberts, W. O. COLLOIDAL SILICA Fundamentals and Applications. *Int. J. Numer. Methods Fluids* **2003**, *41* (1), 1–1. https://doi.org/10.1002/fld.463.

(13) Hsiao, I.; Fritsch-decker, S.; Leidner, A.; Al-rawi, M.; Hug, V.; Diabaté, S.; Grage, S. L.; Meffert, M.; Stoeger, T.; Gerthsen, D.; et al. Biocompatibility of Amine-Functionalized Silica Nanoparticles : The Role of Surface Coverage. **2019**, *1805400*, 1–11. https://doi.org/10.1002/smll.201805400.

(14) Ritter, H.; Brühwiler, D. Accessibility of Amino Groups in Postsynthetically Modified Mesoporous Silica. *J. Phys. Chem. C* **2009**, *113* (24), 10667–10674. https://doi.org/10.1021/jp901983j.

(15) Rosenholm, J. M.; Lindén, M. Wet-Chemical Analysis of Surface Concentration of Accessible Groups on Different Amino-Functionalized Mesoporous SBA-15 Silicas. *Chem. Mater.* **2007**, *19* (20), 5023–5034. https://doi.org/10.1021/cm071289n.

(16) Liu, S.; Han, M. Y. Silica-Coated Metal Nanoparticles. *Chem. - An Asian J.* **2010**, *5* (1), 36–45. https://doi.org/10.1002/asia.200900228.

(17) Li, S.; Wan, Q.; Qin, Z.; Fu, Y.; Gu, Y. Understanding Stöber Silicas Pore Characteristics Measured by Gas Adsorption. *Langmuir* **2015**, *31* (2), 824–832. https://doi.org/10.1021/la5042103.

Appendix

Table A-1. Physicochemical characterization provided by Nanocomposix for the aminated silica nanoparticles purchased. TEM images were acquired with a JEOL 1010 Transmission Electron Microscope, and hydrodynamic diameter/zeta potential was acquired with a Malvern Zetasizer Nano ZS.

	Sample ID	Diameter (TEM, nm)	Hydrodynamic Diameter (nm)	Zeta Potential (mV)	Solvent
B3	50 nm NH_2	48 ± 3	83	+33.9	Ethanol
	80 nm NH_2	80	-	-	Dried
	100 nm NH_2	97	-	-	Dried
B2	20 nm NH_2	22.6 ± 2.7	64	+20.5	Ethanol
	50 nm NH_2	48 ± 3	83	+33.9	Ethanol
	80 nm NH_2	79.7 ± 5.9	108.7	+43.4	Ethanol
	100 nm NH_2	97 ± 6 nm	144 nm	+64 mV	Ethanol
B1	50 nm NH_2	47 ± 3	88	+34	Ethanol
	80 nm NH_2	79.7 ± 5.9	108.7	+43.4	Ethanol
	100 nm NH_2	97 ± 6 nm	144 nm	+64 mV	Ethanol